# Synthesis and Characterization of Ferrocenyl-Containing Porphyrins and Tetraazaporphyrins

A THESIS
SUBMITTED TO THE FACULTY OF THE GRADUATE SCHOOL
OF THE UNIVERSITY OF MINNESOTA
BY

Anatolii Purchel

IN PARTIAL FULFILLMENT OF THE REQUIREMENTS
FOR THE DEGREE OF
MASTER OF SCIENCE

Advised by Dr. Victor Nemykin

August 2013

# Acknowledgements

Firstly, I would like to express my appreciation to my advisor Professor Victor Nemykin for his help and encouragement throughout my education, for teaching me, and for providing his support in all aspects of my being here. I would like to thank Dr. Pavlo Solntsev, Dr. Semen Dudkin, and Dr. Eranda Maligaspe for guidance in lab. I am also thankful to Tony Wertish for help with some experiments, to Jared Sabin for teaching me how to use some of the instrumentation, and to all former and present members of lab 212 for creating a friendly and supportive atmosphere, which helped me to accomplish these results. Lastly, I would like to thank the UMD Chemistry and Biochemistry Department as a whole for its support and the National Science Foundation for funding (Grants CHE – 0809203, CHE – 0922366, and CHE – 1110455) and the Minnesota Supercomputing Institute.

Part one is reprinted with permission from *Journal of Porphyrins and Phthalocyanines*. Characterization of the unusual metal-free, zinc, chloroindium, and ferrocenylindium 5,10,15,20-tetraferrocenylporphyrin anion-radicals by spectroelectrochemical, DFT, and TDDFT approaches, Victor N. Nemykin, Ping Chen, Pavlo V. Solntsev, Karl M. Kadish, *Journal of Porphyrins and Phthalocyanines*, **16**, 793 (2012). DOI: 10.1142/S1088424612500745, Copyright @ 2012 World Scientific.

For my family

&

To those trying to change the world

# Table of Contents

# List of Tables

# List of Figures

# List of Schemes

# Introduction

Organometallic complexes which can form a mixed-valence state are an important class of compounds. This types of molecules are subdivided into three groups, according to the Robin – Day classification[1,2,3,4], and division is based on electron-transfer process between two metallocenters. In a Class I mixed-valence system[2], metal centers do not comunicate between each other and valences are localized on a single site. Electron transfer process in such molecules does not occur and distinct sites with different specific valences cannot easily interconvert. Class II systems[2] are intermediate in character. There is some localization of distinct valences, but there is also low activation energy for their interconversion, therefore making electron transfer process inducible via thermal or radiation excitation. In these types of molecules electron transfer process is relatively slow, and allows investigation of electron transfer processes by variety of spectroscopic methods. Class III mixed-valence systems[2] have completely delocalized valence states of the several metal states and are considered as valence average molecules. Graphical representation of all three systems can be seen in Figure 1.

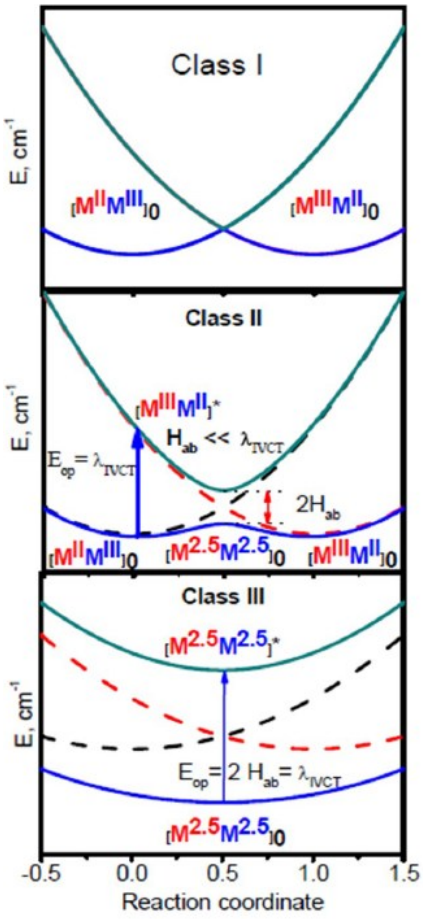


***Figure 1**: Robin and Day Classification for Mixed-Valence State Compounds*

The following two chapters report the redox and photophysical properties of ferrocene containing metal-free and metal-containing porphyrins, and tetraazaporphyrins. Each compound was characterized using variety of techniques such as NMR spectroscopy, UV-Vis and MCD, electrochemistry, spectroelectrochemistry, in order to test their abilities as light-harvesting systems[10], optical limiting devices[11], as well as their incorporation into molecular based electronic devices[5,6,7,8,9] (multibit data storage, sensors).

# Part 1 - Reduction of meso-Ferrocenyl Containing Porphyrins

## Introduction:

Nano-sized molecular based platforms for optoelectronic and switchable redox-driven devices are of great technological interest[12]. Formation of the mixed-valence states in polynuclear transition-metal complexes particularly those containing ferrocene, are responsible for the properties which are discussed below. Poly(ferrocene)-containing compounds with accessible mixed-valance properties at low potentials represent an important class of organometallics which are potentially useful in molecular electronics[13]. Ferrocenyl-containing porphyrins[14,15,16], tetraazaporphyrins[17], phthalocyanines[18], and corroles[19] have been intensively studied in the past few years because of their rich and reproducible redox chemistry as well as for their specific spectroscopic properties. Such types of aromatic macrocycles were considered as potential candidates for use in redox

switchable optical and fluorescent markers active in NIR area, as well as for multibit information storage devices[5,6,7,8,9]. In particular it was found that mixed-valence states are accessible in transition metal and metal-free 5, 10, 15, 20-tetraferrocenylporphyrins (MTFcP) as well as in metal-free 5,10,15-triferrocenyl-20-phenylporphyrin, 5,10-diferrocenyl-15,20-diphenylporphyrin, and 5,15-diferroce-nyl-10,20-diphenylporphyrin, which makes these compounds prospective species for multibit information storage elements[14m,o,q]. Previously it was shown that meso-tetraferrocenyl porphyrins undergo four reversible oxidations and two reversible reductions[7] (Figure 2). Although the oxidation behavior of poly(ferrocenyl)-containing porphyrins is currently well-understood, there is no information available on the spectroscopy and electronic structure of these compounds in their reduced forms. In order to gain insight into the influence of organometallic substituents on the electronic spectroscopy and electronic structure of $[MTFcP]^{\cdot-}$ systems, we have explored their reduction under spectroelectrochemical conditions and gained new insights into their electronic structure using density functional theory (DFT) methods.

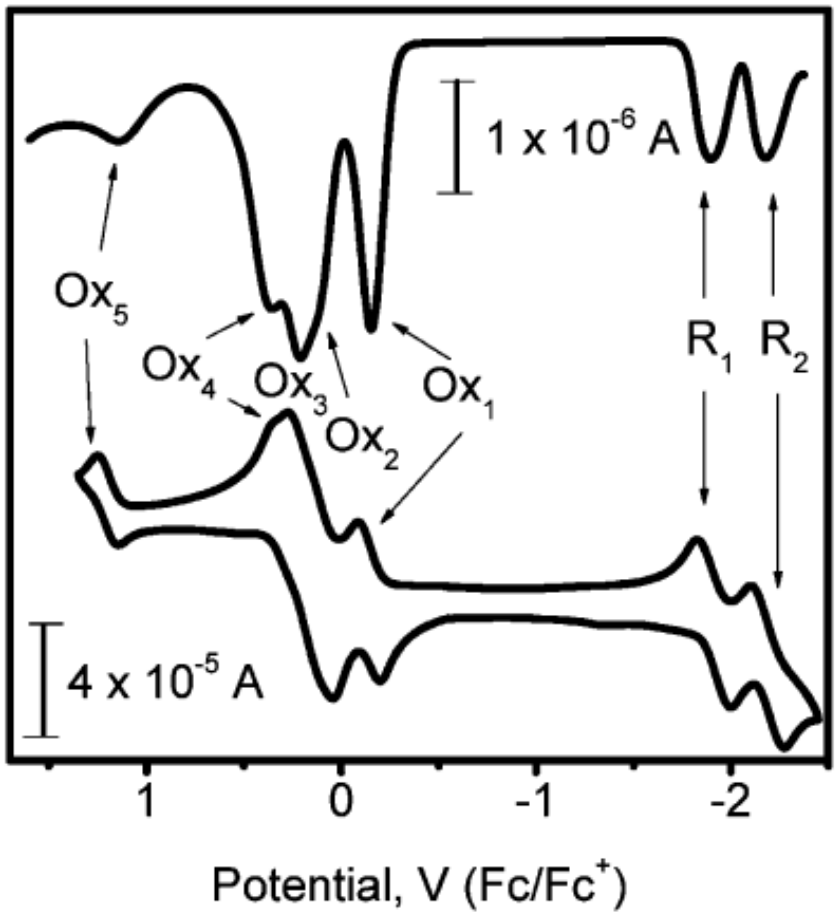


***Figure 2**: DPV(top) and CV (bottom) results of $H_2$TFcP in an o-DCB/TFAB system*[7]

## Synthesis

Previous synthetic procedures[14l,20] were optimized in order to obtain metal-free, transition – metal and main group elements substituted 5,10,15,20-tetraferrocenyl porphyrin. As can be seen in Scheme 1, metal-free porphyrin was prepared using previously described procedure[14l] and futher purification was carried out using alumina column.

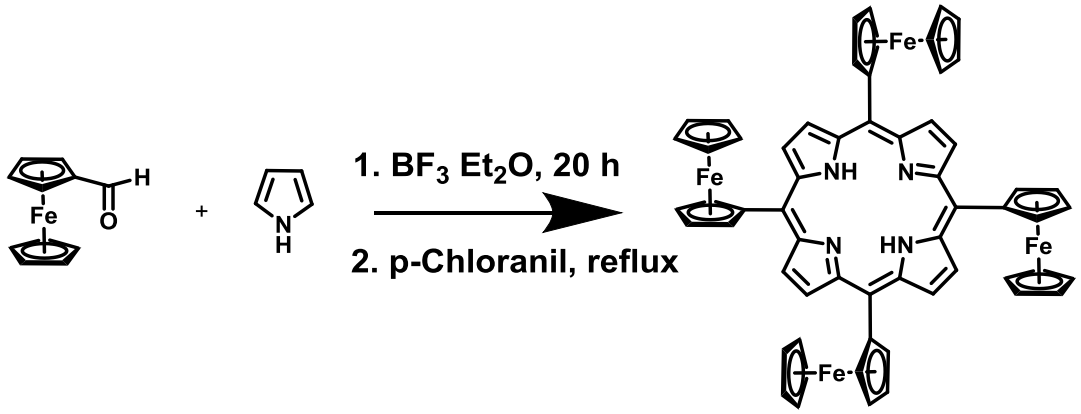


***Scheme 1***: *Preparation of $H_2$TFcP (1)*

Metal-free 5,10,15,20-tetraferrocenyl porphyrin was used as the parent precursor for insertion of indium, zinc, cobalt(II), cobalt(III), and palladium ions.

Due to non-planar structure of tetraferrocenyl porphyrin[14l], and also its lower stability, introduction of different metals in the porphyrin cavity required specially developed procedure, because standard techniques such as refluxing of metal salt in DMF with porphyrin could not be applied. As it is shown in Schemes 2 – 7, several different procedures were applied in order to synthesize $[Co^{III}TFcP]^+$, $Co^{II}TFcP$, PdTFcP, ClInTFcP, FcInTFcP, and ZnTFcP. One of the approaches was to deprotonate metal – free porphyrin using non-nucleophilic base, and then introduce a metal to the porphyrin cavity. This procedure was used for obtaining ClInTFcP and $Co^{II}TFcP$. Another way to synthesize metal-containing porphyrins required to find appropriate solvent and reaction condition. And for synthesis of FcInTFcP reaction between ferrocene-lithium salt and ClInTFcP was used. Using this approach, axially coordinated to indium chlorine was substituted by ferrocene.

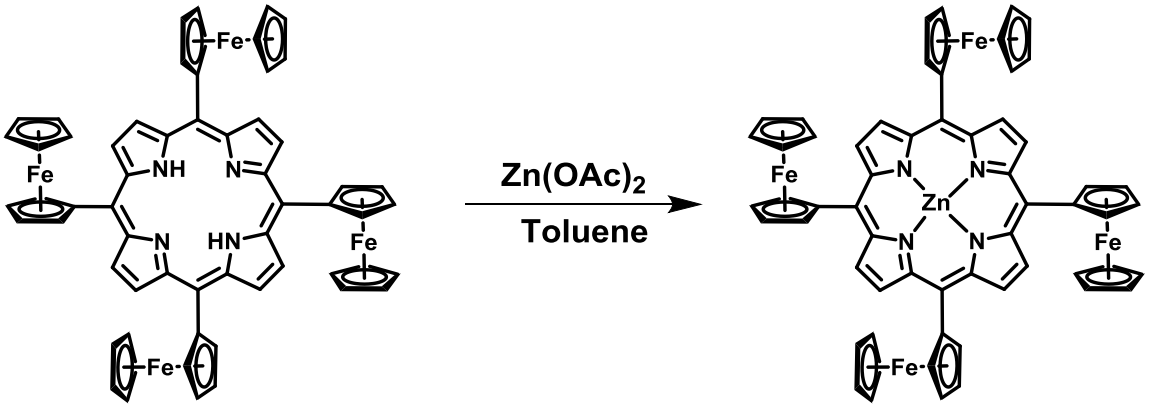


***Scheme 2***. *Preparation of ZnTFcP*

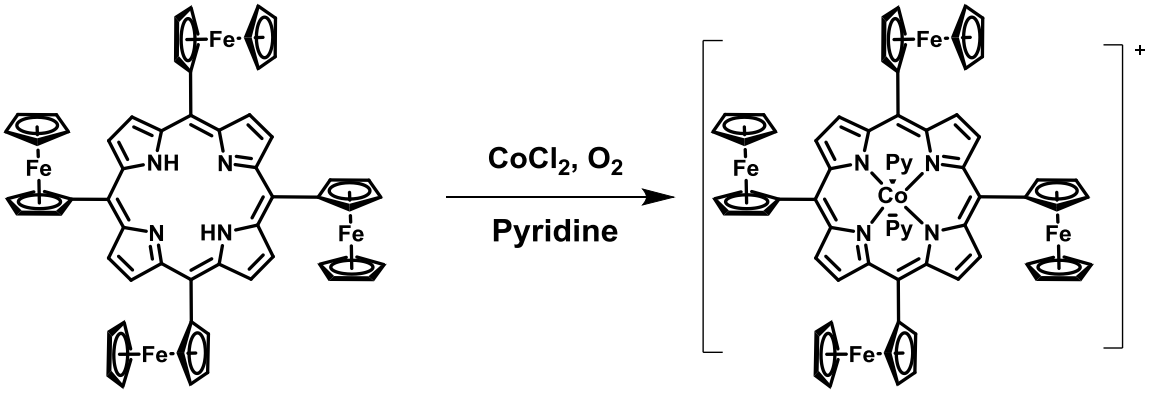


***Scheme 3***. *Preparation of* $[Co^{III}TFcP]^{+}$

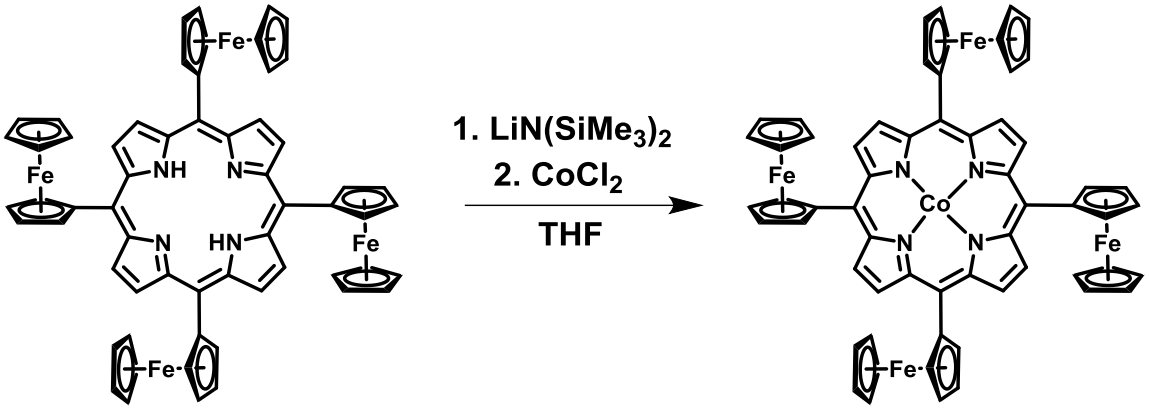


***Scheme 4***. *Preparation of $Co^{II}$TFcP*

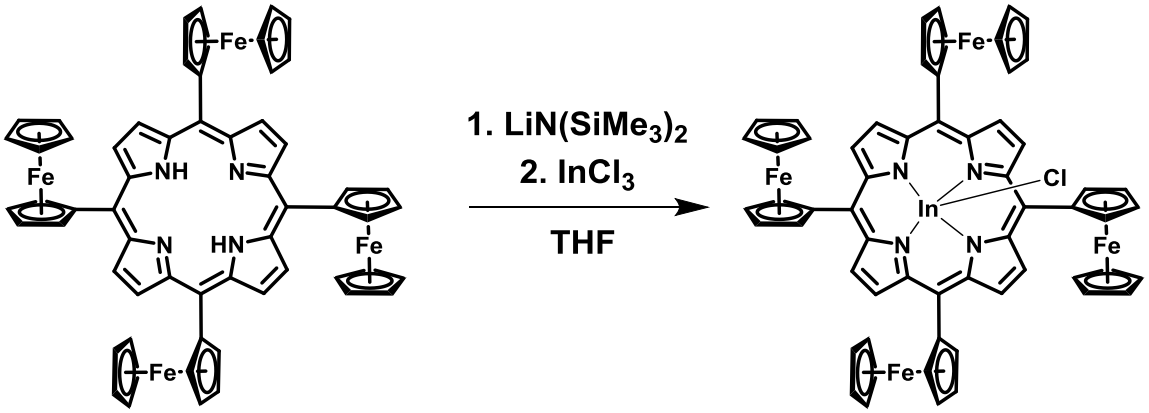


***Scheme 5***. *Preparation of ClInTFcP*

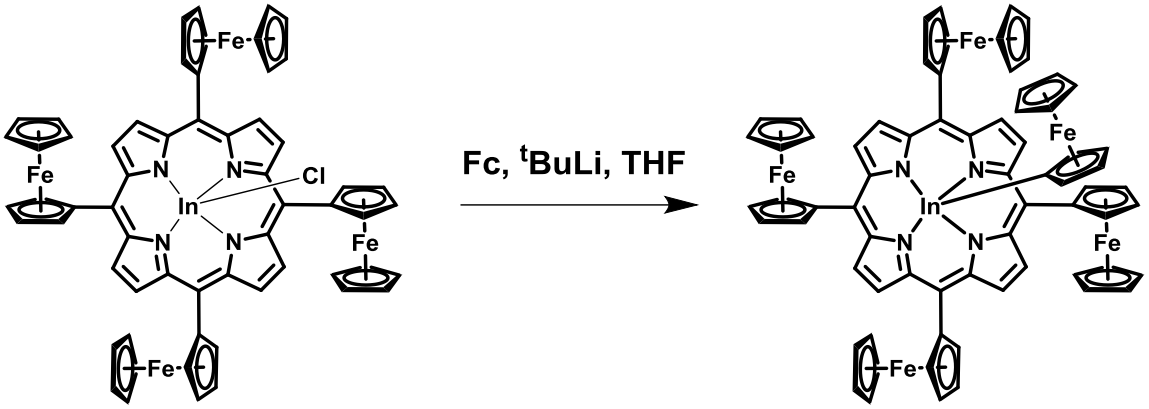


***Scheme 6***. *Preparation of FcInTFcP*

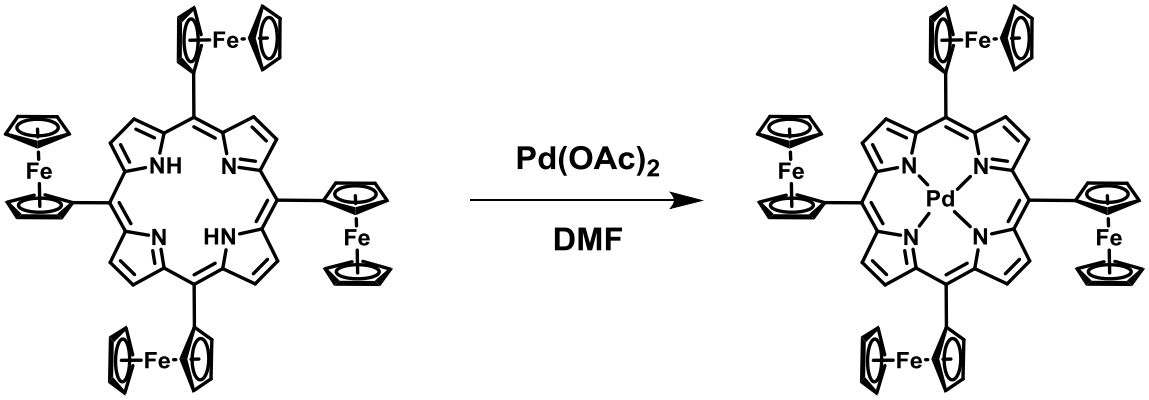


***Scheme 7***. *Preparation of PdTFcP*

All of the further purifications of tetraferrocenyl porphyrin analogues were conducted on Alumina columns. Due to low stability of products, silica gel could not be used in this case.

In Figures 3 – 8 UV–Vis–NIR spectra are shown. Metal-free meso-substituted tetraferrocenyl porphyrin $H_2$TFcP, exhibits an intense Soret band at 433 nm and two Q-

bands 664 nm and 728 nm. All metal–containing complexes exhibit Soret band at around 430 nm and only one Q-band at around 720 nm.

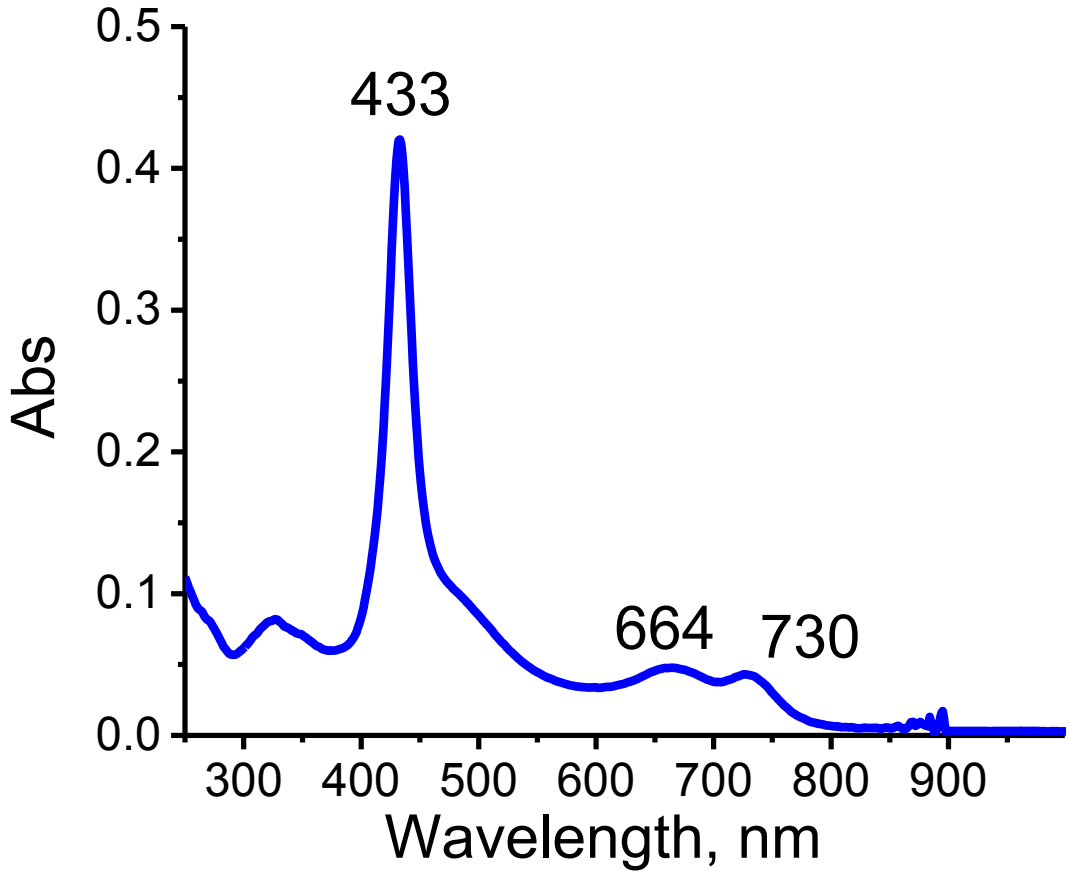


***Figure 3***. *UV – Vis spectrum of $H_2TFcP$*

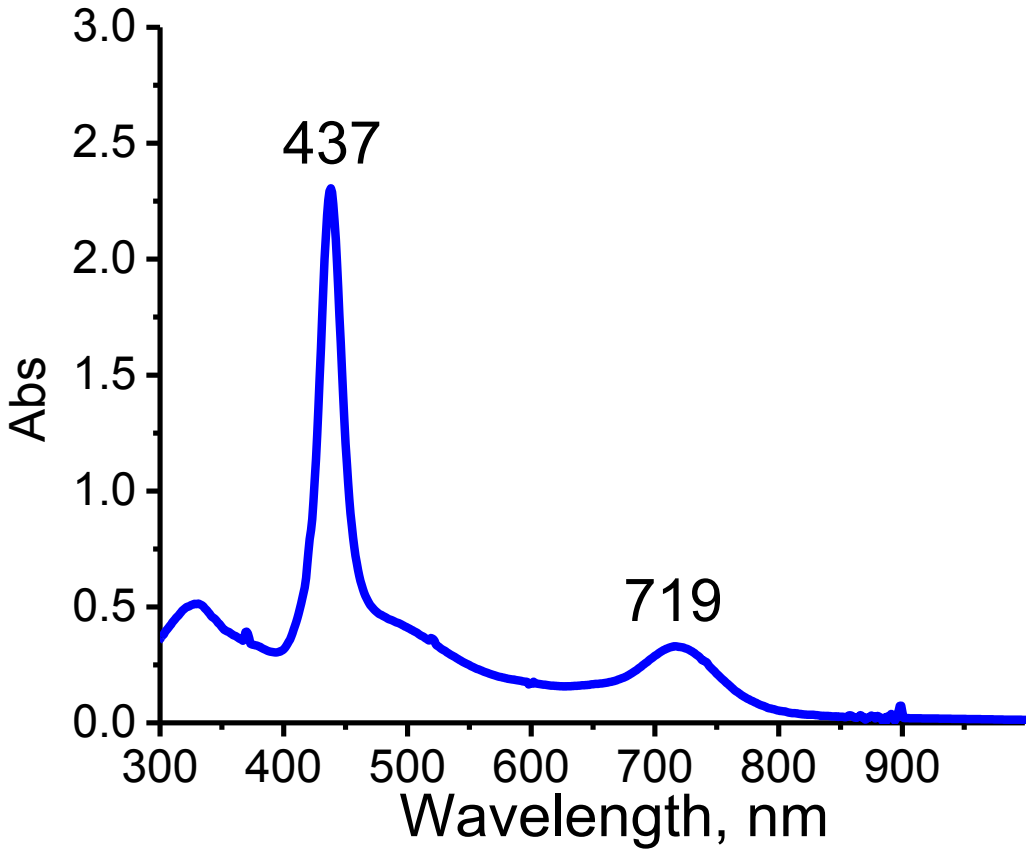


***Figure 4***. *UV – Vis spectrum of ClInTFcP*

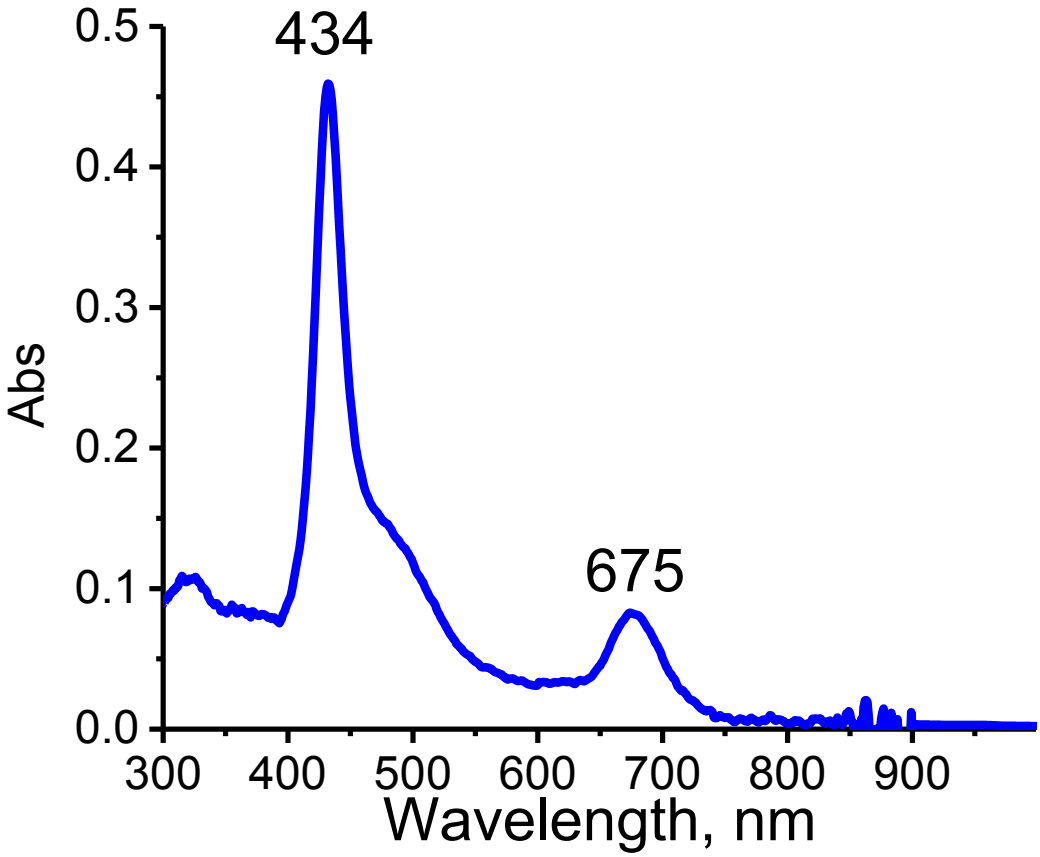


***Figure 5***. *UV – Vis spectrum of ZnTFcP*

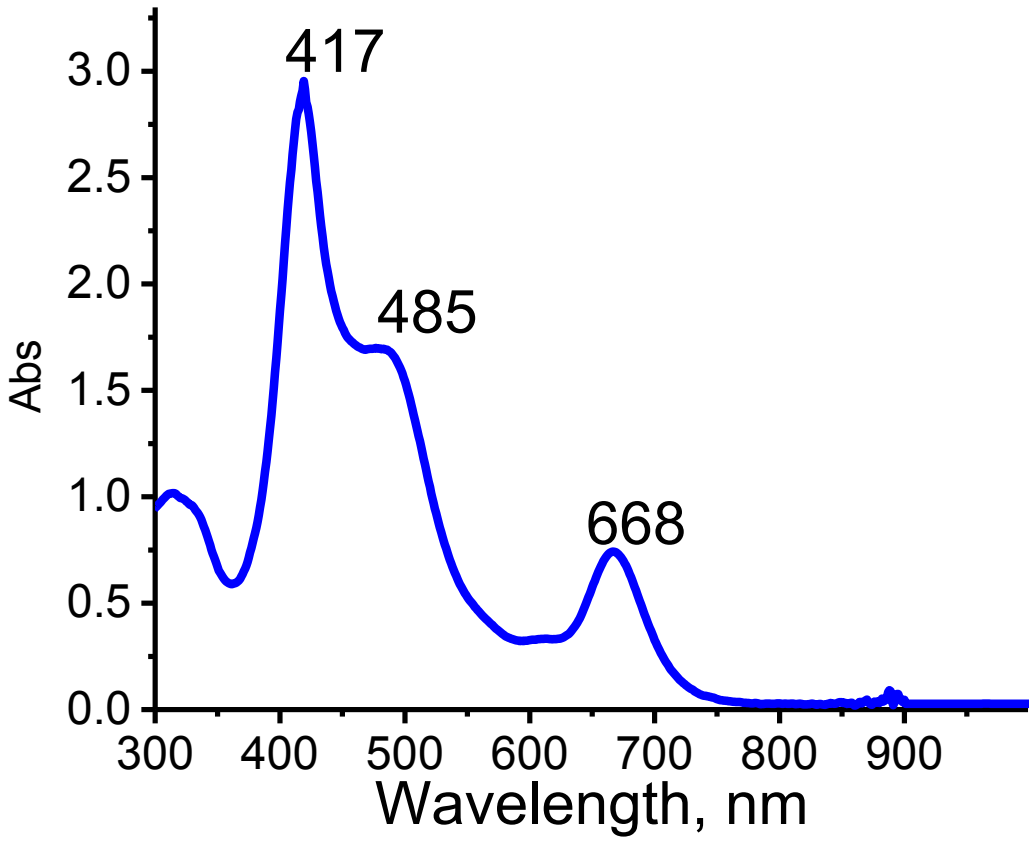


***Figure 6***. *UV – Vis spectrum of $Co^{II}TFcP$*

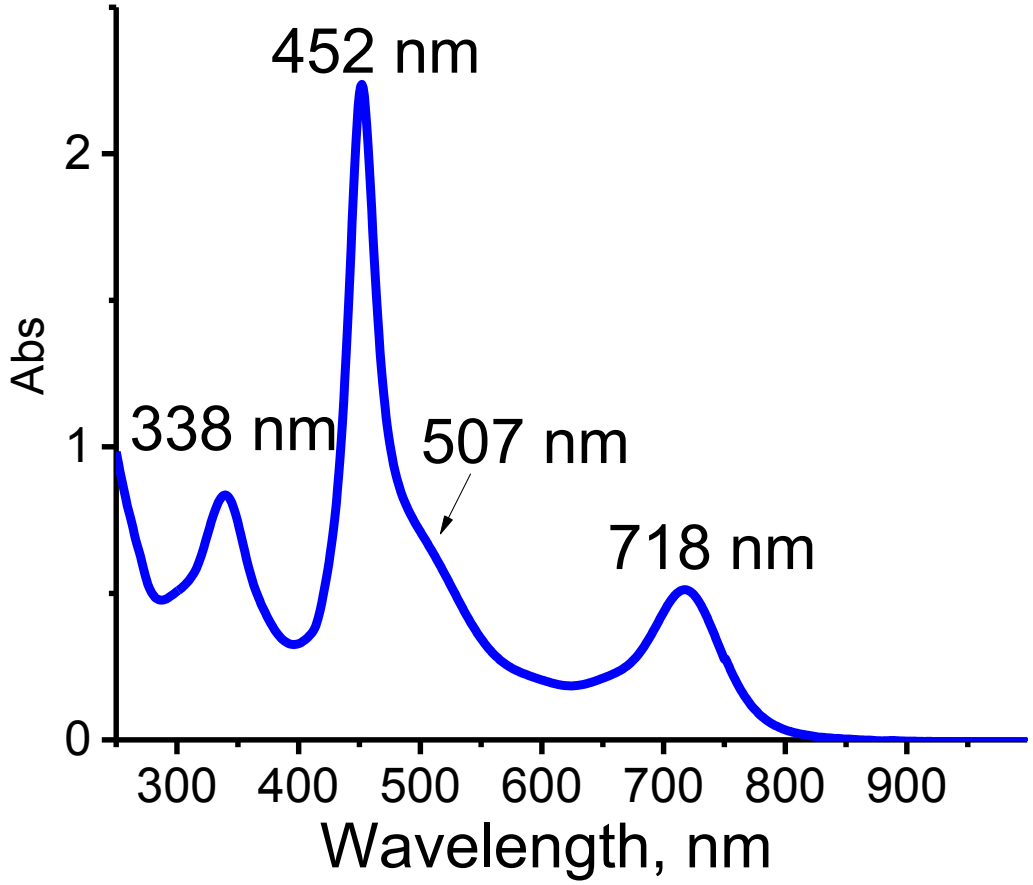


***Figure** 7. UV – Vis spectrum of* $[Co^{III}TFcP]^{+}$

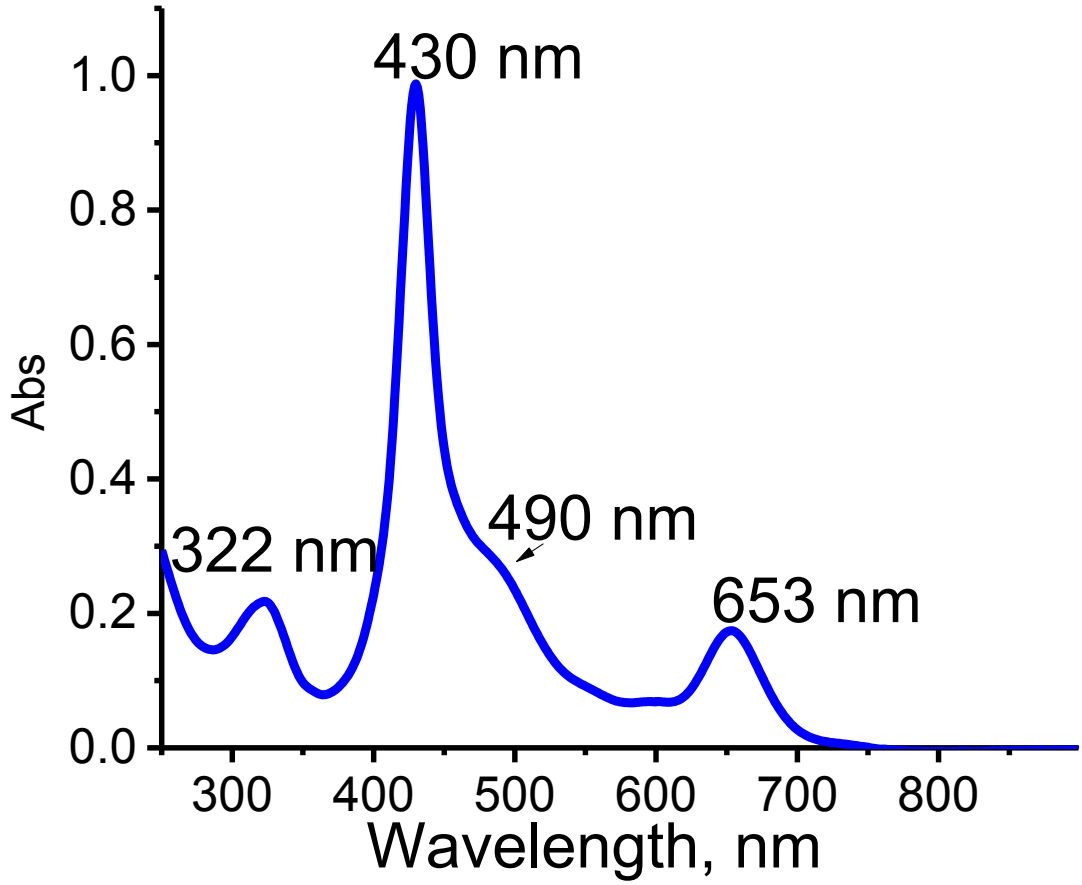


***Figure 8***. *UV – Vis spectrum of PdTFcP*

**NMR Spectra:**

The $H_2$TFcP reactant itself exhibits five different proton signals (Figure 9). The porphyrin ring, composed of four pyrroles, shows two of those signals, one of them being from its β-pyrrolic position. This proton lies far downfield. The second one originating

from the porphyrin core is forn inner NH-pyrrolic protons, which are found in the upfield position with negative value of chemical shift due to π-system ring current[21]. The last three signals on the NMR spectrum come from the ferrocene fragments connected to mesa-positions of the porphyrin. This depicts the pattern of mono-substituted ferrocene which contributes alpha proton signal, a beta proton signal, and Cp-H signal to the spectrum.

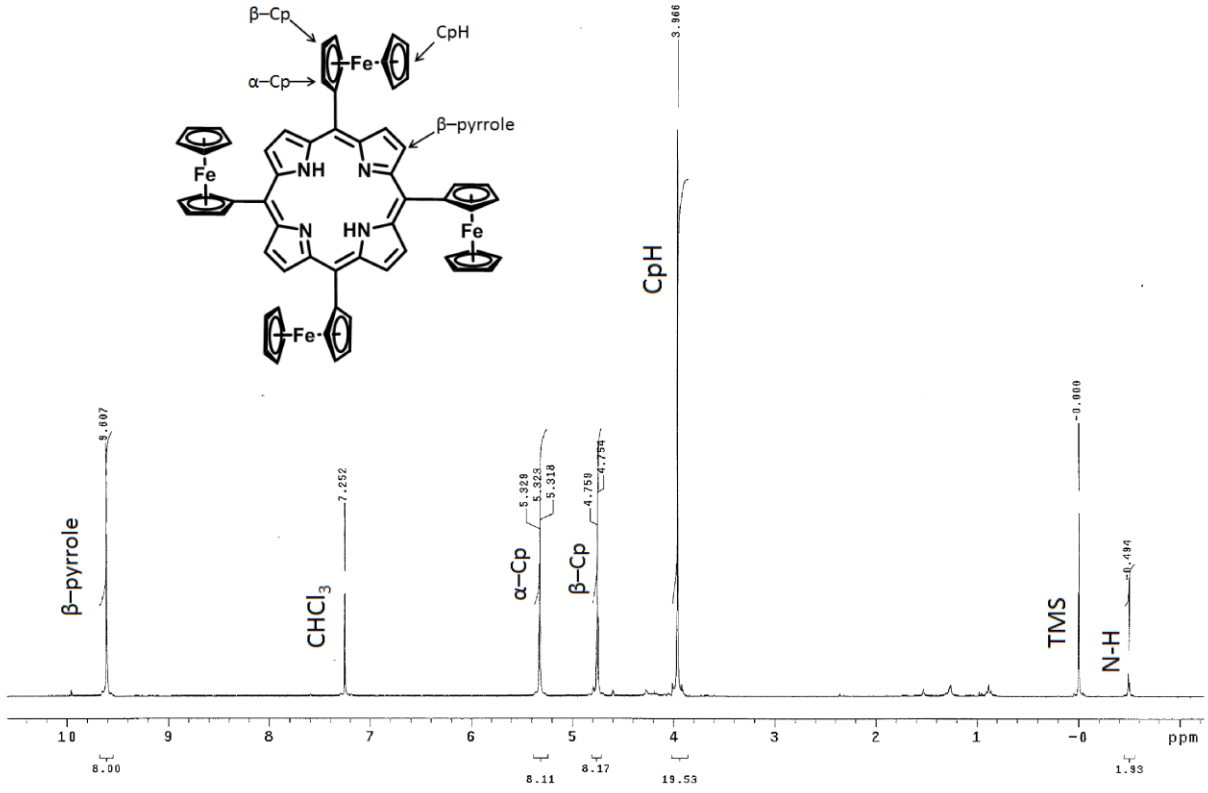


***Figure 9***. *$^1$H-NMR spectra of $H_2$TFcP in $CDCl_3$, 500MHz*

After introduction of the metal in the porphyrin cavity, one of the distinct changes on the NMR spectra is disappearance of the N – H signal at **-0.5 ppm** due to substitution of the hydrogens with metal cation (Figures 10 – 12).

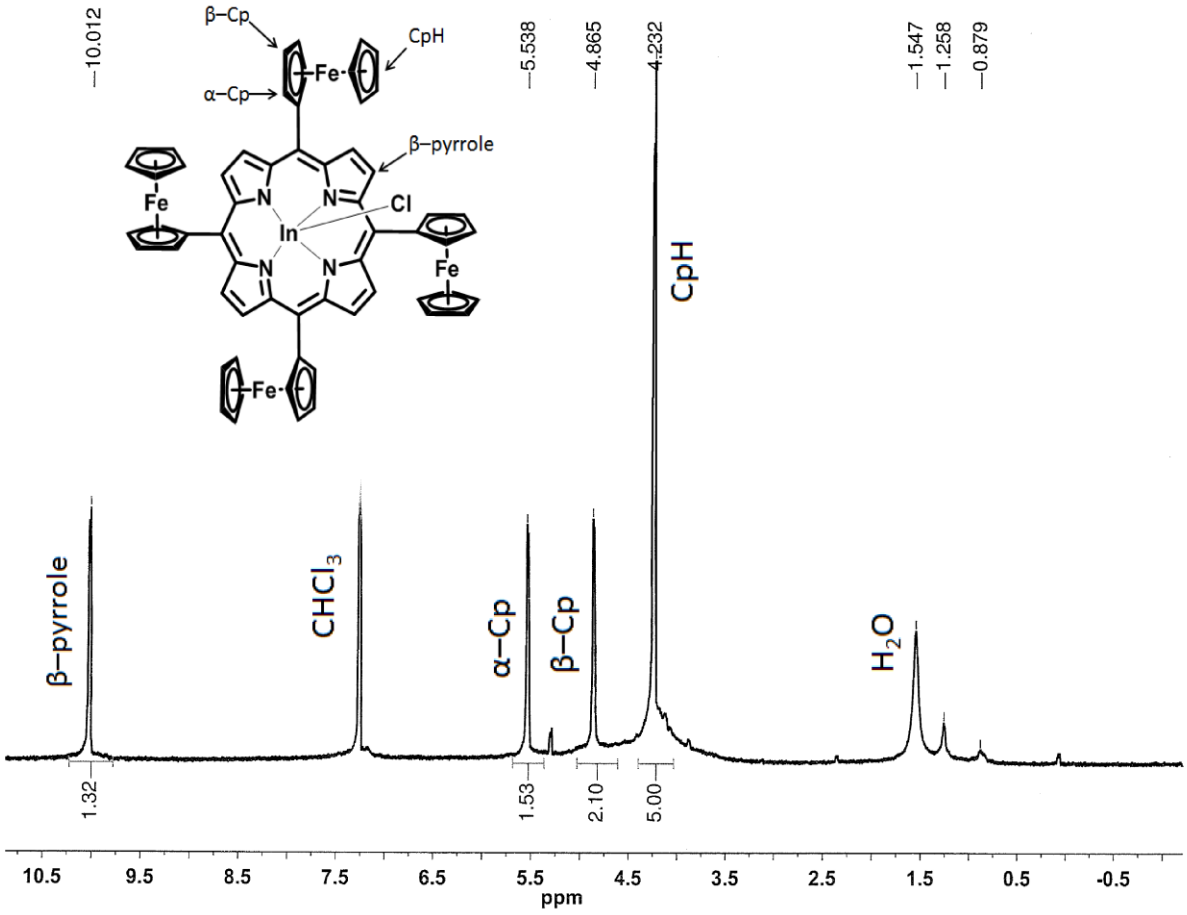


***Figure 10***. *$^{1}$H-NMR spectra of ClInTFcP in $CDCl_3$, 500MHz*

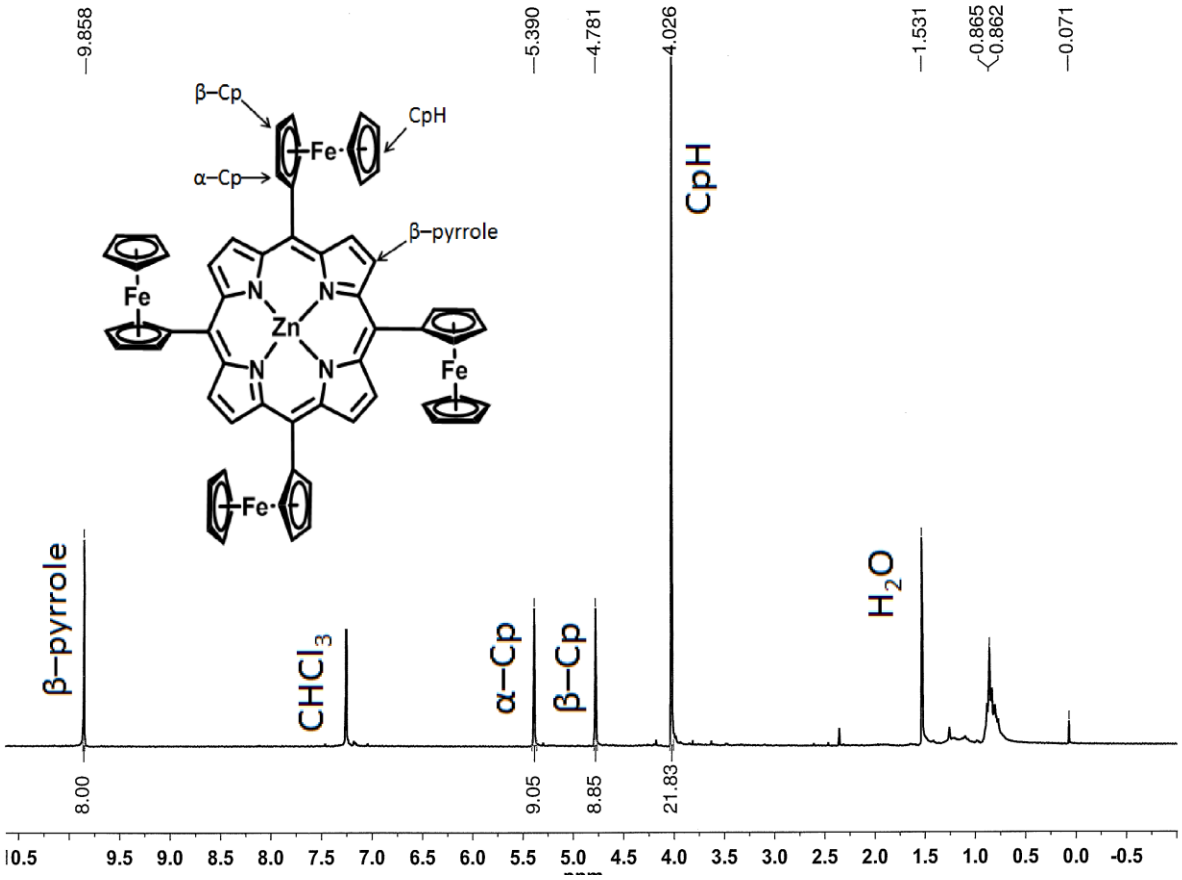


***Figure 11***. *$^{1}$H-NMR spectra of ZnTFcP in $CDCl_3$, 500MHz*

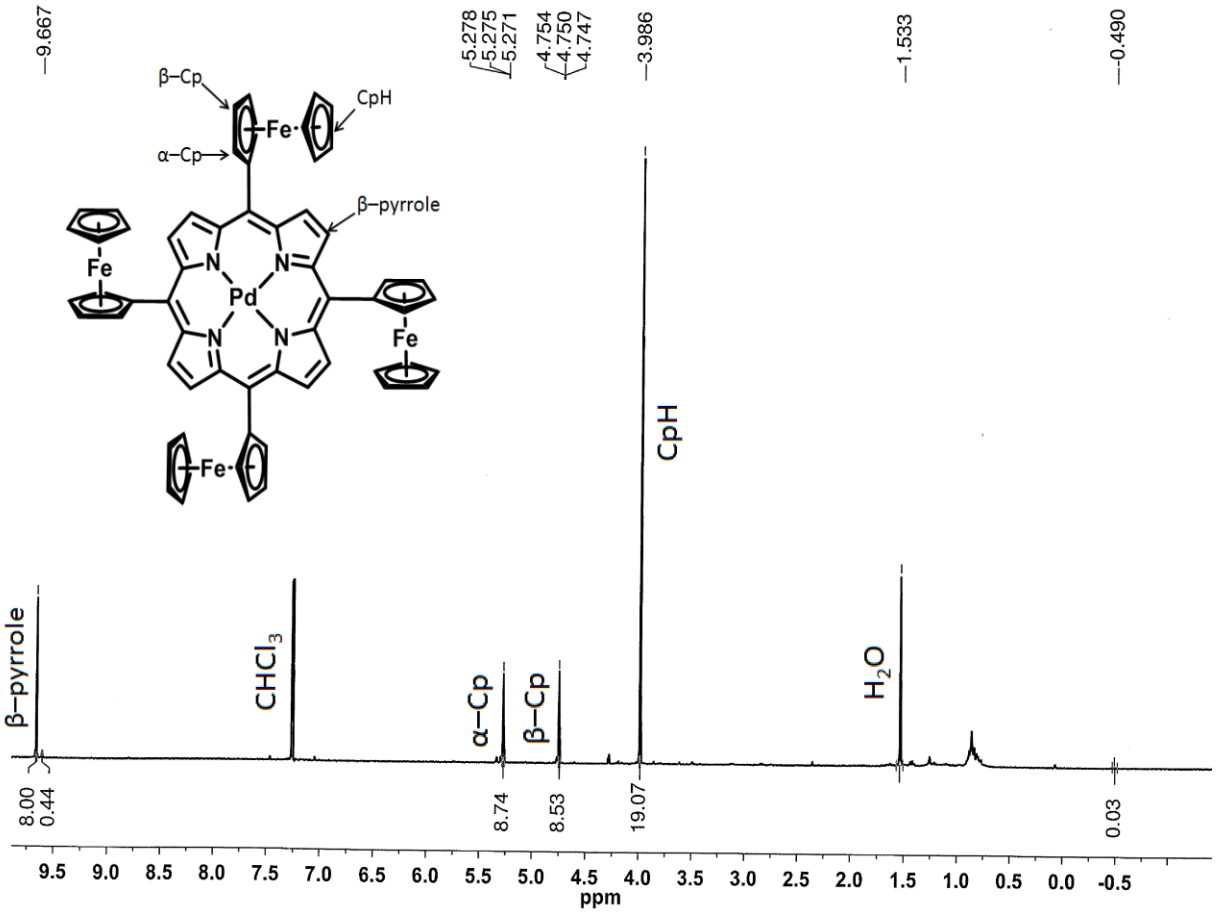


***Figure 12***. *$^{1}$H-NMR spectra of PdTFcP in $CDCl_3$, 500MHz*

## Electrochemistry

Previously cyclic voltammetry (CV), differential pulse voltammetry (DPV), and square wave voltammetry (SWV) were used to evaluate the redox capabilities of the substituted and metal-free 5,10,15,20-tetraferrocenyl porphyrins[14m,q]. It is well-known that polarity of the solvent and nature of the electrolyte could affect electron-transfer processes in poly(metallocenyl)-containing compounds, including ferrocene-based

oxidation waves in the $H_2$TFcP, ClInTFcP, FcInTFcP, ZnTFcP complexes[14m]. Thus, to minimize the interactions of the solvent the interactions of the solvent and electrolyte with the redox active complex, the non-coordinating electrolyte, tetrakis(perfluorophenyl)borate (TFAB), and low-polarity solvent DCM were used to assess their electrochemical behavior. In agreement with the previous studies on ferrocene-containing porphyrins, experimentally observed redox processes of MTFcP complexes (Figure 13) can be separated into three distinctive regions: (i) the four single-electron ferrocene-centered oxidations located between -0.1 and +0.35 V; (ii) porphyrin core/central metal single electron oxidation processes experimentally observed at potentials higher than +0.5 V; (iii) porphyrin core single electron reduction waves observed at potentials more negative than -1 V.

Although the oxidation behavior of poly(ferrocenyl)-containing porphyrins is currently well-understood, there is no information available on the spectroscopy and electronic structure of these compounds in their reduced forms. In order to gain insight into the influence of organometallic substituents on the electronic spectroscopy and electronic structure of $[MTFcP]^{\cdot-}$ systems (Figures 13), their reduction under spectroelectrochemical conditions was explored and new insights into their electronic structures using density functional theory (DFT) methods were gained.

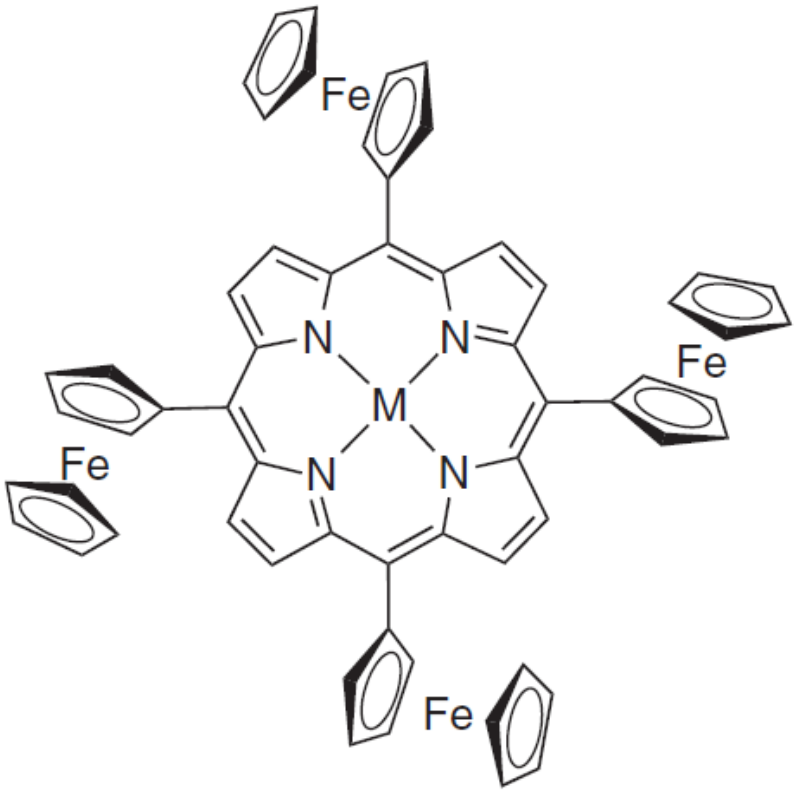


***Figure 13**: Tetraferrocenyl porphyrins, discussed in this chapter.*

Redox properties of the MTFcP complexes presented in Figure 13 were earlier investigated in DCM/TFAB (DCM = dichloromethane) and *o*-DCB/TBAP (*o*-DCB = *o*-dichlorobenzene and TBAP = tetra-n-butylammonium perchlorate) systems using cyclic voltammetry (CV) and differential pulse voltammetry (DPV) approaches. Previous electrochemical studies of the MTFcP systems in DCM/TFAB and *o*-DCB/TBAP

systems suggested that all reductions are porphyrin-centered and thus should not be significantly affected by the nature of the solvent and the electrolyte[14m]. Since the choice of the solvent and electrolyte is less critical for generation of $[MTFcP]^{\bullet-}$ anion-radicals, we used more traditional DCM/TBAP system for electrochemical (Figures 14 – 17) and spectroelectrochemical experiments (Figures 18 – 21).

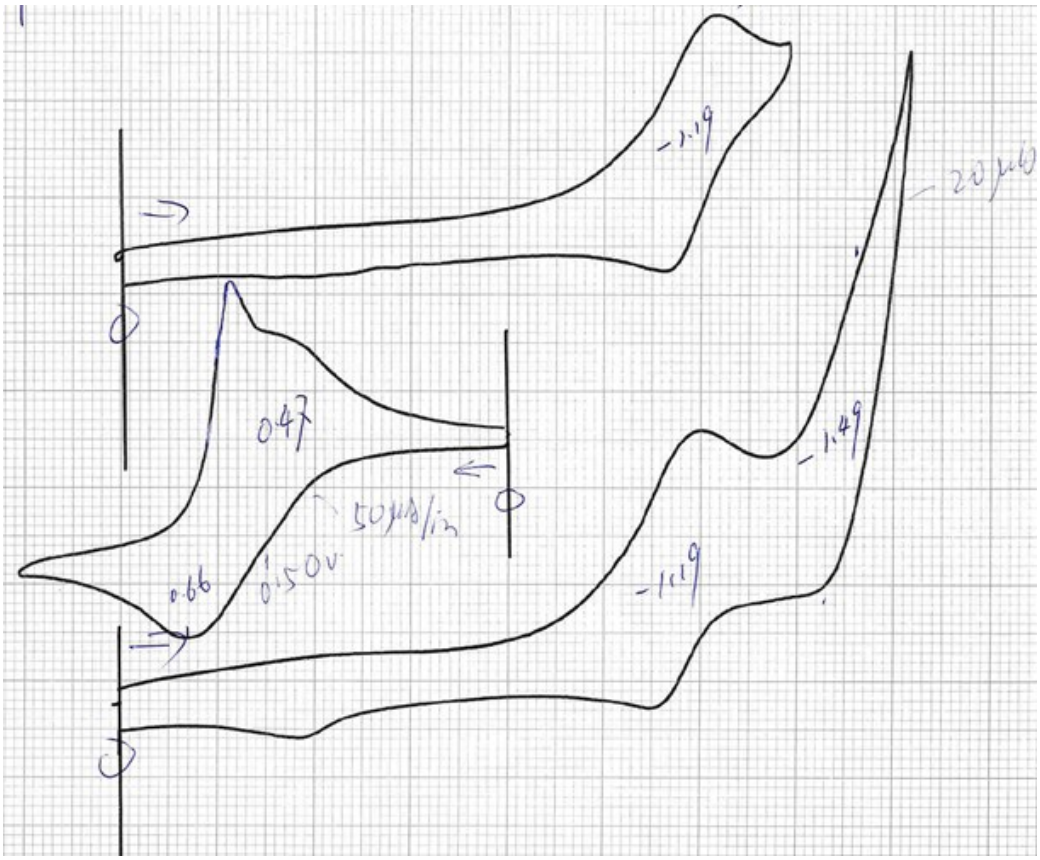


***Figure 14***. *Cyclic voltammetry plot for ClInTFcP. System – DCM/TBAP (0.2 M); scan rate – 10 mV/s; reference electrode – SCE*

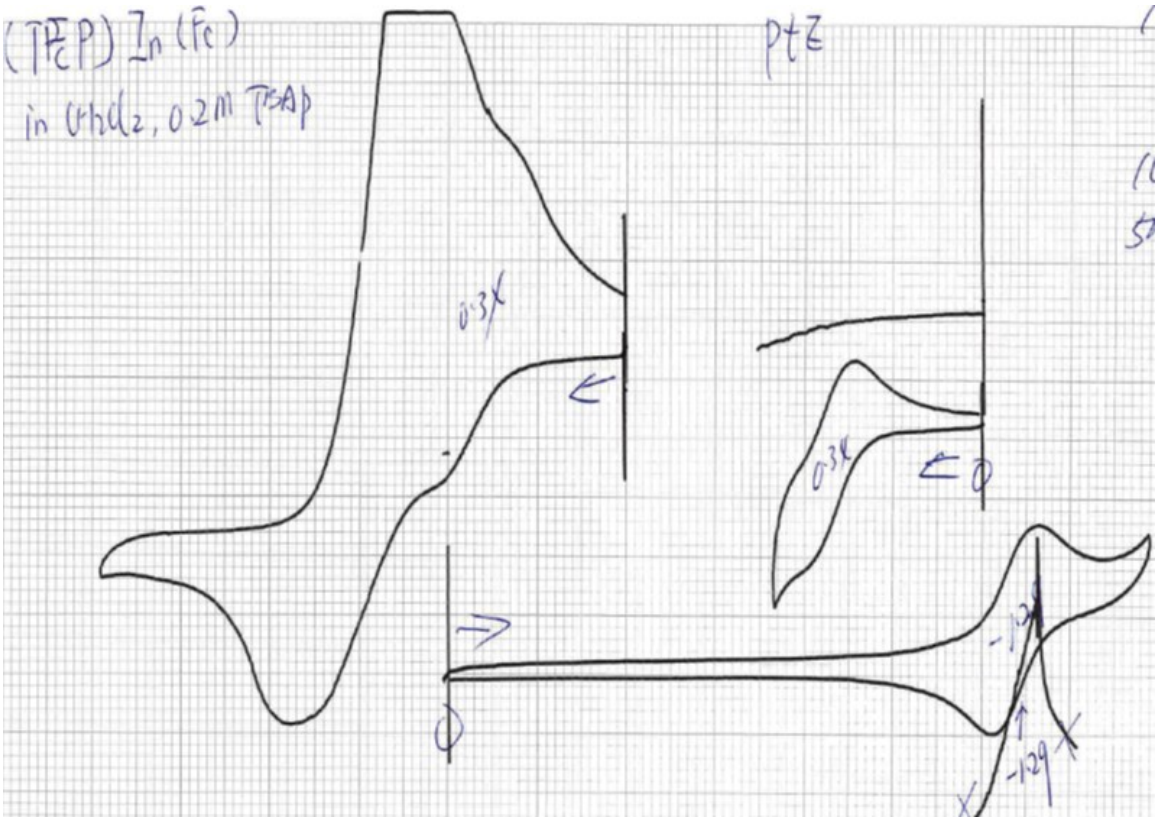


***Figure 15***. *Cyclic voltammetry plot for FcInTFcP. System – DCM/TBAP (0.2 M); scan rate – 10 mV/s; reference electrode – SCE*

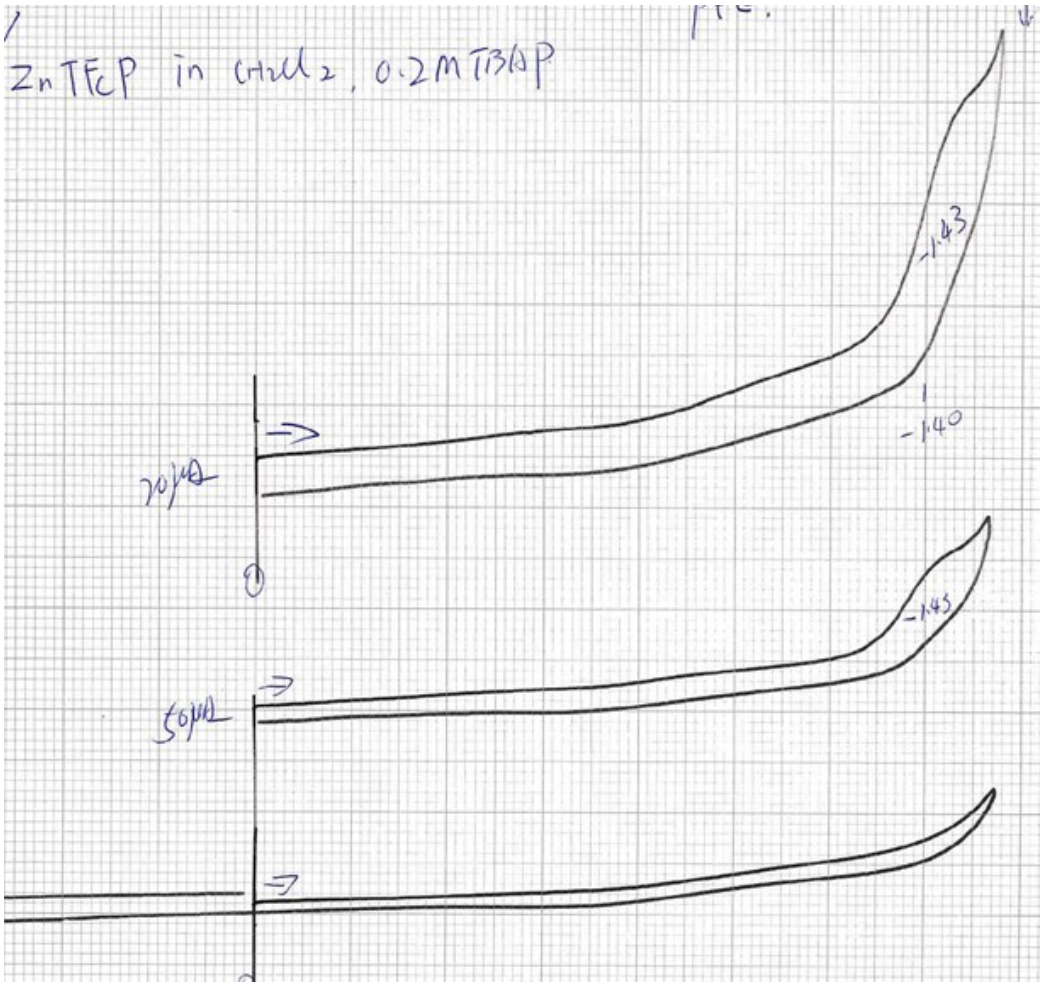


***Figure 16***. *Cyclic voltammetry plot for ZnTFcP. System – DCM/TBAP (0.2 M); scan rate – 10 mV/s; reference electrode – SCE*

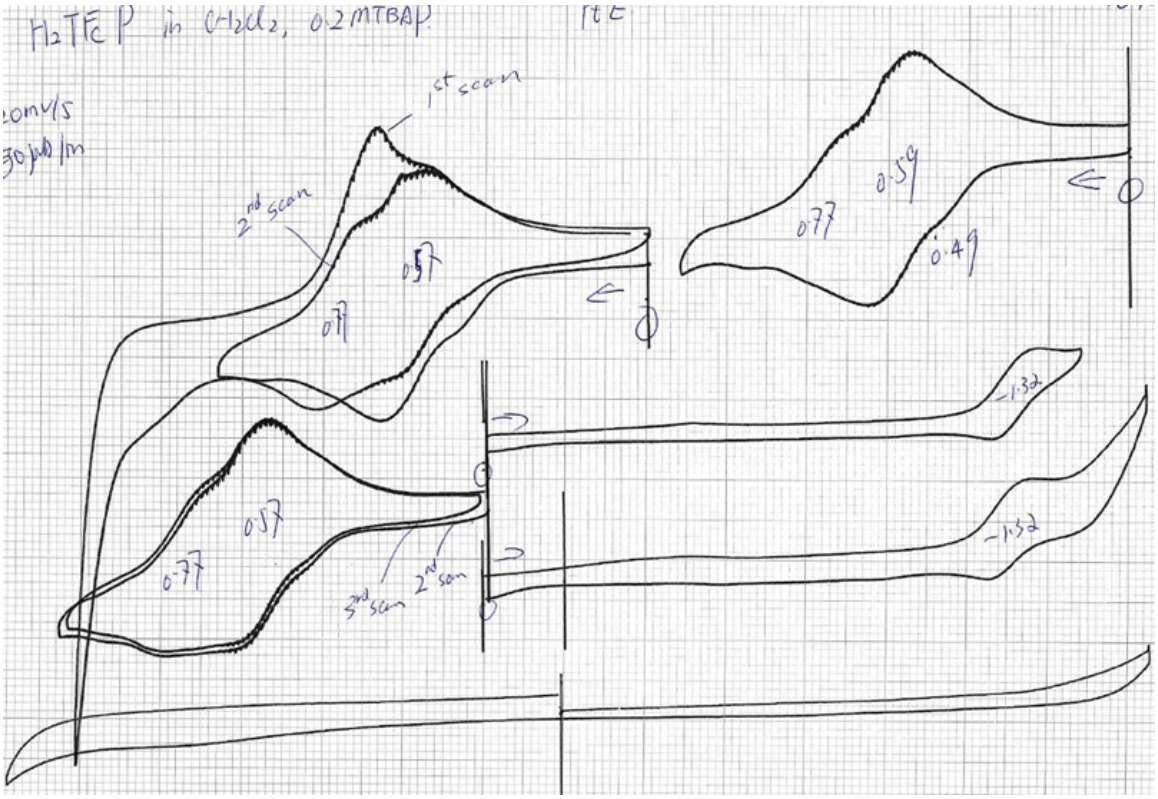


***Figure 17****. Cyclic voltammetry plot for $H_2$TFcP. System – DCM/TBAP (0.2 M); scan rate – 10 mV/s; reference electrode – SCE*

Indeed, in all three solvent/electrolyte systems, $H_2$TFcP and ClInTFcP show two reversible reduction processes, while ZnTFcP and FcInTFcP compounds undergo only a single reduction process within the solvent potential window (Table 1). In order to characterize the UV-vis spectroscopic signatures of $[MTFcP]^{\cdot-}$ anion-radicals, we monitored the spectral changes as a function of time during the first controlled potential reduction in a thin-layer cell (Figures 18 – 21).

***Table 1. Reduction potentials for MTFcP complexes determined in different solvent/electrolyte systems[7]. All potentials are in Volts and relative to $Fc/Fc^+$ couple***

| Compound | Solvent/Electrolyte | | | | | |
|---|---|---|---|---|---|---|
| | DCM/TFAB[7] | | DCM/TBAP[7] | | o-DCB/TBAP[7] | |
| | $R_1$ | $R_2$ | $R_1$ | $R_2$ | $R_1$ | $R_2$ |
| $H_2$TFcP | -1.78 | -2.06 | -1.80 | | -1.86 | -2.10 |
| InClTFcP | -1.68 | -2.02 | -1.67 | -1.97 | | |
| InFcTFcP | -1.80 | | -1.77 | | | |
| ZnTFcP | -2.03 | | -1.91 | | -2.04 | |

Spectroelectrochemistry has often been used to identify the spectrum of an *in situ* generated species during controlled potential electrolysis after determining the redox potentials for oxidation or reduction by cyclic voltammetry (CV) or differential pulse voltammetry (DPV) experiments. The generated UV-Vis spectra could then be compared to spectra obtained after chemical oxidation or reduction of the same compounds to aid in an assignment of the electron transfer site. Usually, the UV-vis spectra of one-electron reduced tetra(aryl)porphyrins exhibits a characteristic broad NIR band between 800 and 900 nm as well as a relatively narrow Soret-type band, which is shifted to lower or higher energy by 20–30 nm with respect to the Soret band of the initial neutral porphyrin[22,23]. This is also the case for the currently investigated compounds where close comparison between UV-vis spectra of $[MTFcP]^{-\cdot}$ and earlier characterized $[MTPP]^{-\cdot}$ (M = 2H, Zn, and InCl) anion-radicals provides additional insights into the degree of *meso*-substituent–

porphyrin core interactions.

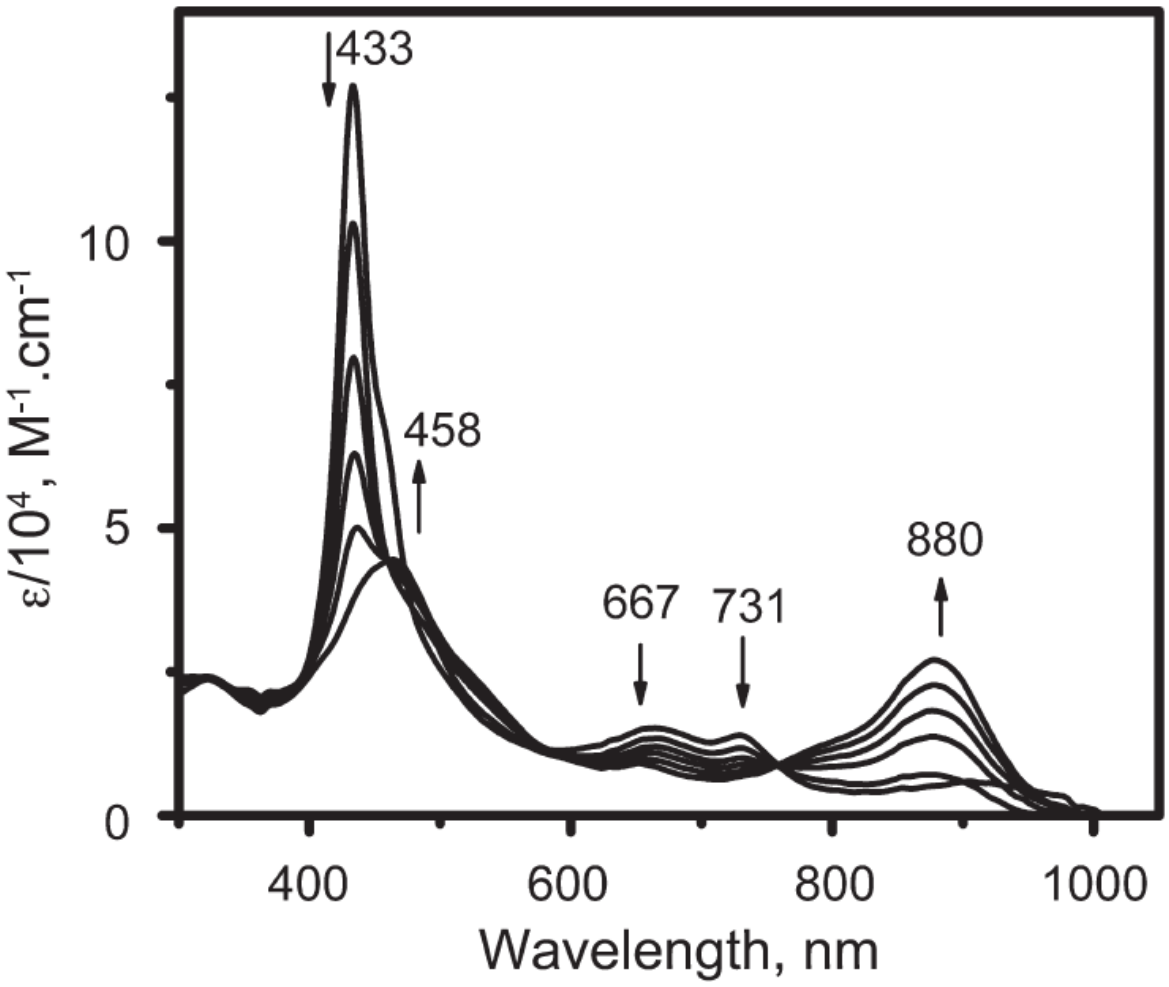


***Figure 18**: Transformation of $H_2TFcP$ into $[H_2TFcP]^{\cdot-}$ under spectroelectrochemical conditions in a DCM/TBAP system. The applied potential was -1.55 V vs. SCE*

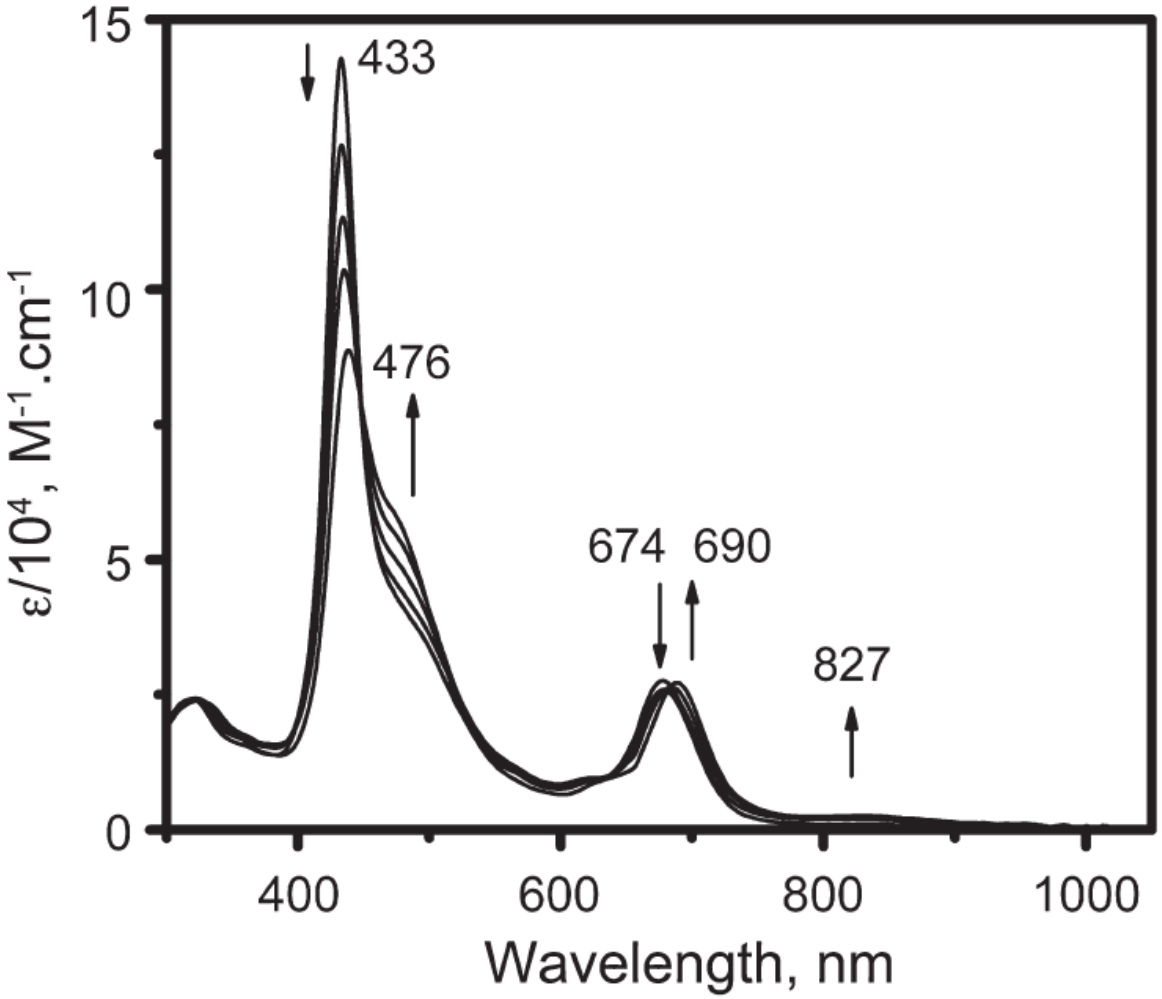


***Figure 19**: Transformation of ZnTFcP into [ZnTFcP]˙⁻ under spectroelectrochemical conditions in a DCM/TBAP system. The applied potential was -1.60 V vs. SCE*

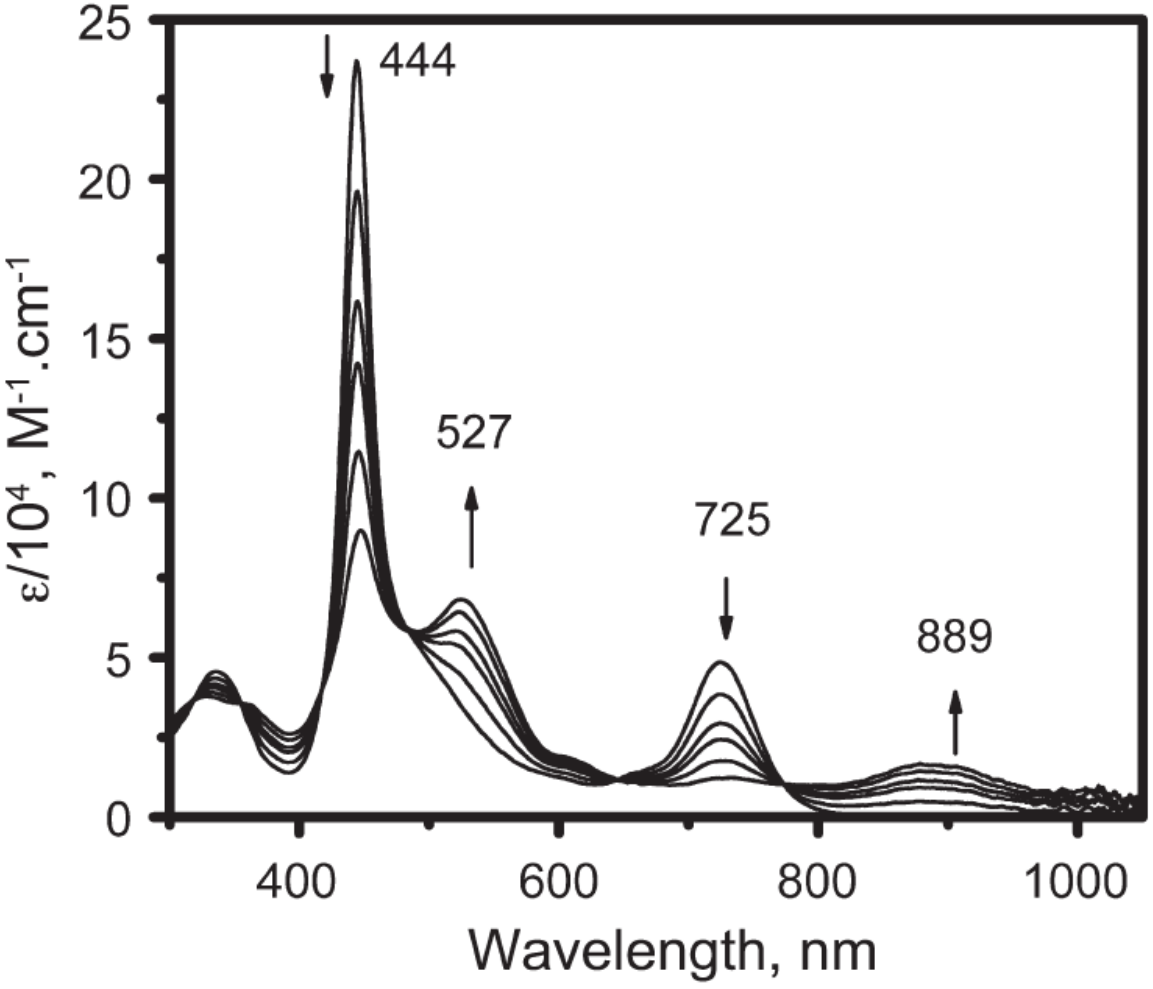


***Figure 20**: Transformation of FcInTFcP into [FcInTFcP]˙¯ under spectroelectrochemical conditions in a DCM/TBAP system. The applied potential was -1.40 V vs. SCE*

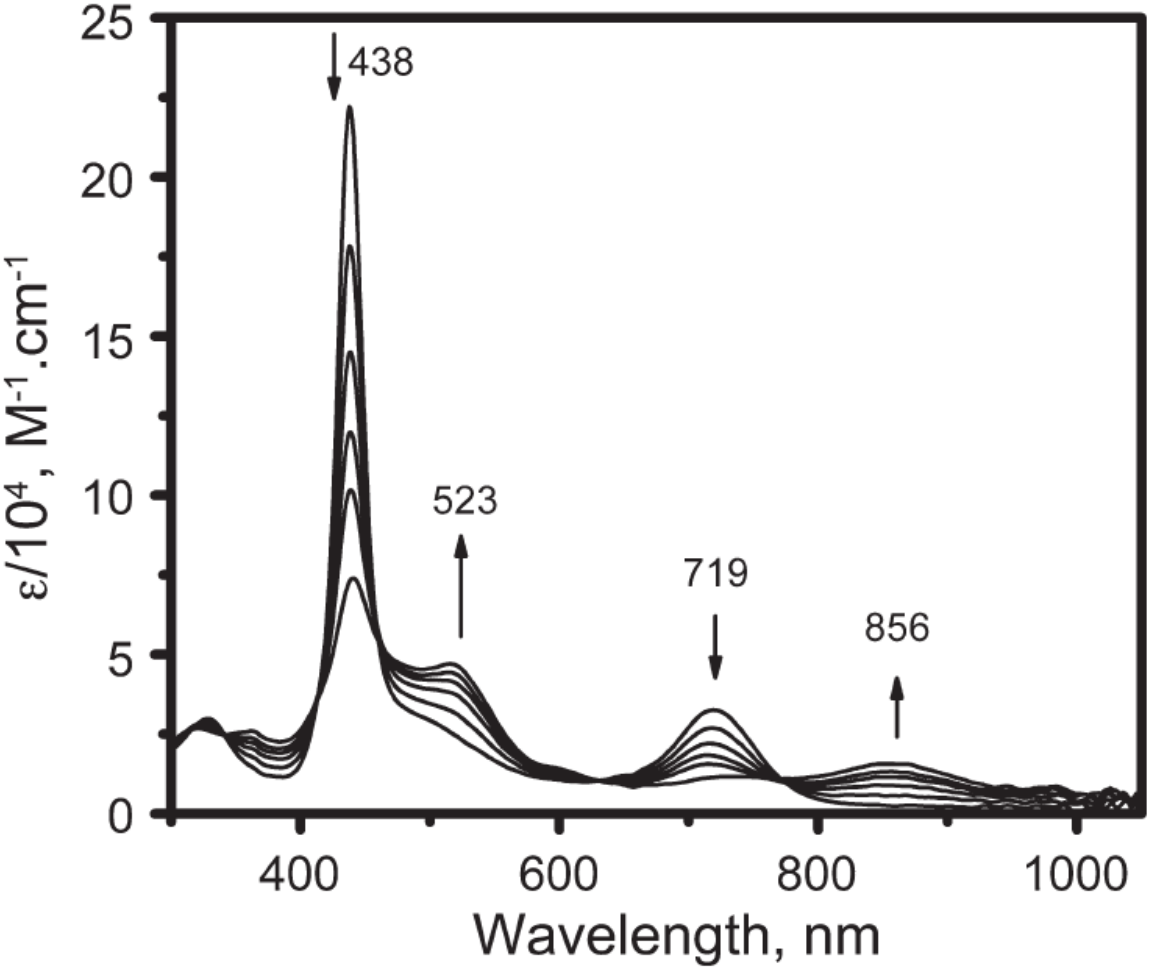


***Figure 21:*** *Transformation of ClInTFcP into [ClInTFcP]˙¯ under spectroelectrochemical conditions in a DCM/TBAP system. The applied potential was -1.35 V vs. SCE*

During electrochemical reduction of the $H_2$TFcP complex at -1.55 V *vs.* SCE, the Soret band at 433 nm decreases in intensity, became significantly broader, and shifts to 458 nm. At the same time, two characteristic Q-bands located at 667 and 731 nm disappear, while a new broad band at 880 nm appears in the NIR region (Figure 18). Wilson and co-workers investigated the reduction of $H_2$TPP to the $[H_2TPP]^{\cdot-}$ anion-

radical in DMF by spectroelectrochemical and EPR methods[23a]. The $[H_2TPP]^{-\cdot}$ anion-radical had a red-shifted Soret band from 418 to 448 nm, in addition to a set of bands in the visible region at 625, 683, 765 and 873 nm. In the current study, an 880 nm band observed during the one-electron reduction of $H_2TFcP$ can be attributed to the formation of its corresponding anion-radical.

Spectroelectrochemical transformation of ZnTFcP into the $[ZnTFcP]^{-\cdot}$ anion-radical is presented in Figure 19. When the reduction was carried out at an applied potential of -1.60 V *vs.* SCE, the Soret band initially located at 433 nm decreased in intensity and a new broad band grew at 476 nm. At the same time, the intensity of the Q-band did not change significantly, but it red shifted from 674 to 690 nm. Finally, a low intensity band at 827 nm was also observed in the UV-vis spectrum of the final product. A red shift of the Soret and Q-bands in ZnTPP were observed by Wilson and co-workers during reduction in DMF and the resulting product was assigned to the $[ZnTPP]^{-\cdot}$ anion-radical[23b].

Changes in the UV-vis spectra of ClInTFcP and FcInTFcP during reduction of the corresponding neutral compounds at -1.67 and -1.77 V *vs.* SCE, respectively, are almost identical to each other and are presented in Figures 20 and 21. The spectrum of neutral ClInTFcP and FcInTFcP consists of an intense Soret band centered at 438 or 444 nm and a broad Q-band centered at 719 or 725 nm, respectively. The difference in $\lambda_{max}$ between the two porphyrins reflects the electron-donating properties of s-bonded ferrocene ligand in FcInTFcP. During reduction both the Soret and Q-bands decrease in intensity and the new bands centered at 523 and 856 nm ($[ClInTFcP]^{-\cdot}$) or 527 and 889 nm ($[FcInTFcP]^{-\cdot}$)

appear. Again, such behavior is consistent with what has earlier been reported by Kadish and co-workers during reduction of ClInTPP under similar experimental conditions[23c]. Kadish and co-workers also reported that the initial Soret band located at 428 nm for ClInTPP decreased in intensity and new bands characteristic of the $[ClInTPP]^{-\bullet}$ anion-radical appeared at 452, 733, and 874 nm during the controlled potential reduction. Taking into account the fact that the Soret and Q-bands of ClInTFcP and FcInTFcP are both red-shifted as compared to the ClInTPP analogue, it is easy to confirm the formation of $[ClInTFcP]^{-\bullet}$ and $[FcInTFcP]^{-\bullet}$ anion-radicals during one-electron reduction of the parent molecules.

One of the interesting observations that was found during spectroelectrochemical experiments, was that the anion-radical band intensity at 827 nm for $[ZnTFcP]^{-\bullet}$ Complex is significantly lower compared to the same band intensity observed in $[H_2TFcP]^{-\bullet}$, $[ClInTFcP]^{-\bullet}$, and $[FcInTFcP]^{-\bullet}$ complexes. To eliminate the possibility of any side-reactions during reduction of ZnTFcP complex, several reduction-oxidation cycles were repeated and was found no sign of complex degradation or demetallation. Moreover, spectroelectrochemical experiments conducted on two independent samples of ZnTFcP resulted in identical spectroscopic signatures of $[ZnTFcP]^{-\bullet}$ radical-anions. In order to get further insight into the spectroscopic differences of $[MTFcP]^{-\bullet}$ complexes, several other transition-metal tetraferrocenyl porphyrins needs to be investigated.

## Chemical Reduction:

In order to elucidate additional spectroscopic features of the reduced porphyrins (*i.e.* MCD or EPR) chemical reduction was carried out on the MTFcP complexes using a variety of reducing agents. In the Figures 22 – 25 are shown reductions of MTFcP using Sodium amalgam alloy. No additional bands are formed and slow degradation of the initial MTFcP is proceeding therefore making it impossible to reduce the porphyrin with Na/Hg alloy.

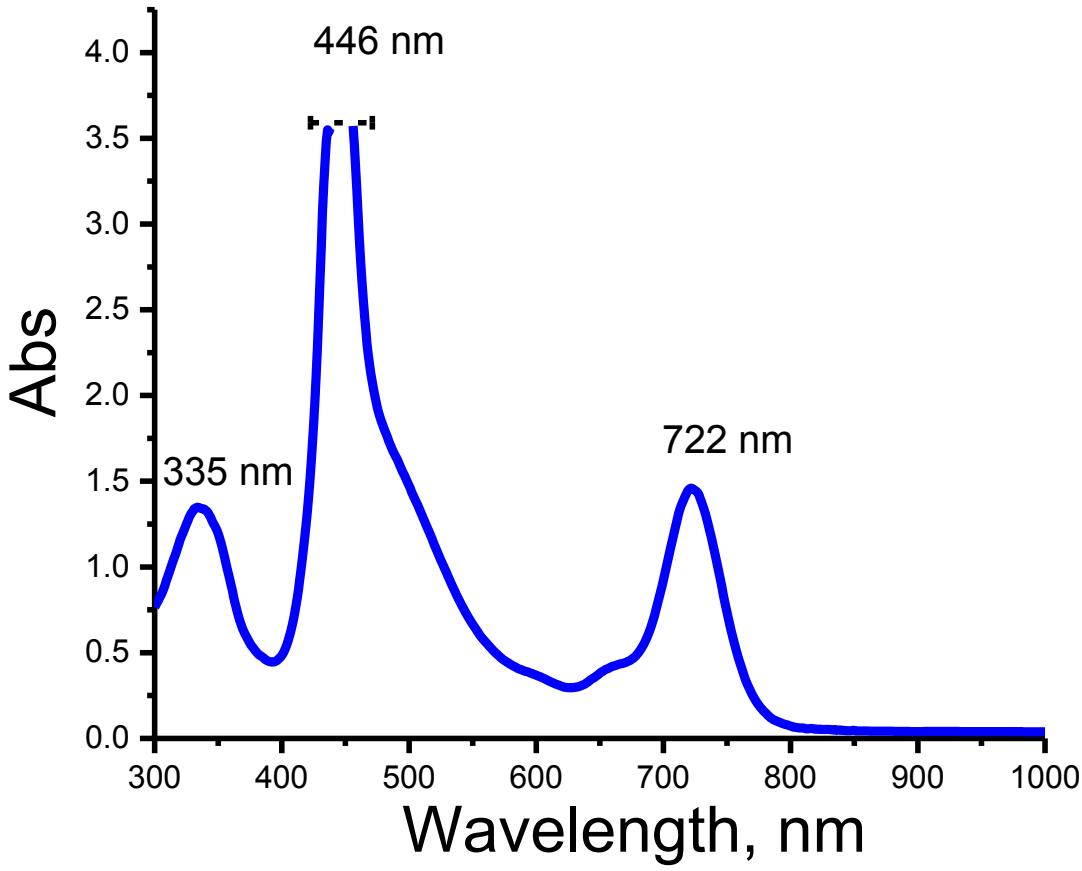


***Figure 22.*** *Chemical reduction of $H_2$TFcP using Na/Hg alloy in DCM*

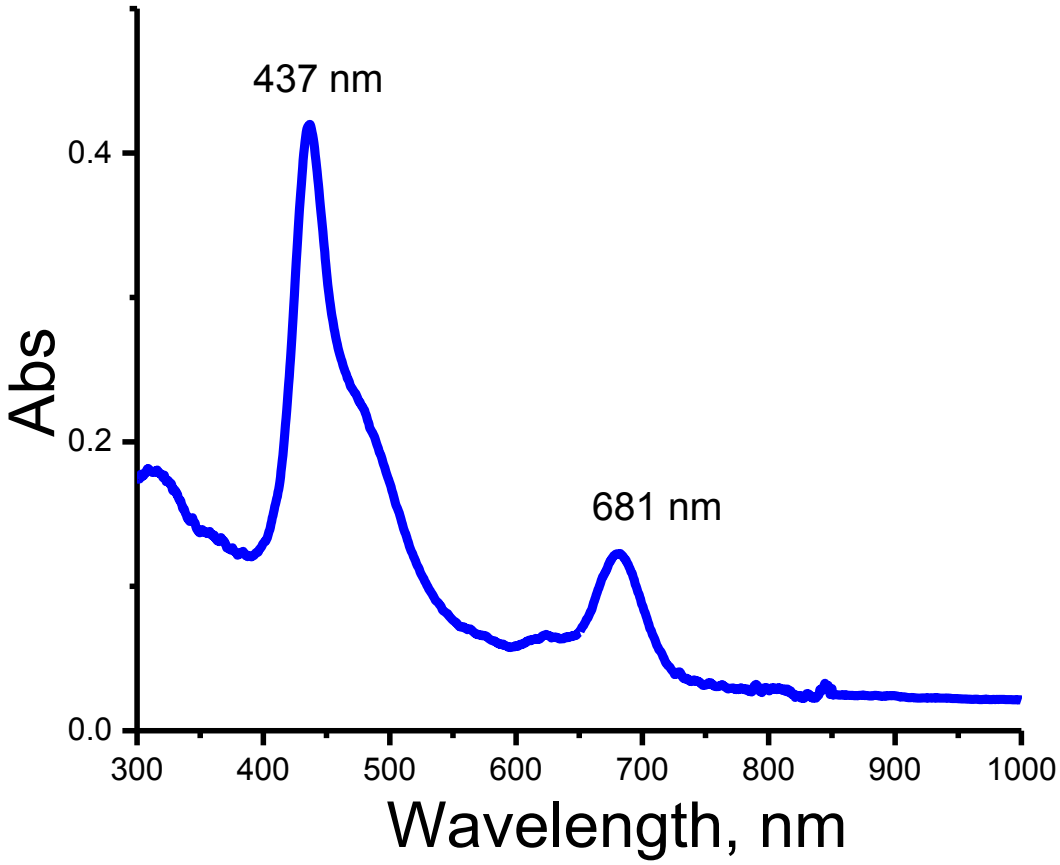


***Figure 23.*** *Chemical reduction of ZnTFcP using Na/Hg alloy in DCM*

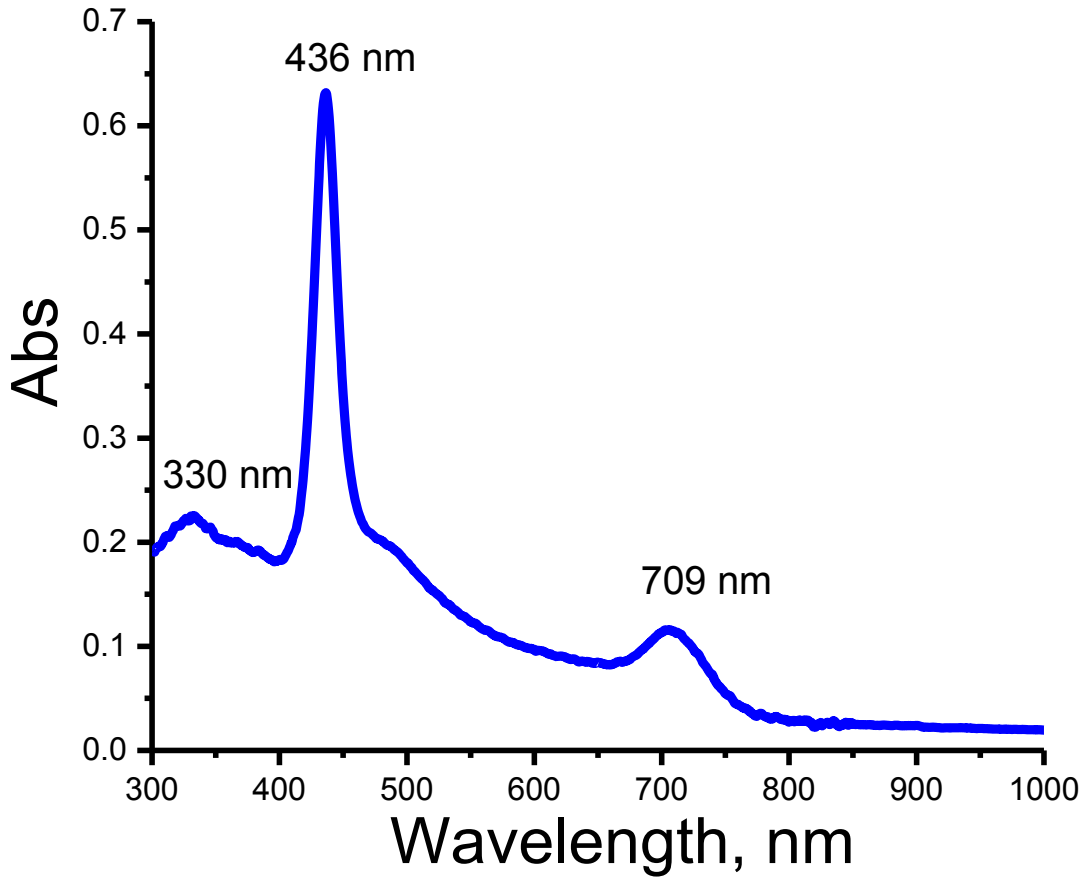


***Figure 24.*** *Chemical reduction of ClInTFcP using Na/Hg alloy in DCM*

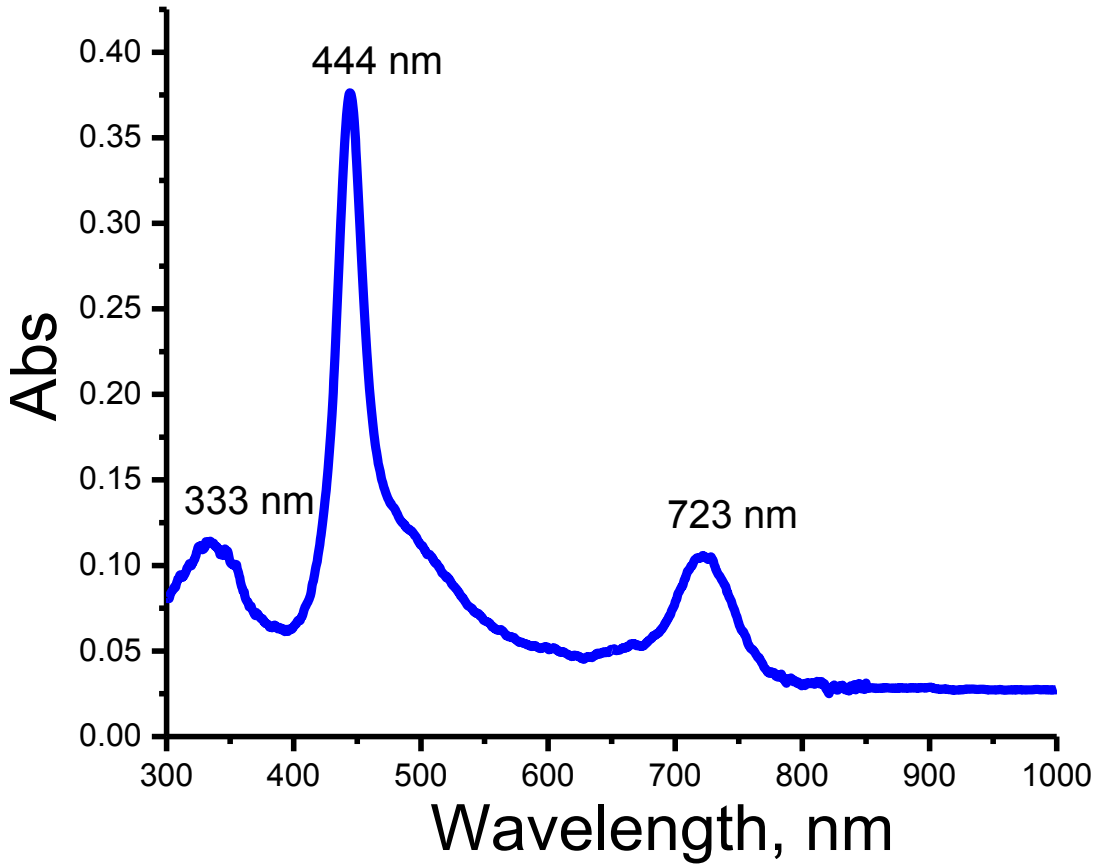


***Figure 25.*** *Chemical reduction of FcInTFcP using Na/Hg alloy in DCM*

No dramatic changes were observed during reduction with Na/K alloy. In the Figures 26 – 27 are shown spectra of the complexes before and after reduction. No significant changes occur during this process. Some degradation of the porphyrin is observed.

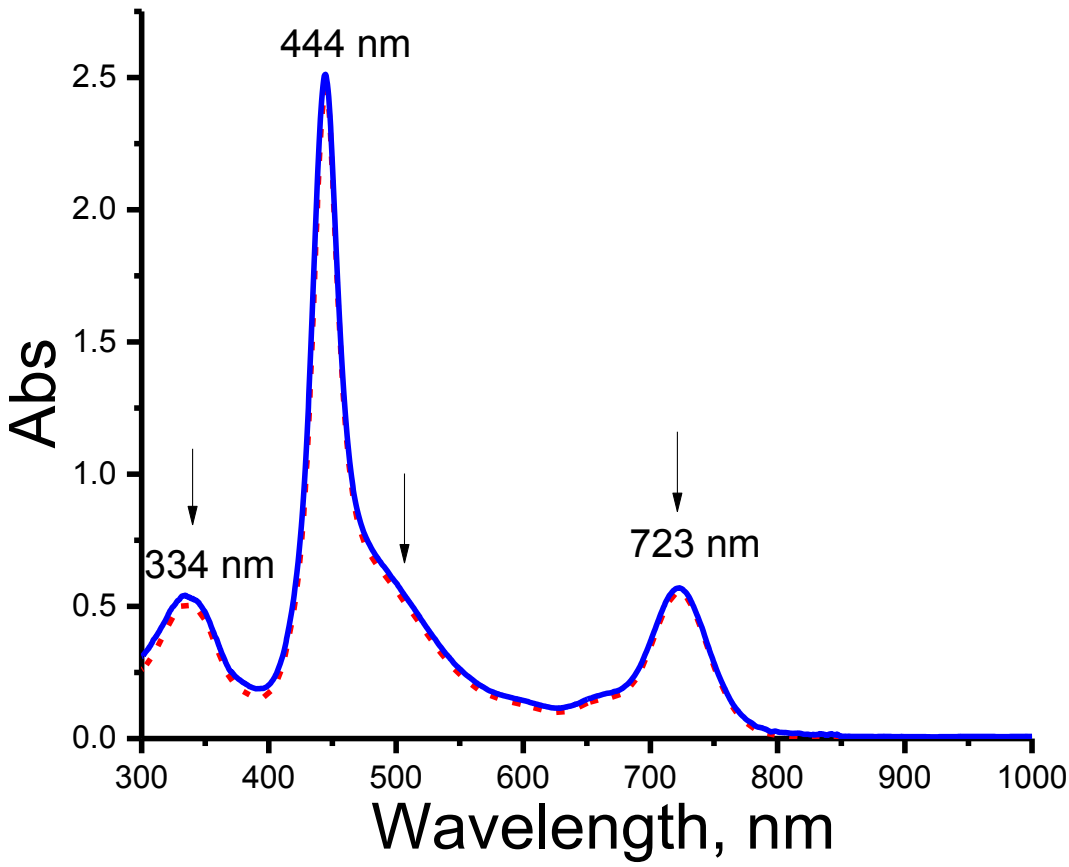


***Figure 26.*** *Chemical reduction of FcInTFcP using Na/K alloy in DCM*

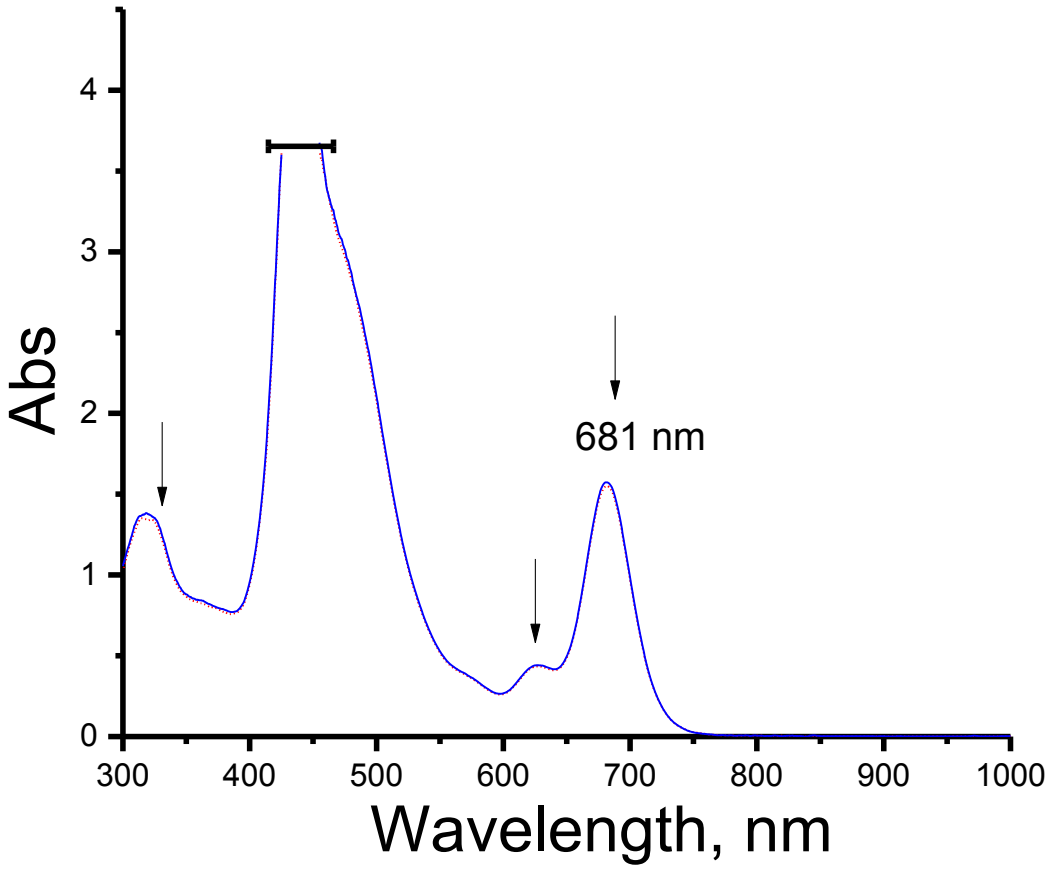


***Figure 27.*** *Chemical reduction of ZnTFcP using Na/K alloy in DCM*

Apart from results, obtained with previous reducing agents, hydrazine hydrate ($N_2H_4 \cdot H_2O$) in DMF gave some changes in UV-Vis spectra, but unfortunately, obtained anion radicals were not stable long enough. To elucidate bands which showed up due to reduction from bands which were a result of absorption of $N_2H_4 \cdot H_2O$ UV–Vis absorption spectrum of mixture of $N_2H_4 \cdot H_2O$ and DMF was recorded (Figure 28). As we can see, two intense bands at 1063 and 1252 nm appear due to the presence of $N_2H_4 \cdot H_2O$ in the

solvent. In Figures 29, 31, 33, 35 are shown reductions of different complexes of meso-ferrocenyl substituted porphyrins with different metals. Bands, which are spectroscopic signatures of anion – radical formation ($[MTFcP]^{-\bullet}$) appear upon addition of $N_2H_4 \cdot H_2O$ to the porphyrin solution in DMF. Additionally, stability test was conducted (Figures 30, 32, 35, 36) in order to estimate stability of the obtained anion – radical. It shows, that obtained products are not stable long enough

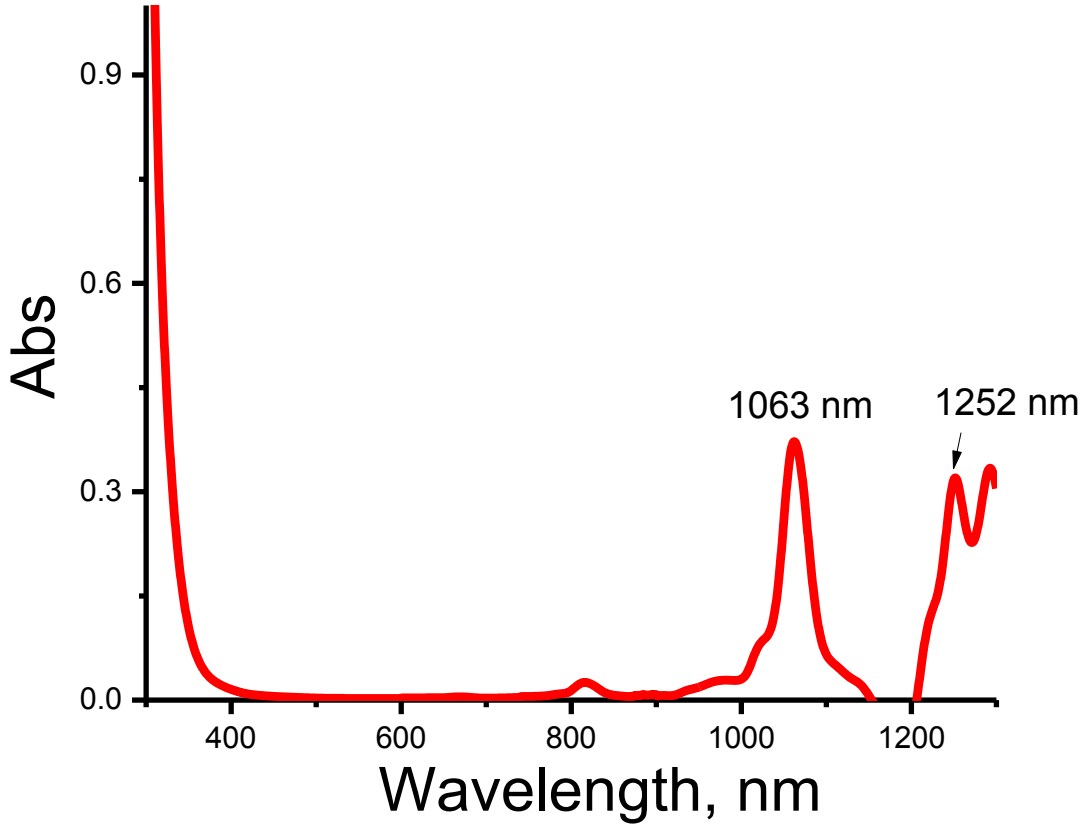


***Figure 28.*** *UV – Vis absorption spectrum of the solution of $N_2H_4 \cdot H_2O$ in DMF*

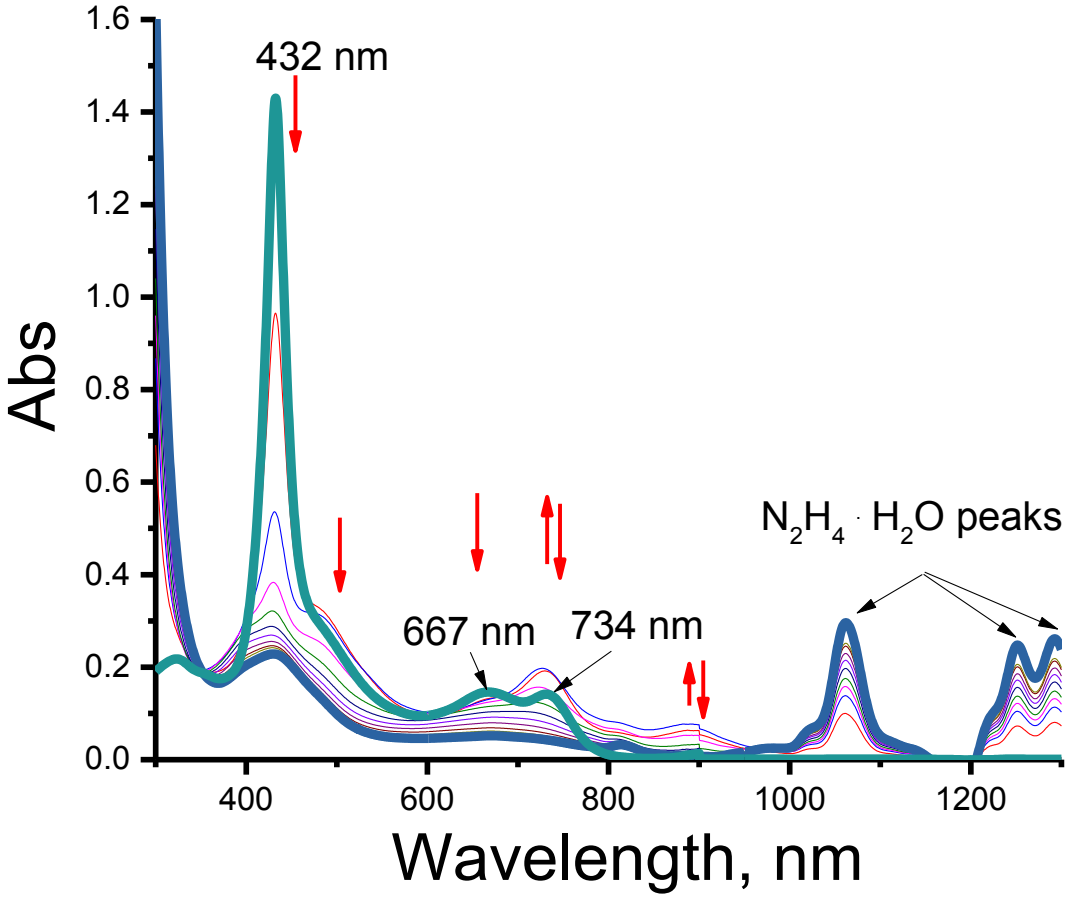


***Figure 29.*** *Reduction of $H_2TFcP$ with $N_2H_4 \cdot H_2O$ in DMF*

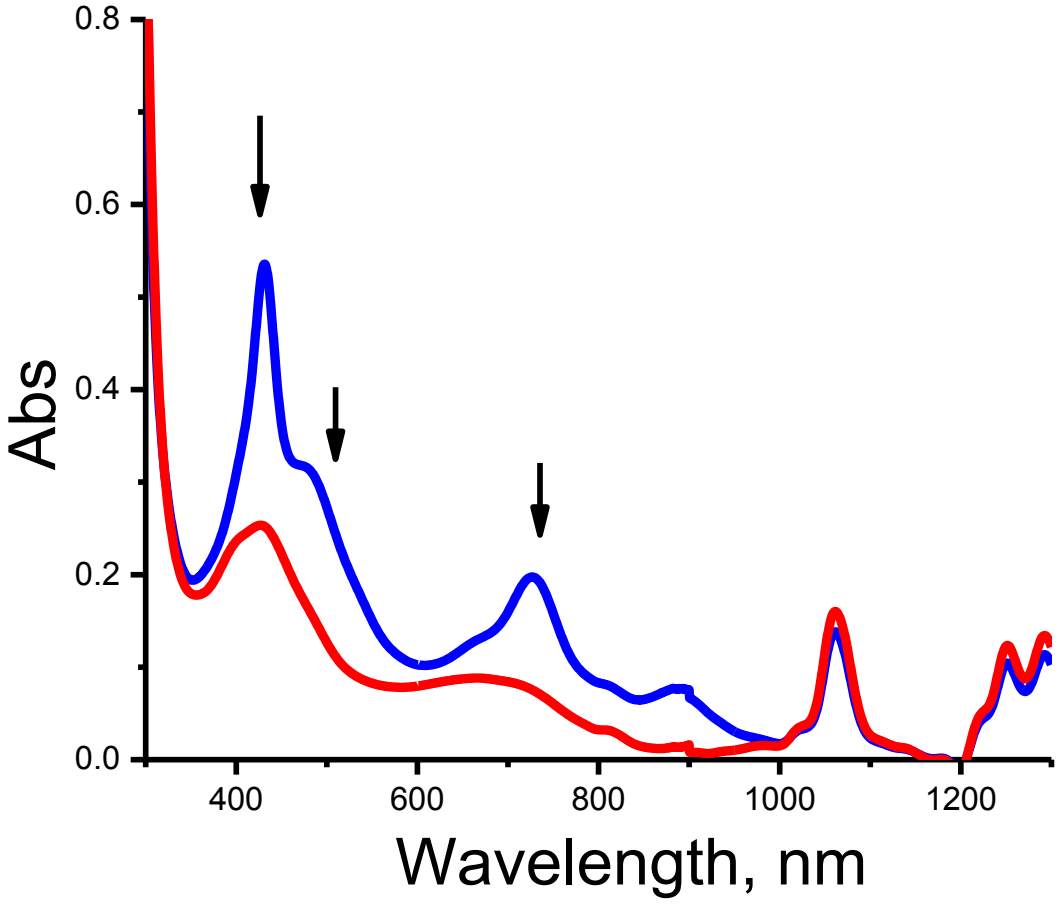


***Figure 30***. *Stability test for $[H_2TFcP]^{\cdot-}$ after addition of $N_2H_4 \cdot H_2O$ to $H_2TFcP$ in DMF. Blue – after addition of 2.3 mmol of $N_2H_4 \cdot H_2O$; red – after 30 min of waiting period*

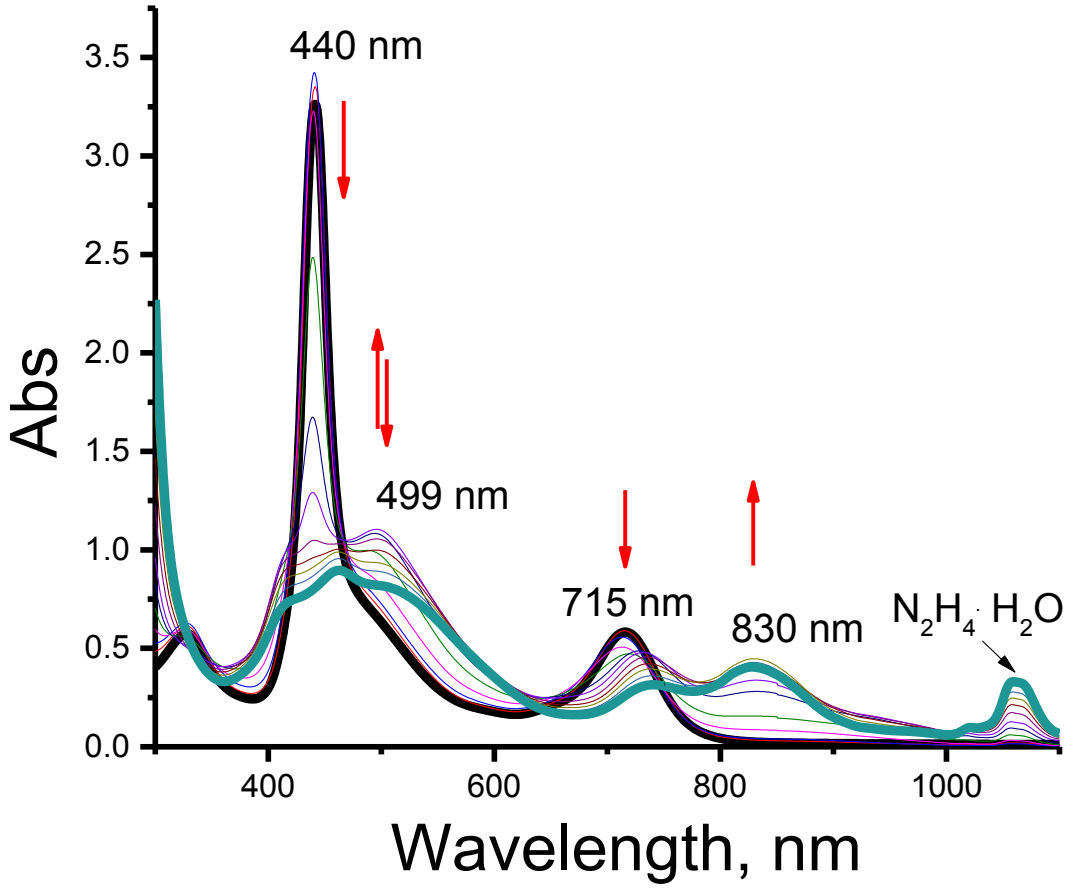


***Figure 31.*** *Reduction of ClInTFcP with $N_2H_4 \cdot H_2O$ in DMF*

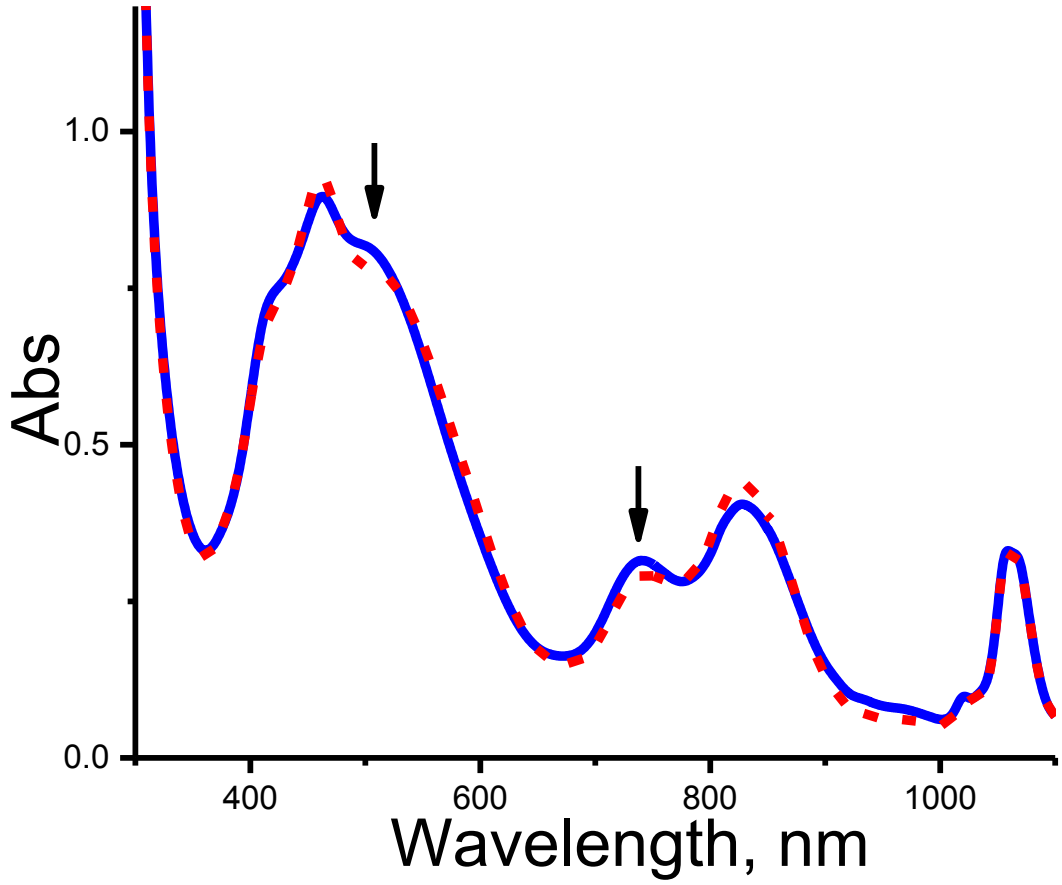


***Figure 32**. Stability test for [ClInTFcP]˙¯ after addition of $N_2H_4 \cdot H_2O$ to ClInTFcP in DMF. Blue – after addition of 2.3 mmol of $N_2H_4 \cdot H_2O$; red – after 30 min of waiting period*

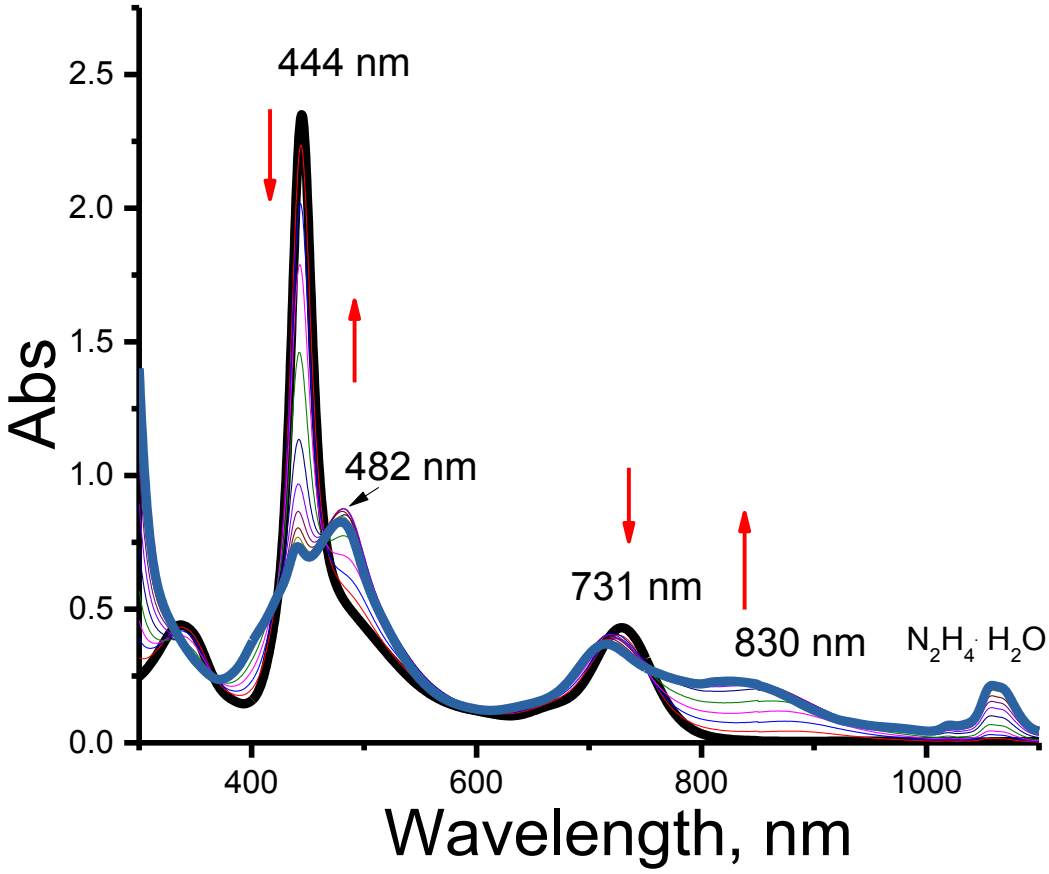


***Figure 33.*** *Reduction of FcInTFcP with $N_2H_4 \cdot H_2O$ in DMF*

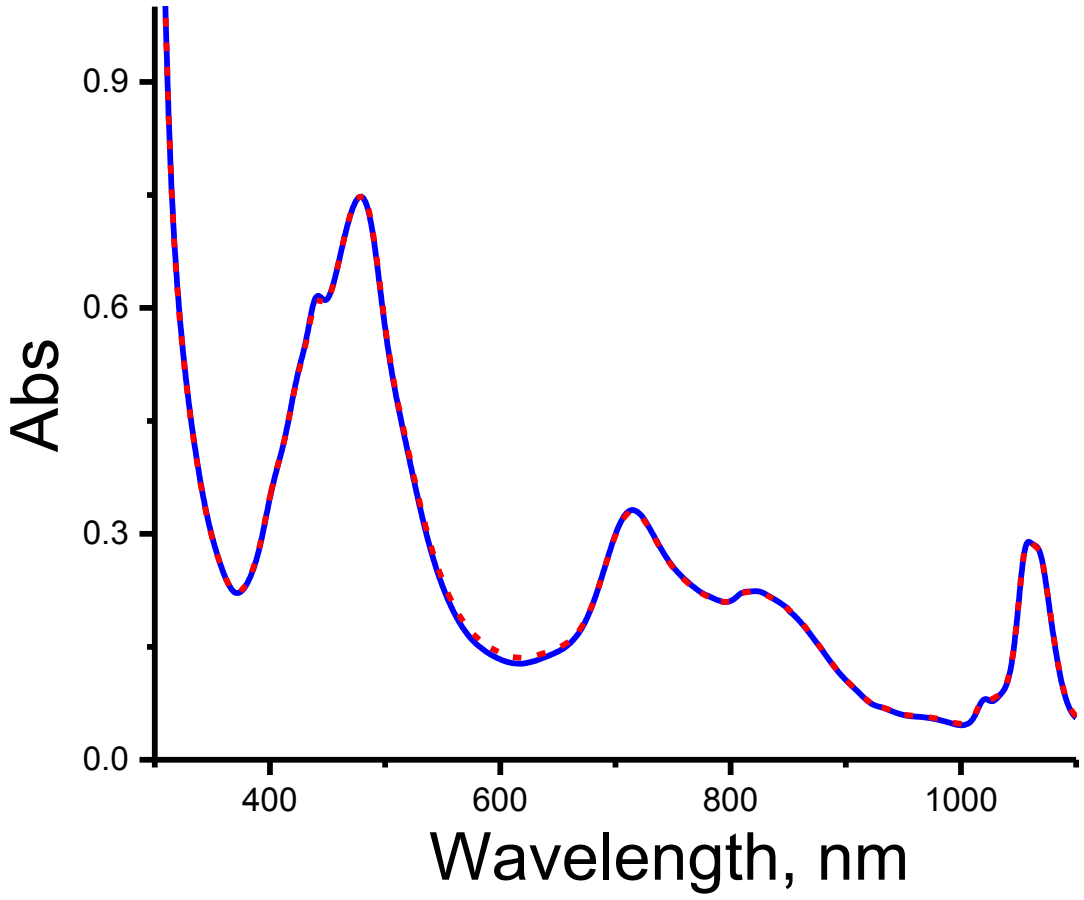


***Figure 34**. Stability test for [FcInTFcP]˙¯ after addition of $N_2H_4 \cdot H_2O$ to FcInTFcP in DMF. Blue – after addition of 2.3 mmol of $N_2H_4 \cdot H_2O$; red – after 30 min of waiting period*

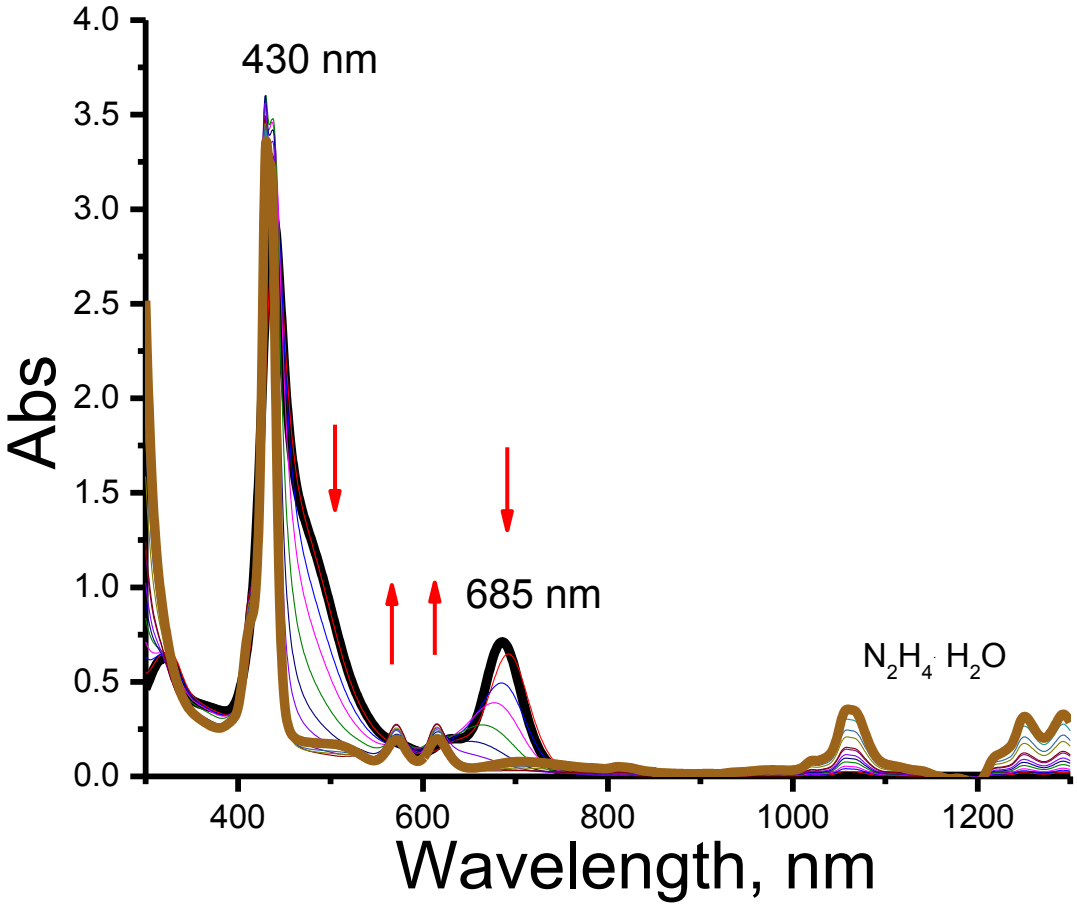


***Figure 35.*** *Reduction of ZnTFcP with $N_2H_4 \cdot H_2O$ in DMF*

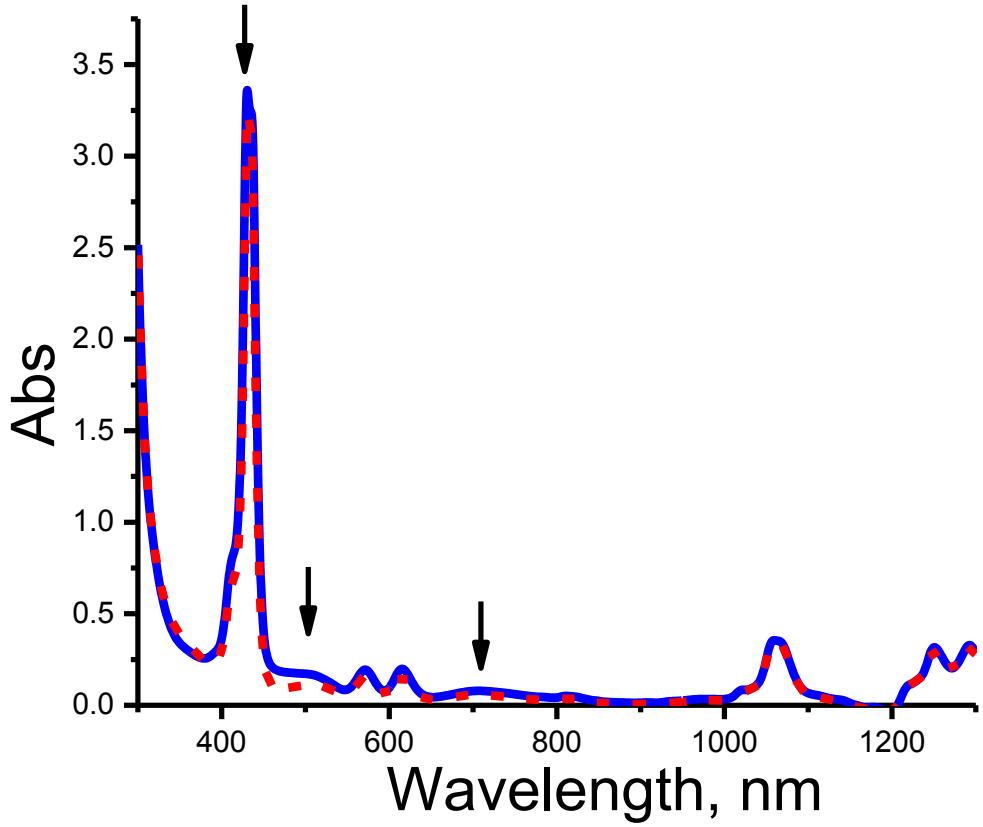


***Figure 36***. *Stability test for* $[ZnTFcP]^{\bullet-}$ *after addition of* $N_2H_4 \cdot H_2O$ *to ZnTFcP in DMF. Blue – after addition of 2.3 mmol of* $N_2H_4 \cdot H_2O$*; red – after 30 min of waiting period*

Finally, it was concluded that all tested reagents (hydrazine in DMF, Na in THF, Na/Hg in THF, Na/K in THF, $NEt_3$ in DCM or DMF, and $(Cp^*)_2Co$ in DCM or DMF) lead to the formation of $[MTFcP]^{n-}$ mixtures or to a degradation of the reduced complexes, thus prohibiting a further spectroscopic investigation of the $[MTFcP]^{\bullet-}$ anion-radicals.

## Electronic Structures of $[H_2TFcP]^{-\cdot}$

One of the most intriguing spectroscopic features of the electrochemically generated $[MTFcP]^{-\cdot}$ species is their broad Soret bands. Indeed, in all $[MTFcP]^{-\cdot}$ complexes this band is significantly broader compared to the Soret band earlier observed in the corresponding $[MTPP]^{-\cdot}$ anion-radicals. In order to gain further

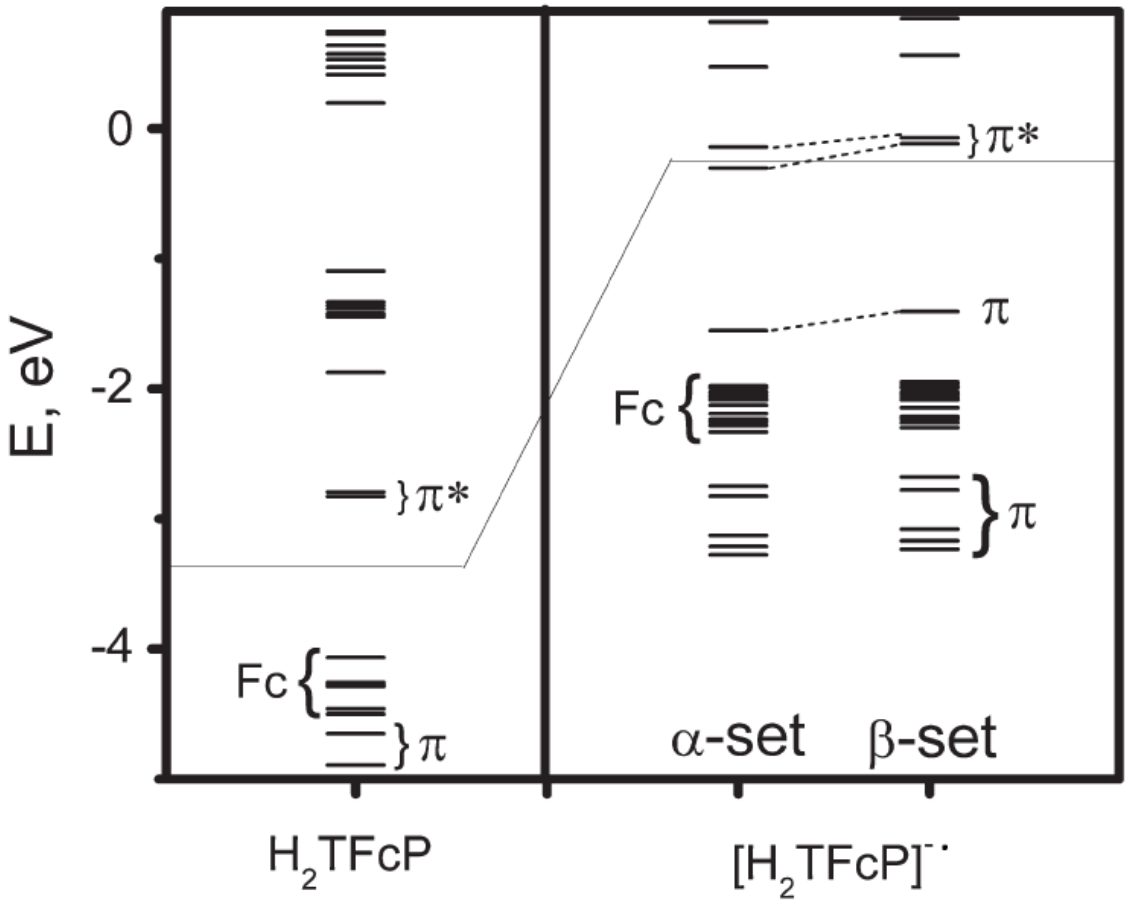


***Figure 37**: MO energy diagram for $H_2TFcP$ and $[H_2TFcP]^{-\cdot}$ complexes calculated at the BP86 DFT level. Occupied and unoccupied MOs are separated by the thin solid line*

insight into the spectroscopic properties and energetics of the $[MTFcP]^-$ complexes, the geometry, electronic structure, and vertical excitation energies of the $[H_2TFcP]^{-\bullet}$ anion-radicals were calculated using a DFT approach, which has previously been shown to provide accurate structure and also explain the electronic and spectroscopic properties of ferrocene-containing compounds including organometallic porphyrins[14l,o,p,16b,24]. The $C_2$ symmetry of the $[H_2TFcP]^{-\bullet}$ system was used in order to avoid complications originating from Jahn-Teller effects associated with the $S_4$ symmetry and corresponding $^2E$ ground state of the $[MTFcP]^{-\bullet}$ anion-radicals. Another advantage of using the $[H_2TFcP]^{-\bullet}$ system to model electronic structures of $[MTFcP]^{-\bullet}$ anion-radicals is that its electronic structure and vertical excitation energies can be directly compared with what has been previously reported for the neutral $H_2TFcP$ complex[14p]. The molecular orbital diagrams and compositions for $H_2TFcP$ and $[H_2TFcP]^{-\bullet}$ calculated by a DFT approach are shown in Figures 37 and 38, respectively, while key molecular orbital surfaces are depicted in Figure 39.

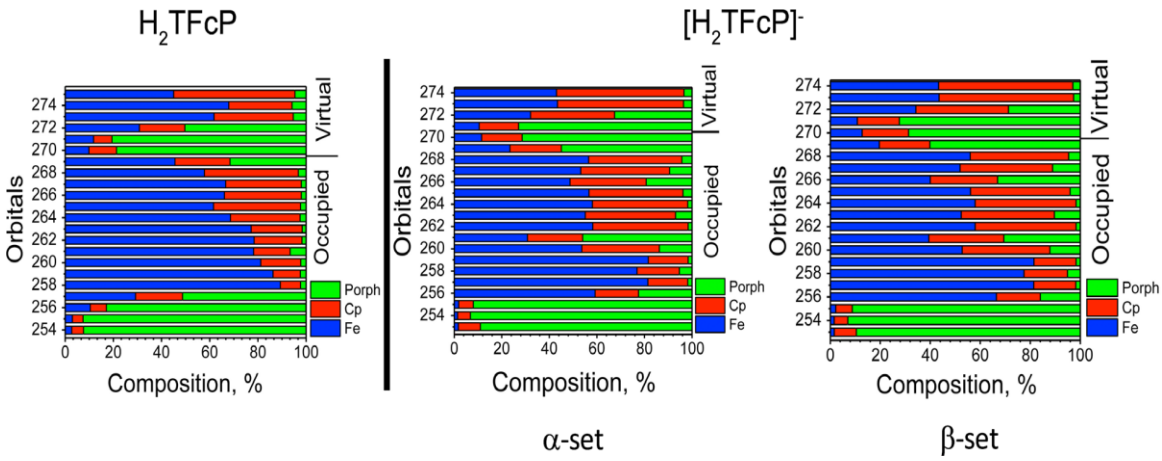


***Figure 38**: Molecular orbital compositions for $H_2TFcP$ and $[H_2TFcP]^-$ systems calculated at the DFT level. Contribution from the porphyrin core is given in green color, contribution from the cyclopentadienyl ligands is given in red color, and contribution from the iron centers is given in blue color*

In the case of the neutral $H_2TFcP$ complex, DFT predicted that nearly degenerate LUMO and LUMO+1 MOs are porphyrin-core centered, while the HOMO to HOMO-11 are predominantly ferrocene-centered MOs with ~30% of the porphyrin core contribution to the HOMO. Expectedly, injection of a single electron into the LUMO results in the formation of a porphyrin-centered $[H_2TFcP]^{-\bullet}$ anion-radical. More importantly, the presence of a single electron in the porphyrin-delocalized SOMO of $[H_2TFcP]^{-\bullet}$ leads to a large spin polarization and a mixing with the HOMO, thus increasing the porphyrin-core contribution from ~30% in $H_2TFcP$ to ~60% in $[H_2TFcP]^{-\bullet}$. As a result, the HOMO in $[H_2TFcP]^{-\bullet}$ transforms from a predominantly ferrocene-centered into a predominantly porphyrincentered MO. The next porphyrin-centered π orbital in the $[H_2TFcP]^{-\bullet}$ complex

is HOMO-9. Again, this MO hasa higher energy compared to the corresponding MO in neutral $H_2$TFcP and is located above the five ferrocenecentered orbitals.

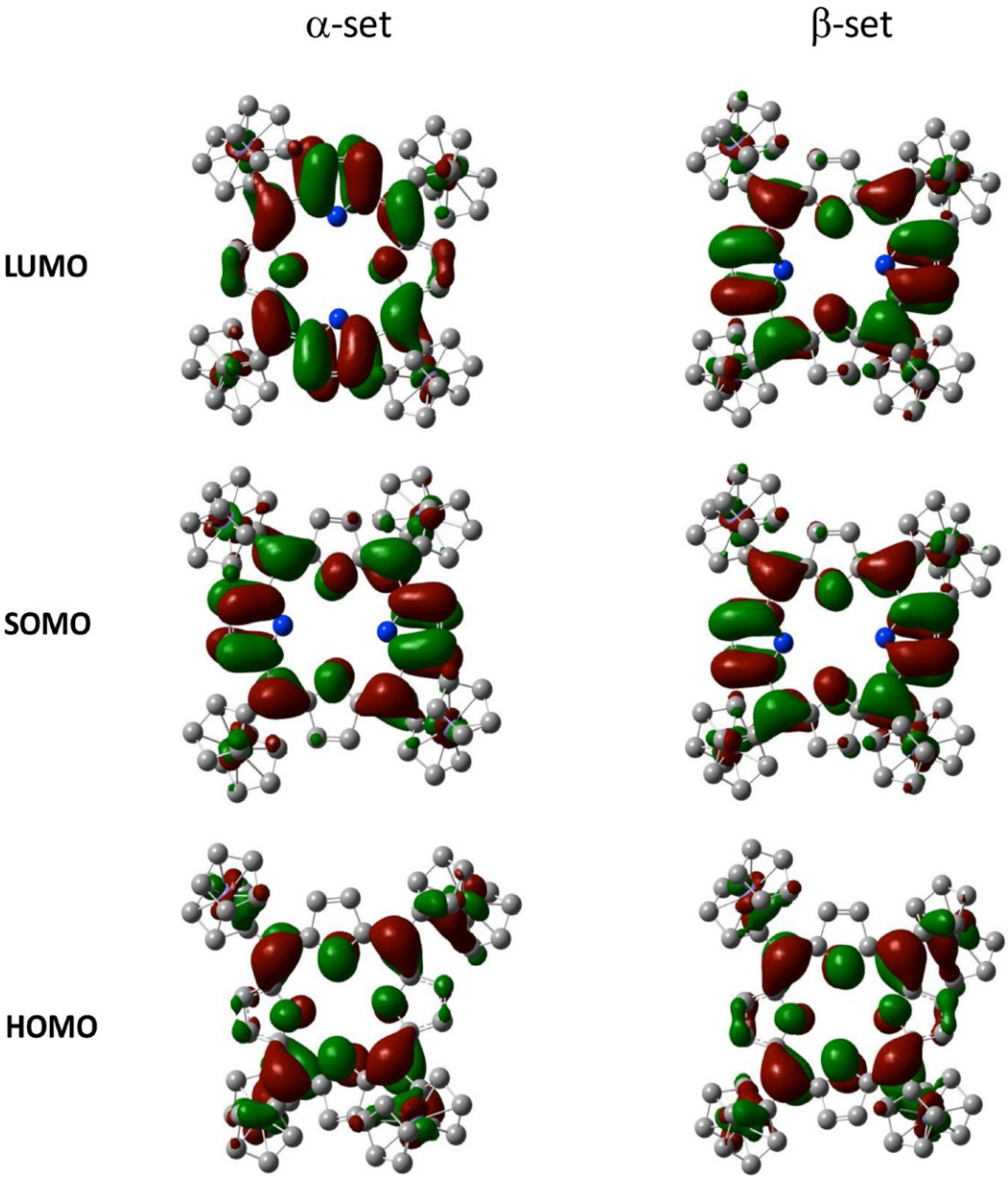


***Figure 39**: Frontier orbitals of $[H_2TFcP]^{\cdot-}$ calculated at the DFT level*

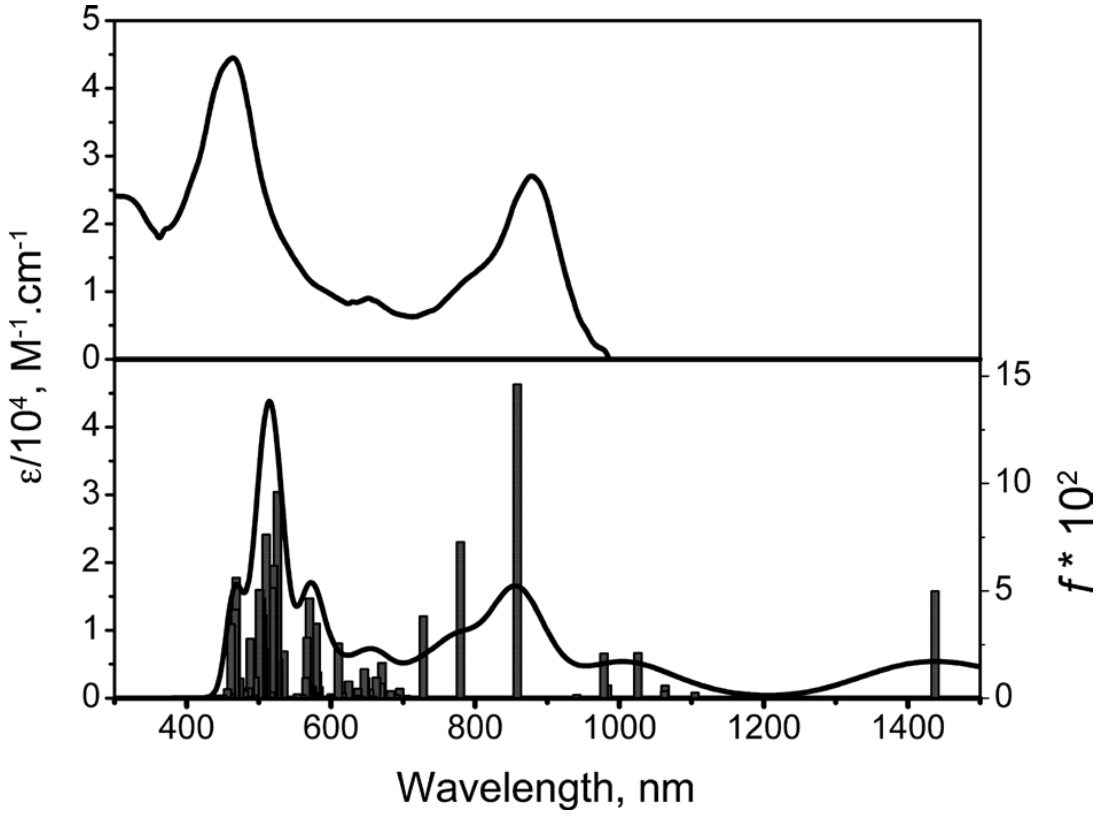


***Figure 40**: Experimental (top) and TDDFT predicted (bottom) UV-vis spectra of the $[H_2TFcP]^{\bullet-}$ complex*

In general, the TDDFT calculations on the $[H_2TFcP]^{\bullet-}$ anion-radical are in a good agreement with the experimental UV-vis data in the spectral region of 300–1100 nm (Figure 40). In particular, TDDFT predicts an intense transition ($f$ = 0.156) at 11690 $cm^{-1}$ (855 nm) originated from 269β (HOMO) → 270β (LUMO) single electron excitation. As expected, the presence of a large number of occupied and virtual ferrocene-centered MOs, results in numerous LMCT and MLCT transitions in the UV-vis region. For instance, TDDFT predicted bands at 12820 $cm^{-1}$ (780 nm) and 13720 $cm^{-1}$ (729 nm) have a main contribution from 270α (SOMO) → 280α (Fc) electron excitation and have

predominant LMCT character. These transitions have lower intensities ( $f$ = 0.0746 and $f$ = 0.0403, respectively), partially overlap with the more intense π – π* transition at 11690 $cm^{-1}$ ( $f$ = 0.156), and could form the higher energy shoulder of the experimentally observed band centered at 880 nm. The SOMO-LUMO difference for the α-set is 0.162 eV and the corresponding 270α (SOMO) → 271α (LUMO, $f$ = 0.001) transition is predicted in the IR region (1405 $cm^{-1}$) and thus cannot be investigated by UV-vis-NIR spectroscopy. Another relatively intense ($f$ = 0.046) excited state predicted by TDDFT is located at 17530 $cm^{-1}$ (570.5 nm), has two predominant contributors (269α → 272α and 257β → 271β) and could be assigned as a mixed MLCT/LMCT transition. The TDDFT predicted intense transition at 18990 $cm^{-1}$ (527 nm) ($f$ = 0.102) predominantly originates from 269β → 278β electron excitation and has LMCT character. More importantly, TDDFT calculations allow us to explain the nature of the broad Soret band experimentally observed in the UV-Vis spectrum of the $[H_2TFcP]^{-\bullet}$ anion-radical at 458 nm. Indeed, TDDFT predicts a large number of individual excited states with predominant π – π*, MLCT, and LMCT characters located in this spectral region, which will significantly broaden experimentally observed bandwidth.

## Conclusions:

In this chapter was reported *in situ* generation and spectroscopic characterization of several 5,10,15,20-tetraferrocenylporphyrin anion-radical species. Anionradicals having the general formula $[MTFcP]^{-\bullet}$ (M =2H, Zn, InCl, and InFc) were prepared *in situ*

for the first time by reduction of the respective neutral MTFcP complexes under spectroelectrochemical conditions. UV-vis spectroscopy reveals the formation of the Soret bands between 458 and 527 nm that are unusually broad for 5,10,15,20-tetra(aryl)porphyrin radical-anions. Additionally, characterization of the electronic structure and the nature of the vertical excitation energies in the $[H2TFcP]^{-\cdot}$ system was obtained on the basis of density functional theory (DFT) and time-dependent DFT (TDDFT) methods. DFT calculations predict that the SOMO in the $[H2TFcP]^{-\cdot}$ anionradical is predominantly localized over the porphyrin core. TDDFT calculations are suggestive of numerous LMCT and MLCT transitions in addition to the expected $\pi - \pi^*$ excitations, which play a key role in the formation of unusual UV-vis spectra in $[MTFcP]^{-\cdot}$ anion-radicals.

# Part 2 – Characterization of Ferrocenyl – Containing Magnesium Tetraazaporphyrins

## Introduction

The generation of energy is one of the most important scientific and technological challenges in the 21st century[30]. And search for more reliable sources of energy are of great importance. Giving the amount of energy which sun is radiating towards Earth, light harvesting has become one of the promising solution to the human's energy need (Table 2).

***Table 2: Yearly Solar Fluxes and Energy Consumption***

| | |
|---|---|
| Solar energy potential* | $3{,}850 \cdot 10^{21}$ J |
| Wind energy potential* | $2.25 \cdot 10^{18}$ J |
| Biomass Potential* | $0.1 – 0.3 \cdot 10^{18}$ J |
| Primary Energy Use (2009) | $0.5 \cdot 10^{18}$ J |
| Electricity, produced in 2009 | $0.06 \cdot 10^{18}$ J |

* - total amount of energy which may be possible to produce on Earth

The commercially available solar cells are currently based on inorganic silicon semiconductors[25]. The demand for silicon will dramatically increase within the next decade and the price for silicon will also rise. Organic solar cells, therefore, appear to be a highly promising and cost-effective alternative for the photovoltaic energy sector. In

this context, dye-synthesized solar cells (DSSC) have attracted considerable attention in recent years[25]. At present, two compounds hold the efficiency record of an overall power conversion efficiency ($\eta$) approaching 11% under standard (Global Air Mass 1.5) illumination (Figure 41).

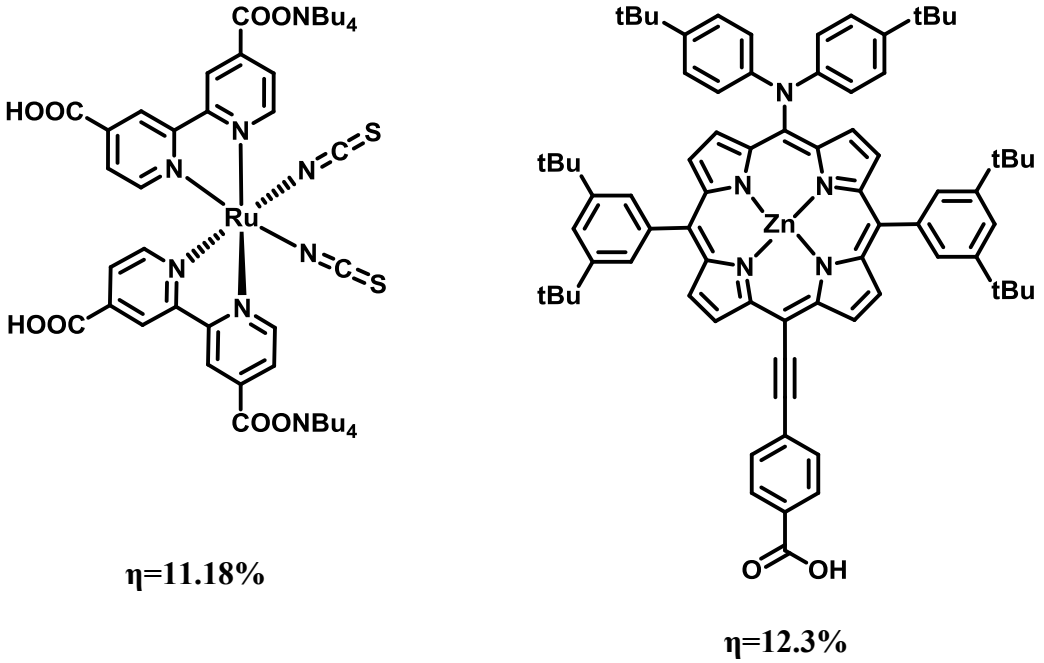


***Figure 41:*** *Ruthenium(II) – polypyridyl complex N719[26,27,28] and meso-derivatized porphyrin with carboxylic acid groups[29] as examples of highly efficient dyes for DSSCs production*

In the last 15 – 20 years a lot of effort has been devoted to the synthesis and investigation of materials for DSSCs: fundamental understanding of the working principles has been gained by means of modeling electrical and optical properties as well as by advanced characterization techniques[31,32].

In this chapter synthesis and properties of two magnesium tetraazaporphyrins will

be discussed, as these compounds combine two types of electronical transitions including $\pi - \pi^*$ and ligand to metal charge transfer bands. Giving their unique spectroscopic signatures, these compounds can be prospective candidates for highly-efficient DSSC production[33]. Also, understanding of the electronic structure and influence of the second set of peripheral substituents on the spectroscopic properties of these complexes can provide us with ability of fine tweaking and precise structure – properties correlation of the end-line industrial products.

## Synthesis:

Two target compounds were synthesized using previously developed schemes[34,35,36,37]. Firstly, cis-dicyanovinyl ferrocene and tricyanovinyl ferrocene (Figure 42) were

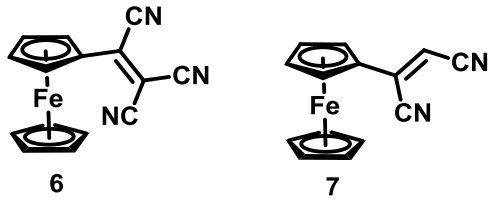


***Figure 42:*** *Precursors for synthesis of target tetraazaporphyrins*

synthesized. For synthesis of tricyanovinyl ferrocene (6) a mercury-free procedure was used[34]. On the Scheme **8** are shown main procedures for synthesis of the target tetraazaporphyrin. Most of the procedures involve use of toxic mercury salts (*a* and *b,*

*scheme 8*), or use of toxic thallium (reaction *c, scheme 8*) that's why a more environmentally-free procedure was used. For direct coupling of ferrocene and tetracyanoethylene, sulfolane was used as a solvent. Interestingly, that any other solvent that was tried did not give satisfactory yields[34].

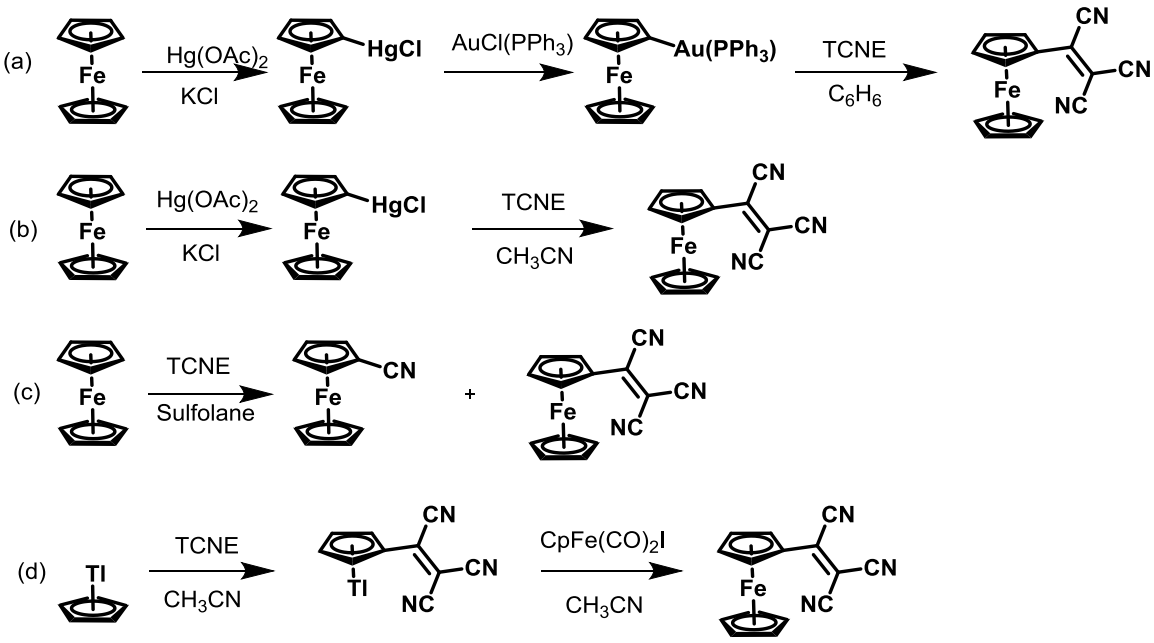


***Scheme 8:*** *Synthetic pathways of a compound* ***6****.*

For compound **7** the most difficult part was the separation of *z* and *e* isomers after first process of iodination of the ethynylferrocene (Scheme 9). After iodination step, reaction with copper (I) cyanide was performed, resulting in a mixture of mono- and di-cyano derivatives, which were further separated and used as a reagent for tetraazaporphyrin synthesis.

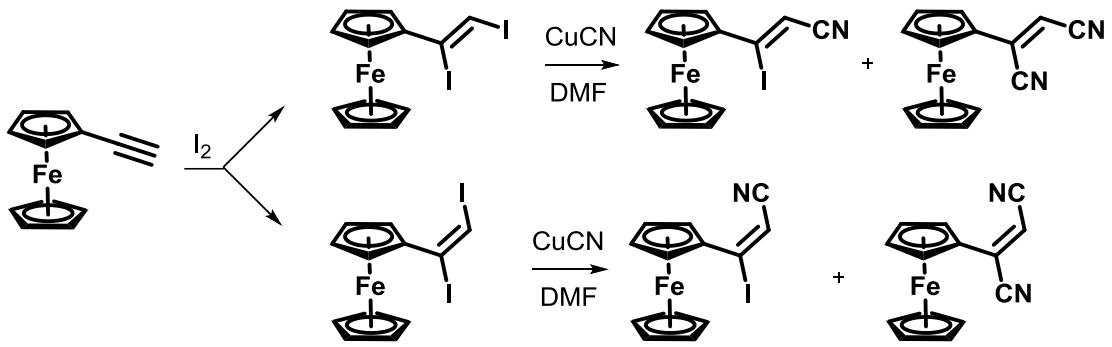


***Scheme 9:*** *Synthetic pathways for preparation of cis- and trans-dicyano substituted vinylferrocenes*

Finally, compounds **8** and **9** were synthesized in the presence of magnesium in 1-butanol (Scheme 10).

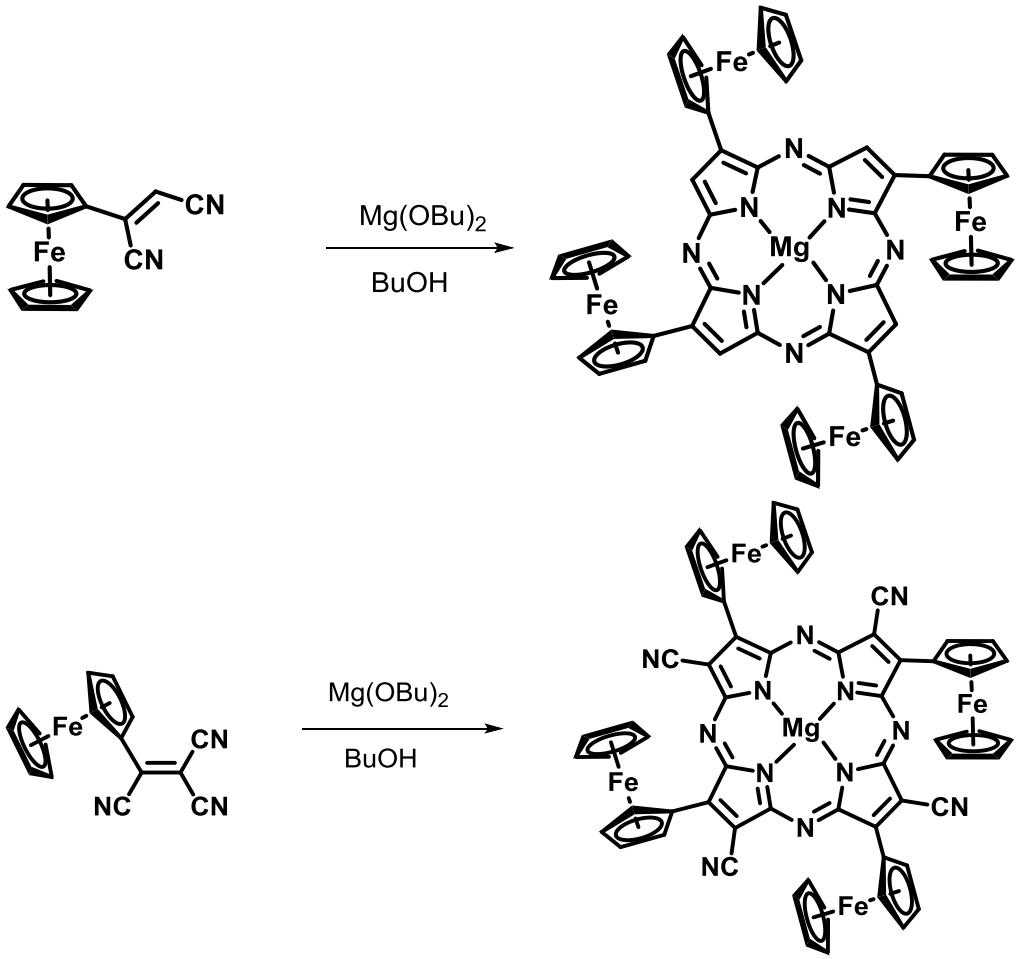


***Scheme 10**: Preparation of 2,7,12,17-tetracyano-3,8,13,18-tetraferrocenyl-5,10,15,20-tetraazaporphyrinatomagnesium (**MgTAP(CN)$_4$Fc$_4$**) and 3,8,13,18-tetraferrocenyl-5,10,15,20-tetraazaporphyrinatomagnesium (**MgTAPFc$_4$**)*

Both of the compounds are stable in the solid state, but in all of the tested solvents they degrade over the several days.

## Positional Isomers and Their Separation

Due to the fact that both reactants **6** and **7** do not have plane of symmetry between C – C double bond, final products can form several positional isomers, which can be differentiated by different position of ferrocene units which are attached to β-pyrrolic positions. On the diagram below (Figure 43) are shown all possible isomers which could be formed. In order to carry out further analysis of the complexes, separation of isomers was attempted. In $MgTAP(CN)_4Fc_4$ CN group has strong dipole moment which significantly changes polarity of the whole molecule, therefore allowing to obtain several different fraction on TLC plate. Unfortunately, separation of $MgTAPFc_4$ could not be performed due to the fact, that polarity of all four isomers is approximately the same.

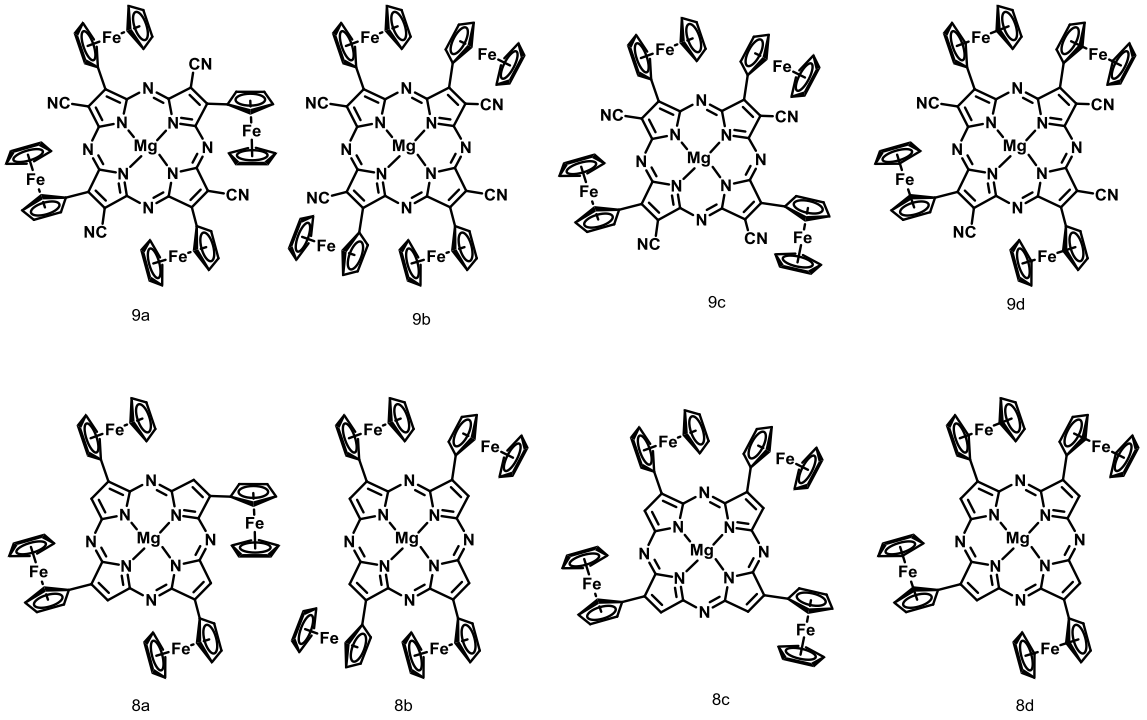


***Figure 43:*** *Different positional isomers of $MgTAP(CN)_4Fc_4$ (9a – 9b) and $MgTAPFc_4$ (8a – 8b). Note, that $\mu_{9a,\ 9b} \sim 0$, $\mu_{9c,\ 9d} > 0$, and $\mu_{8a,\ 8b,\ 8c,\ 8d} \sim 0$, where $\mu$ – overall dipole moment*

Separation of the $MgTAP(CN)_4Fc_4$ was conducted using silica-gel thin-layer chromatography and with Toluene – Ethanol mixture in 10:1 (v:v) ratio. Two main fractions were obtained (Figure 44), and further analysis was carried out using two different fractions as well as initial mixture of positional isomers.

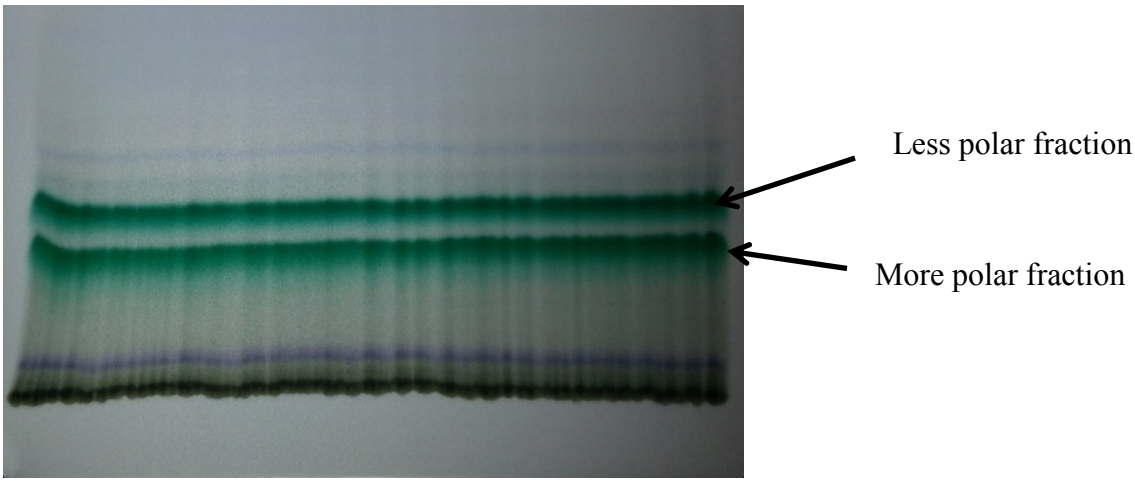


***Figure 44**: Thin-layer chromatography plate after separation of the $MgTAP(CN)_4Fc_4$ using toluene – ethanol as eluent*

## UV-Vis and MCD Spectra

UV-Vis and MCD spectra of **8** and **9** are presented in Figures 45, 46 and remain unchanged over a wide range of concentrations suggesting monomeric states of the target compounds in solution. The assignments of Q and B bands in UV-Vis spectra of **9** are straightforward: there are only two narrow intense bands expected for tetraazaporphyrins in the spectral ranges of 623 and 384 nm in the UV-Vis spectrum of **9**. The assignments can be further confirmed by the MCD spectrum of **9** in which, as expected, both Q and B bands represented by Faraday *A*-terms centred close to the absorption maxima with negative components located at lower energies in both cases. According to the perimeter model, this situation suggests that the ΔHOMO > ΔLUMO in agreement with TDDFT calculations (ΔHOMO is the energy difference between two highest occupied π-orbitals

centred at tetraaazaporphyrin core and ΔLUMO is the energy difference between two lowest energy π*-orbitals centred at the tetraazaporphyrin core)[38]. In addition, another prominent feature was observed in the MCD spectrum of **9** (Figure 46), which is represented by a Faraday *A*-term centred at 895 nm with a negative component at lower energy and corresponds to the intense near-IR band observed in the UV-Vis spectrum of **9**, which will be discussed below. Similarly to **9**, the prominent band observed at 363 nm in the UV-Vis spectrum of **8** and the respective Farday *A*-term centered at 361 nm can be clearly attributed to the B-band.

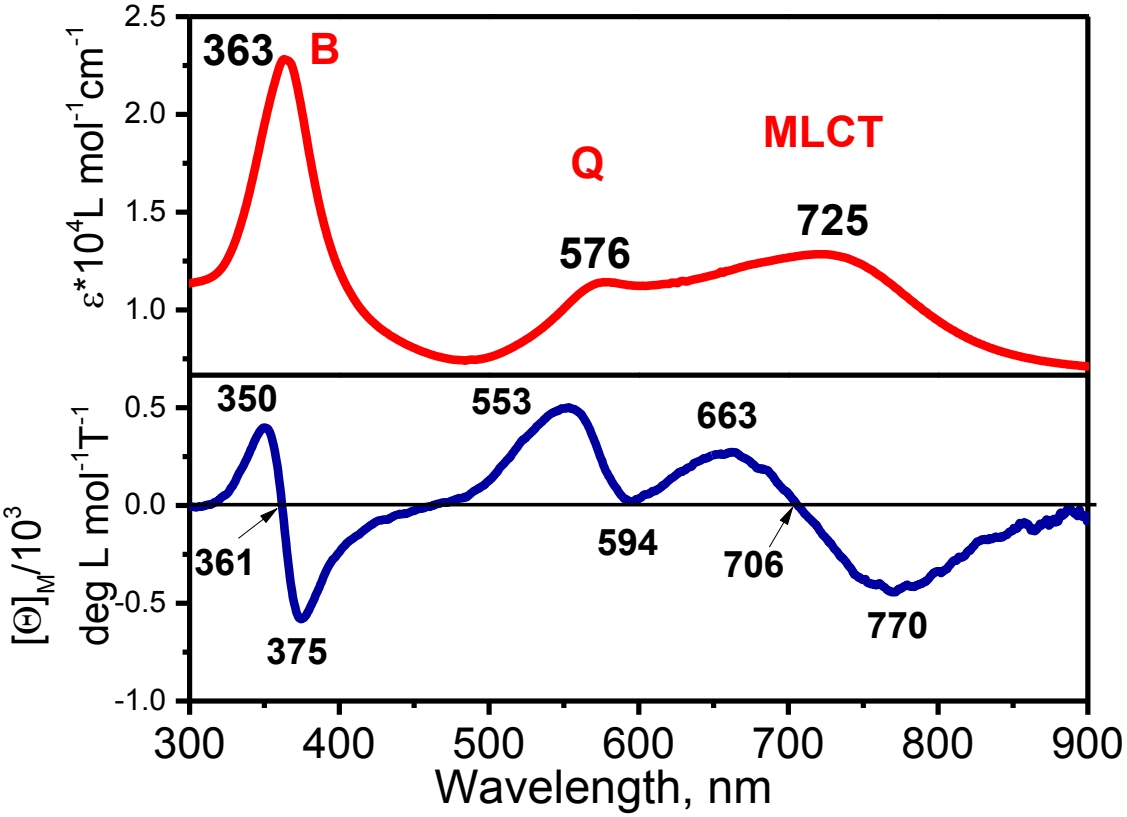


***Figure 45:*** *UV-Vis-NIR (top) and MCD (bottom) spectra of* ***8*** *in DCM*

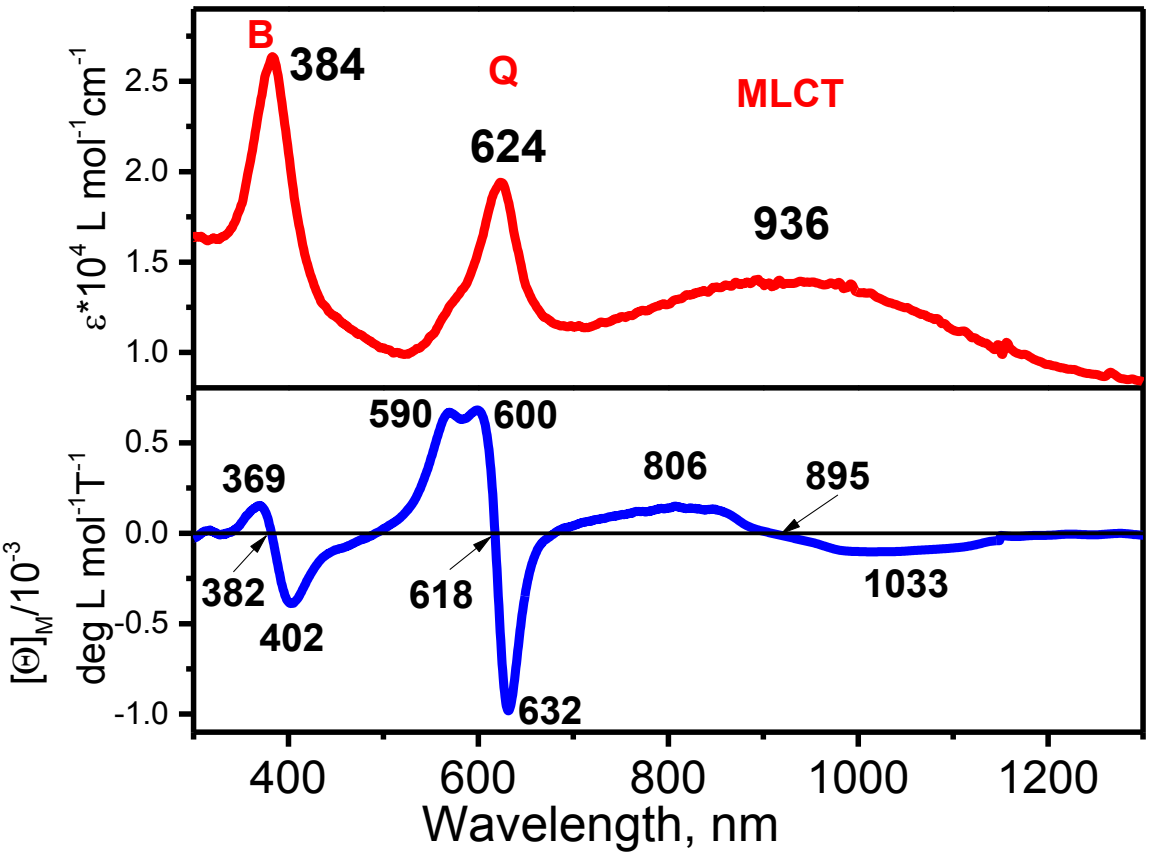


***Figure 46:*** *UV-Vis-NIR (top) and MCD (bottom) spectra of* ***9*** *in DCM*

The band assignments in the near-IR region of the UV-Vis and MCD spectra of **8** are not obvious. In the UV-Vis spectrum of **8**, two intense bands were observed in the visible-to-near-IR region (Figure 45). The first broad band centred at 725 nm overlaps with the narrower band observed at 577 nm. Two positive and one negative signals (going from higher to lower energies) were observed in the MCD spectrum of **8** in this

region (Figure 45). The first two low energy components are cantered close to the maximum of the broad near-IR band observed in the UV-Vis spectrum of **8** and similar to the near-IR band observed in the case of **9**.

## Electrochemistry and Spectroelectrochemistry

Since the oxidation of the ferrocene substituents in poly(ferrocenyl)-contatining macrocycles is sensitive to the nature of solvent and electrolyte,[7,39] the redox properties of **8** and **9** were investigated by cyclic voltammetry (CV) and differential pulse voltammetry (DPV) methods in *o*-dichlorobenzene (*o*-DCB), dichloromethane (DCM), and dimethylformamide (DMF) with TBAF as a non-coordinating electrolyte, while further insight on the first redox process in both systems has been gained on the basis of spectroelectrochemical experiments. In all cases, two oxidation and two reduction processes were observed for **8** and **9** with all processes in **9** shifted to more positive potentials as expected (Figures 47, 48).

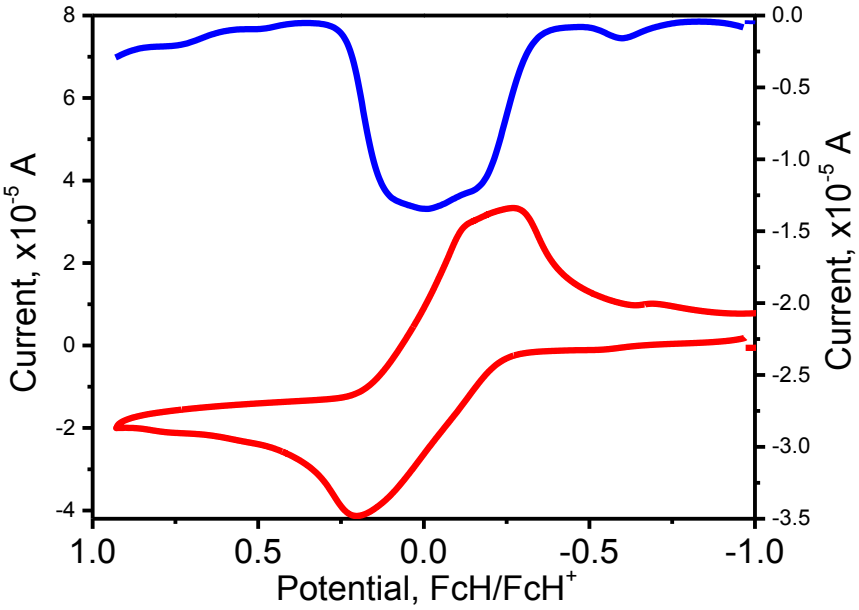


***Figure 47**: CV(red) and DPV(blue) of **8** in DCM/TFAB system*

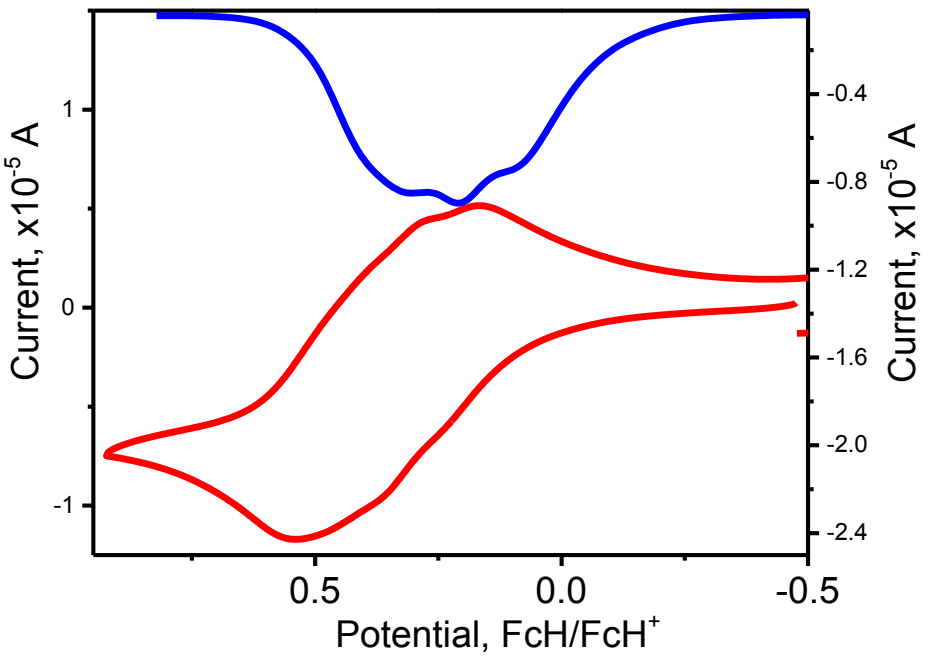


***Figure 48**: CV(red) and DPV(blue) of **9** in DCM/TFAB system*

The first process represents simultaneous four-electron oxidation of ferrocene substituents in **8** and **9**, while the other redox transformations are tetraazaporphyrin core-centered single-electron processes. Some broadening of a signal of ferrocene-centred oxidation suggests that there is some communication between ligands and probable formation of a mixed valance state. But it is unclear if this differentiation in ferrocene oxidation potentials happens due to the presence of four different positional isomers of **8** and **9**. Positional isomers have different type of steric hindrance between large substituents which can be a reason for the observable effect. To answer this question, separation of two different groups of isomers of **9** was carried out as it is described in the

chapter above and electrochemistry was compared to initial mixture of compounds (Figure 49).

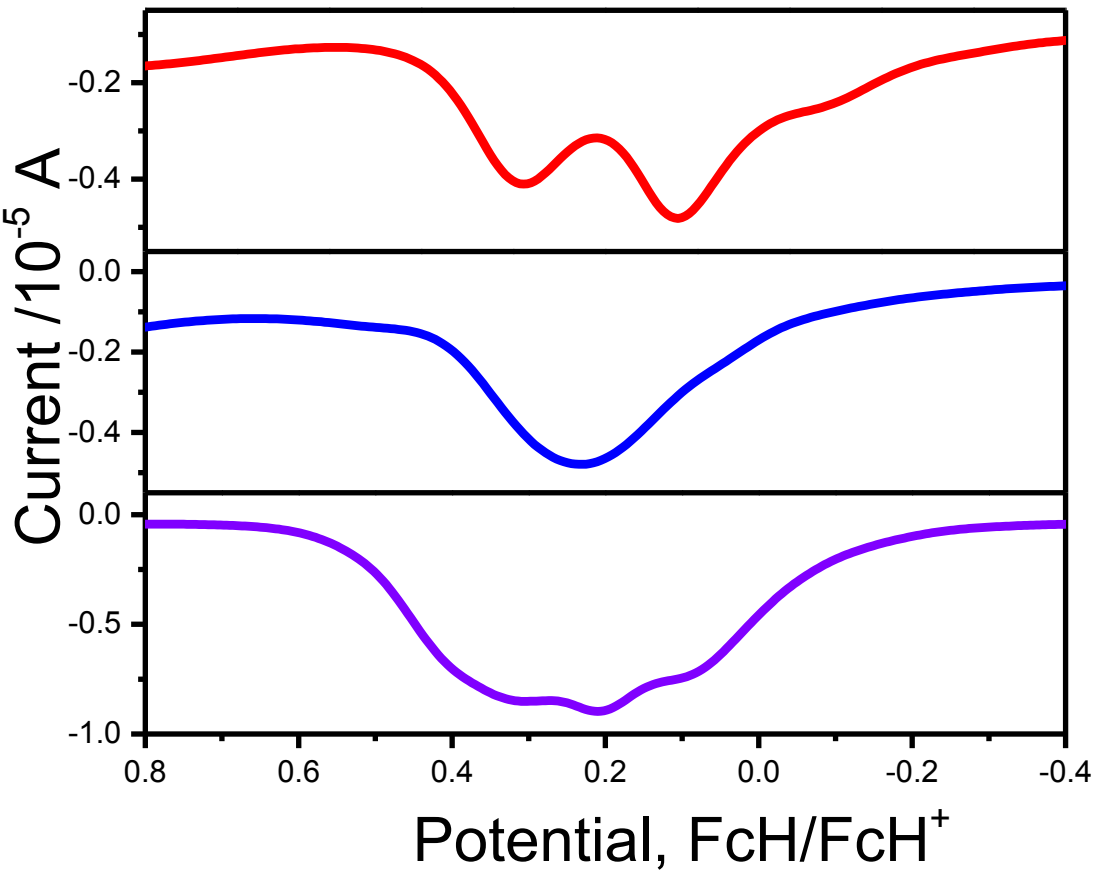


***Figure 49***. *Comparison of DPV experiments for* ***9*** *(bottom),* $\mathbf{9}_{a,b}$ *(top) and* $\mathbf{9}_{c,d}$ *(middle) in DCM/TFAB system*

From the data shown above it is possible to conclude that different positional isomers contribute to the separation of ferrocene oxidation peaks. Since compounds 9a

and 9b have approximately the same polarity, but different steric constrains, it gives two different peaks during oxidation as compared to the 9c and 9d. And DPV's for 9a,b and for 9c,d add up into DPV of initial mixture of all four isomers of $MgTAP(CN)_4Fc_4$.

Spectroelectrochemical experiments conducted in different solvents are also very similar to each other (Figures 50 – 61). As it is shown, two different fractions of a compound **9** as well as initial mixture are also very similar, which can prove that this data is indifferent to type of a positional isomer present in the analysed mixture. Specifically, during electrolysis at the first oxidation potential, the intensity of the NIR MLCT band in **8** and **9** decreases, while the Q-band undergoes a low-energy shift. Additionally, a new low-intensity band in the NIR region is formed (around 1300nm for **9** and 1000nm for **8**), which can be a result of the mixed-valence state formation due to ferrrocene oxidation.

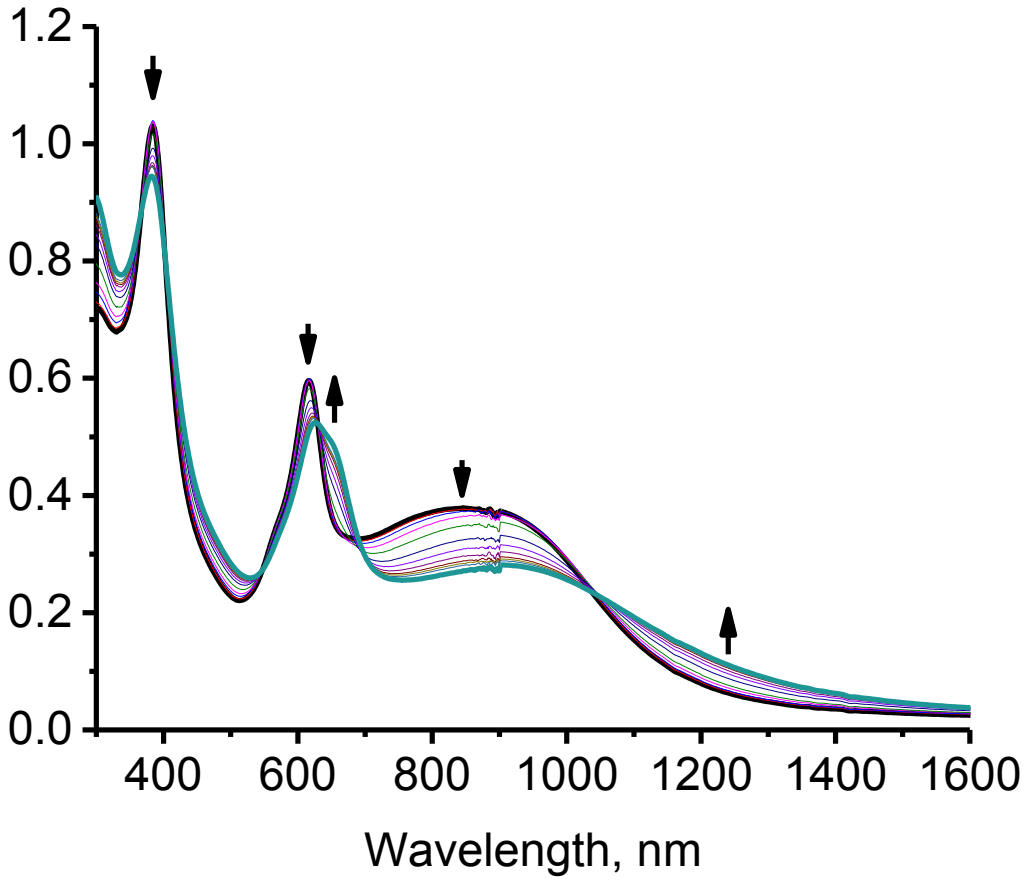


***Figure 50***. *Oxidation of* ***9*** *under spectroelectrochemical conditions in DCM/TFAB system conducted at first oxidation potential*

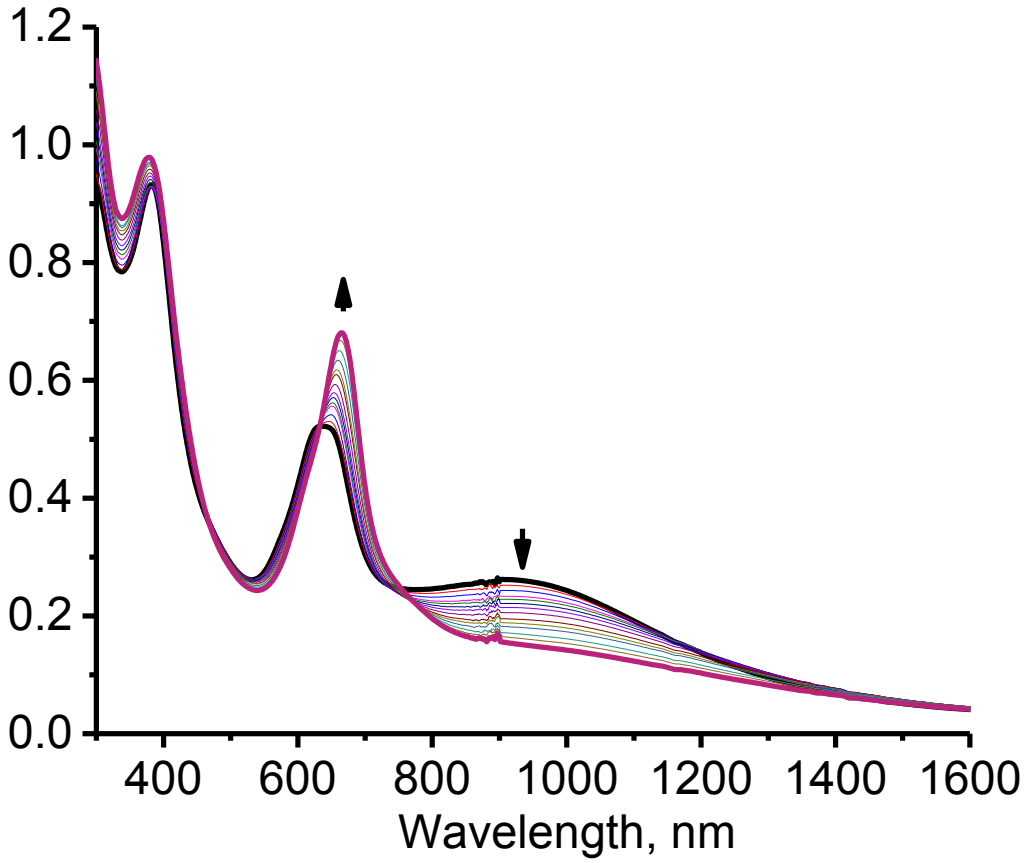


***Figure 51***. *Oxidation of* $\boldsymbol{9^{n+}}$ *under spectroelectrochemical conditions in DCM/TFAB system conducted at second oxidation potential*

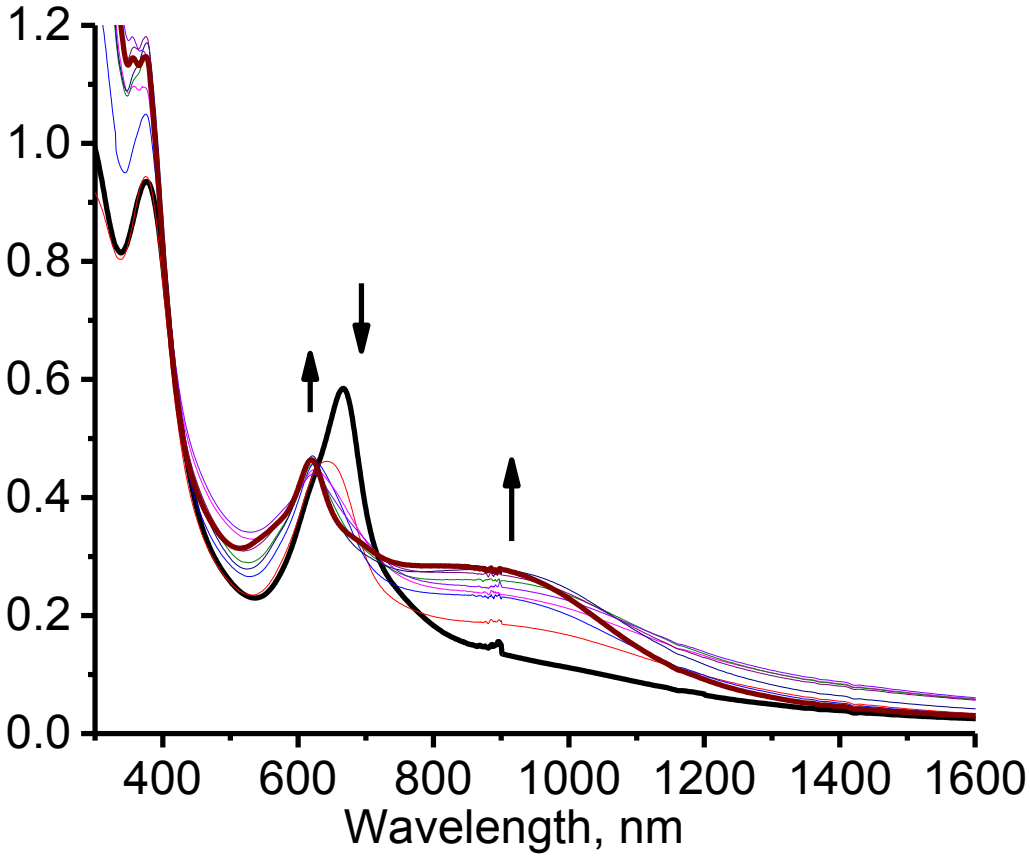


***Figure 52***. *Reduction of* $\boldsymbol{9}^{4+}$ *under spectroelectrochemical conditions in DCM/TFAB system*

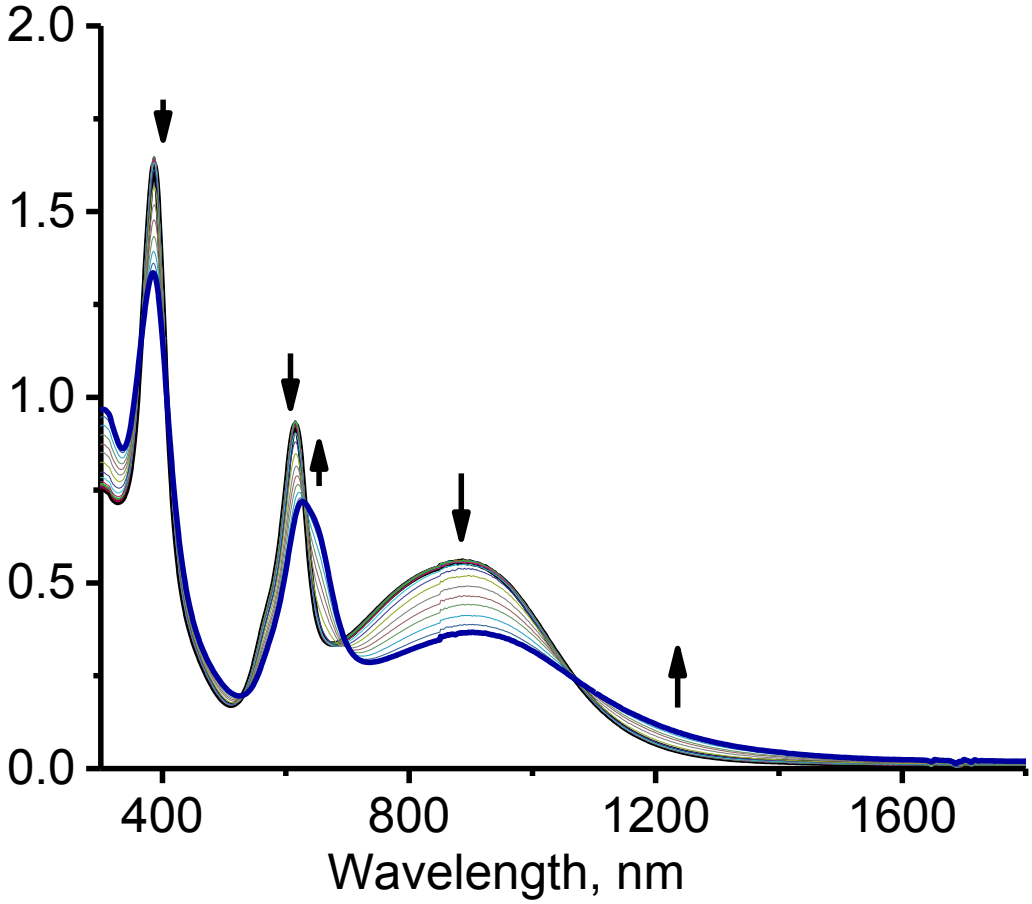


***Figure 53.*** *Oxidation of* ***9a*** *and* ***9b*** *mixture under spectroelectrochemical conditions in DCM/TFAB system conducted at first oxidation potential*

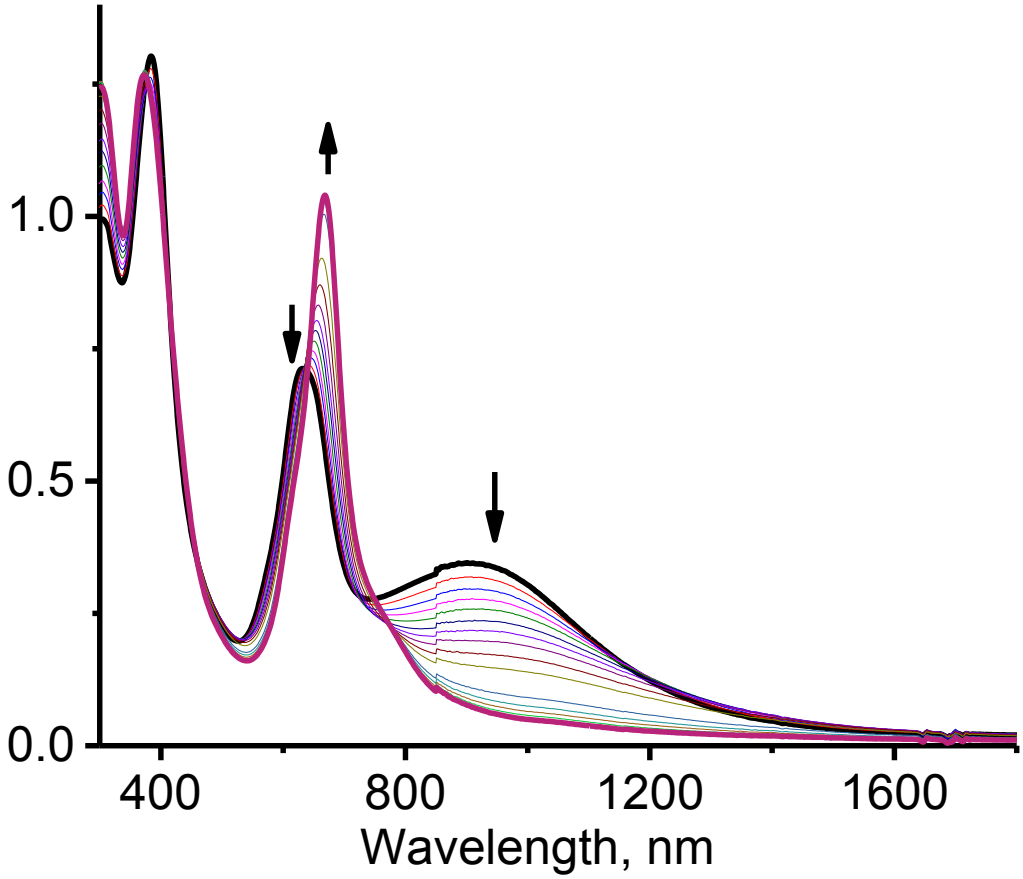


***Figure 54***. *Oxidation of* $\mathbf{9}_{a,b}^{n+}$ *under spectroelectrochemical conditions in DCM/TFAB system conducted at second oxidation potential*

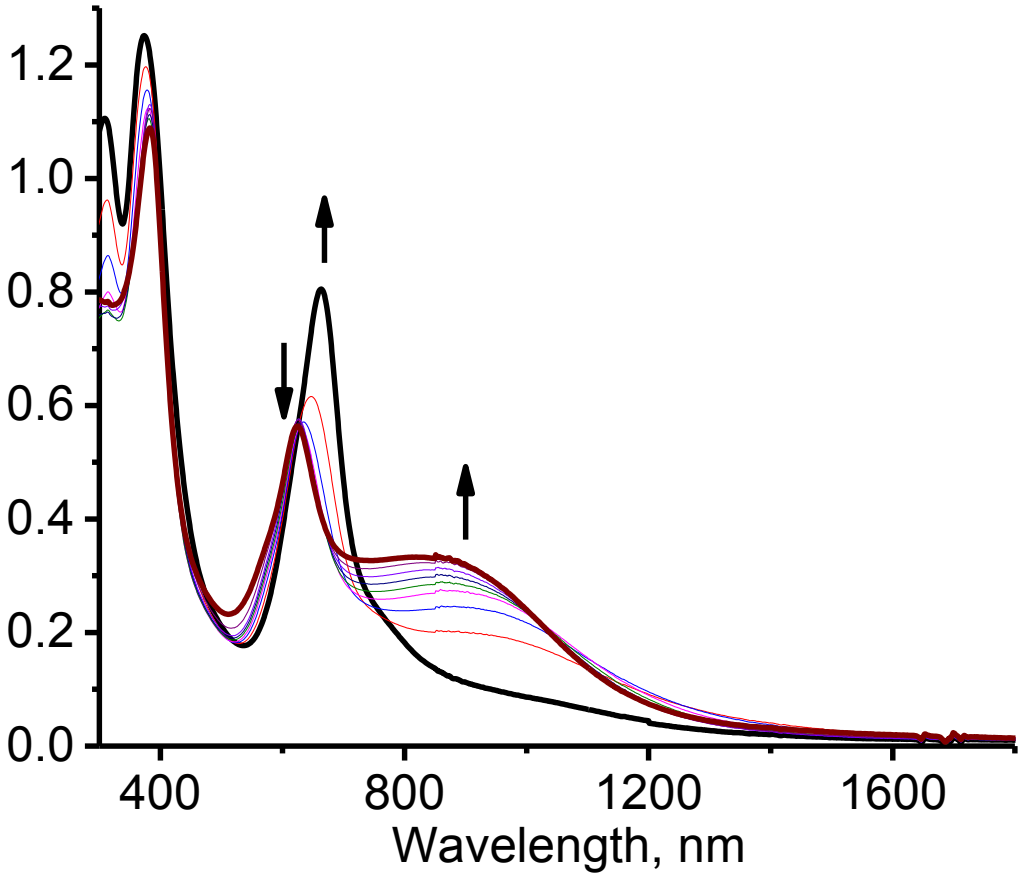


***Figure 55***. *Reduction of* $\mathbf{9}_{a,b}^{4+}$ *under spectroelectrochemical conditions in DCM/TFAB system*

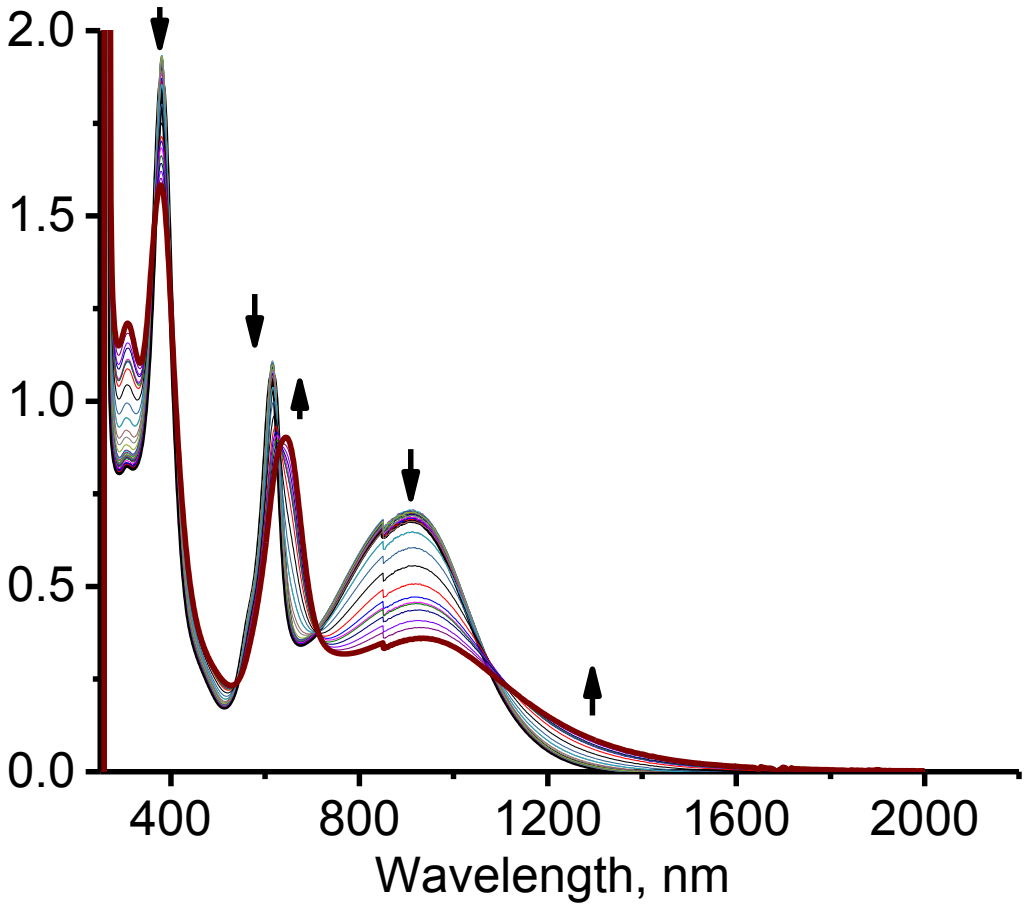


***Figure 56***. *Oxidation of* ***9c*** *and* ***9d*** *mixture under spectroelectrochemical conditions in DCM/TFAB system conducted at first oxidation potential*

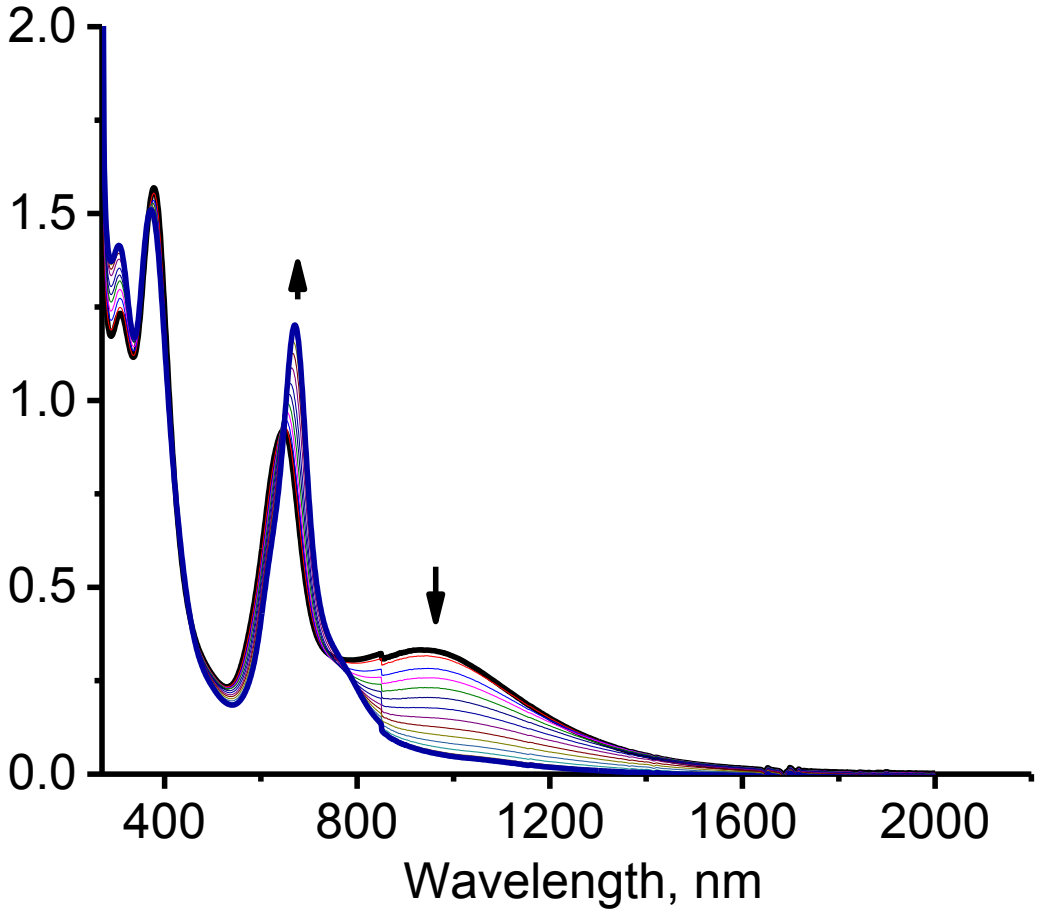


***Figure 57**. Oxidation of $\mathbf{9}_{c,d}^{n+}$ under spectroelectrochemical conditions in DCM/TFAB system conducted at second oxidation potential of $\mathbf{9}_{c,d}$*

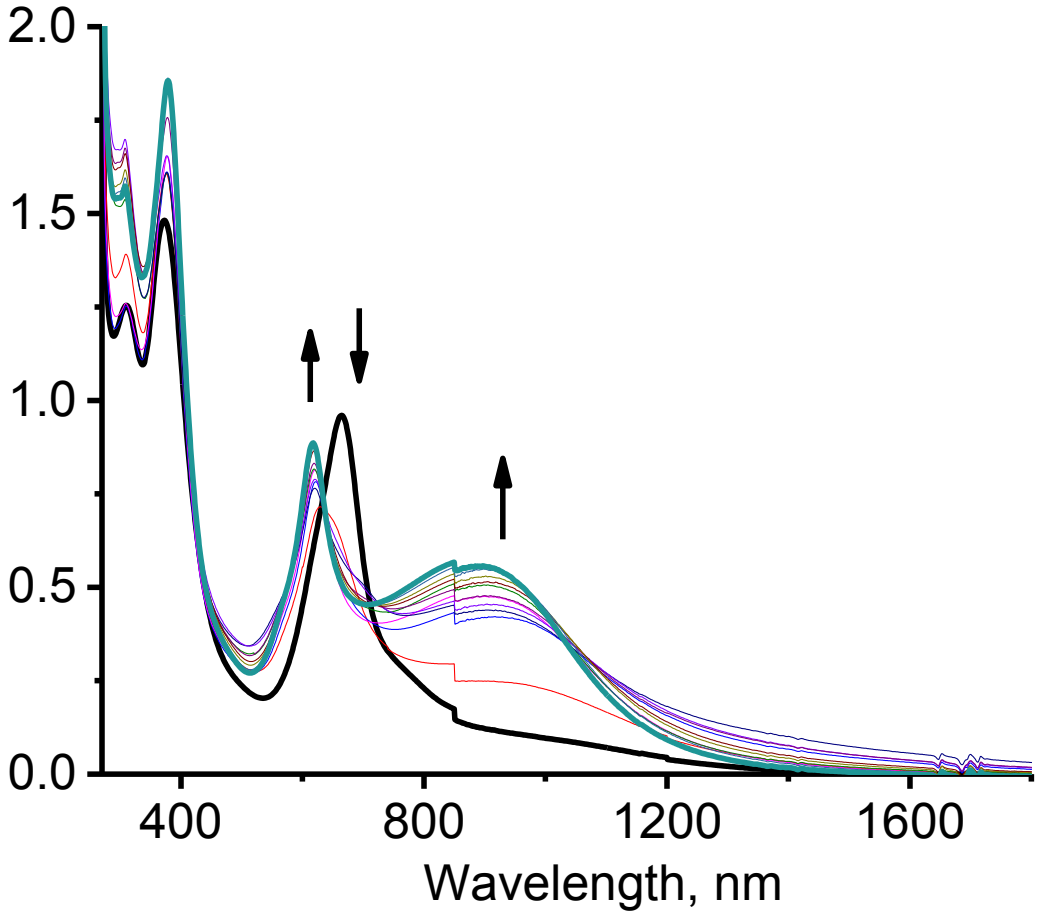


***Figure 58***. *Reduction of* $\mathbf{9}_{c,d}^{4+}$ *under spectroelectrochemical conditions in DCM/TFAB system*

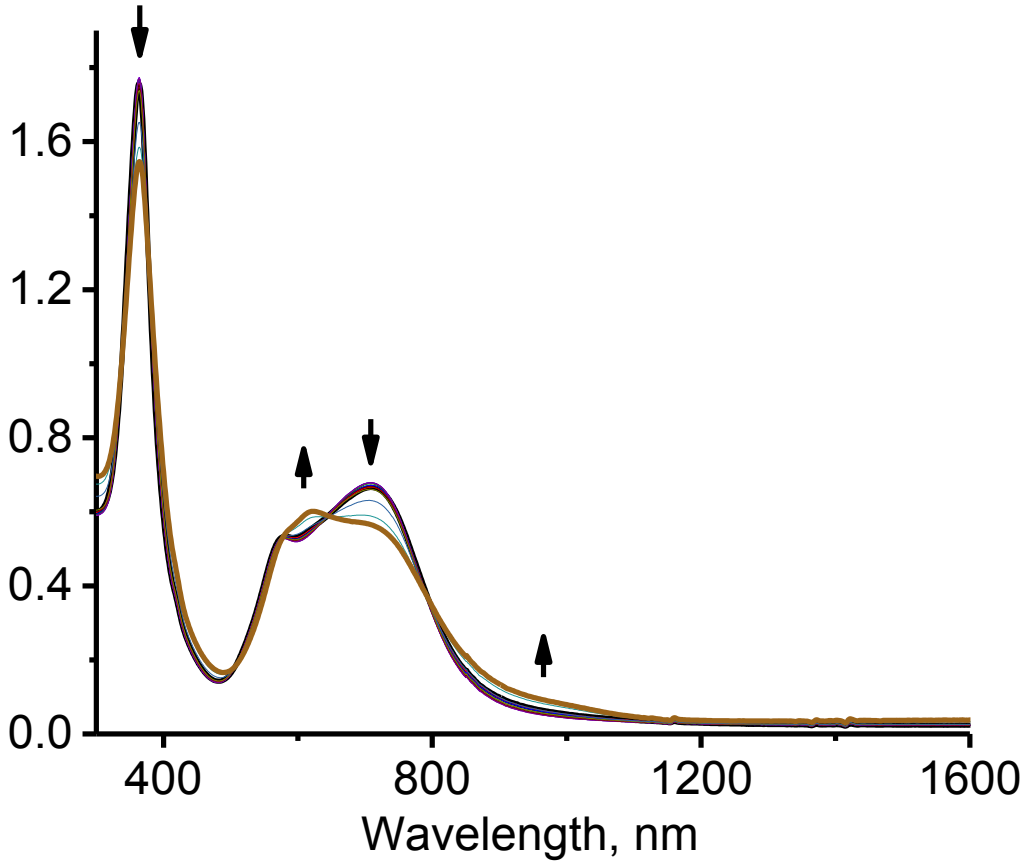


***Figure 59***. *Oxidation of* ***8*** *under spectroelectrochemical conditions in DCM/TFAB system conducted at first oxidation potential*

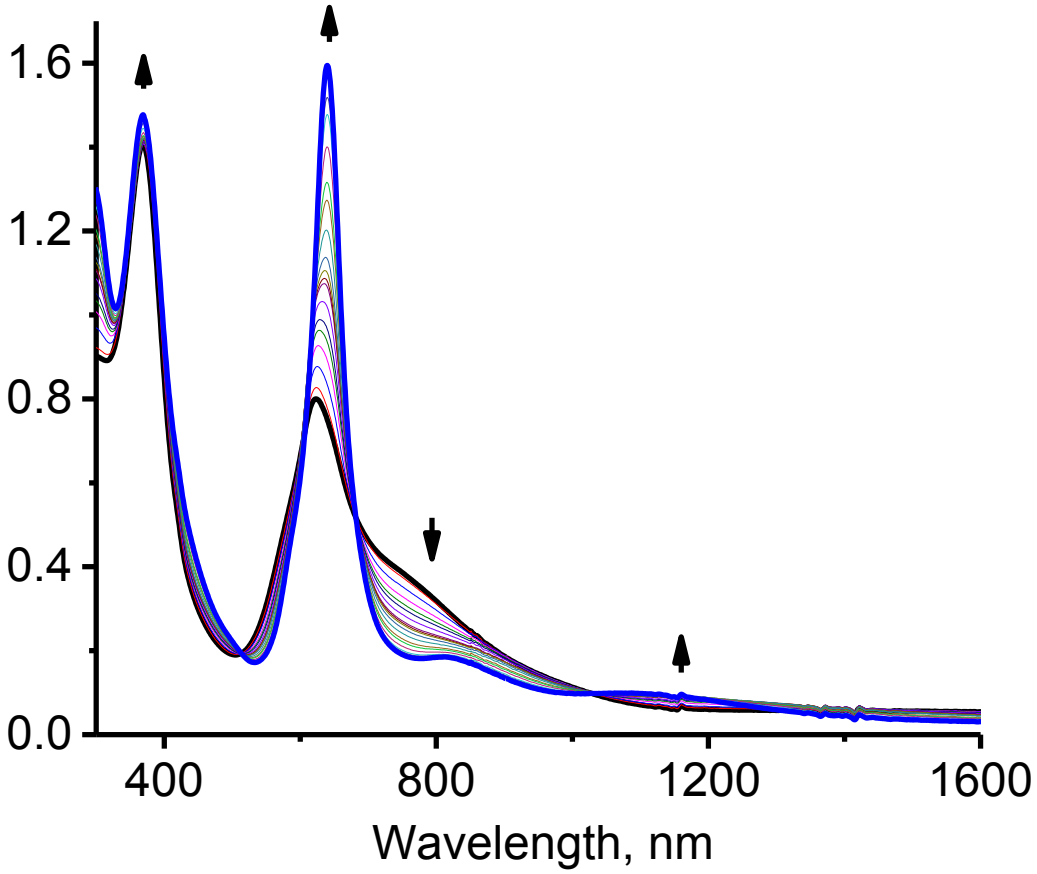


***Figure 60***. *Oxidation of* $\boldsymbol{8^{n+}}$ *under spectroelectrochemical conditions in DCM/TFAB system conducted at second oxidation potential*

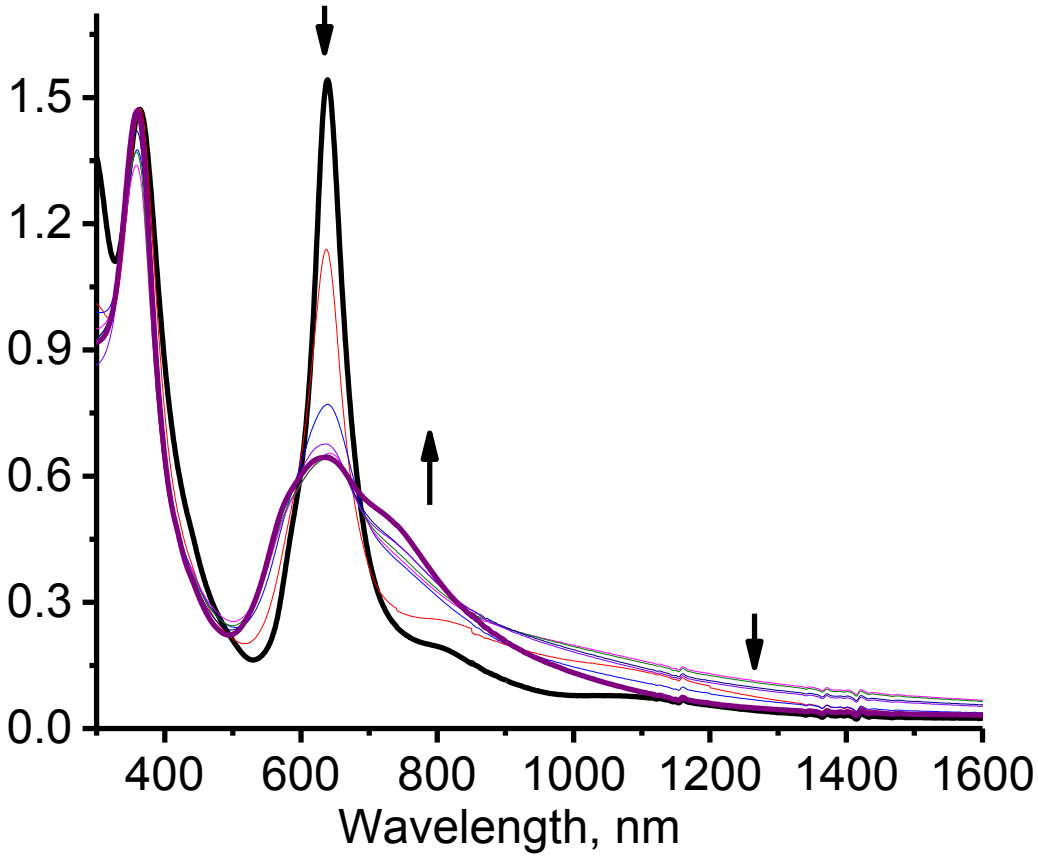


***Figure 61***. *Reduction of* ***8***$^{4+}$ *under spectroelectrochemical conditions in DCM/TFAB system*

Summarizing all the electrochemical data, given above, we can consider the formation of mixed-valance state according to the equations below:

$$\mathbf{MgTAP(CN)_4Fc_4} \xrightarrow{-n\,e^-} \mathbf{[MgTAP(CN)_4Fc_4]^{n+}} \quad \text{first oxidation}$$

$$\mathbf{[MgTAP(CN)_4Fc_4]^{n+}} \xrightarrow{-m\,e^-} \mathbf{[MgTAP(CN)_4Fc_4]^{4+}} \quad \text{second oxidation}$$

$$\mathbf{MgTAPFc_4} \xrightarrow{-n\,e^-} \mathbf{[MgTAPFc_4]^{n+}} \quad \text{first oxidation}$$

$$\mathbf{[MgTAPFc_4]^{n+}} \xrightarrow{-m\,e^-} \mathbf{[MgTAPFc_4]^{4+}} \quad \text{second oxidation}$$

Unfortunately, low stability of the cations and low purity of initial compounds prevents from predicting the exact amount of electrons which are participating in different processes.

## DFT and TDDFT Results

In order to gain insight into the nature of the intense NIR bands observed in UV-vis-NIR and MCD spectra of **8** and **9**, DFT and TDDFT calculations were conducted by Richard Dennison and Dr. Victor Nemykin with the selected results presented in Figures 20 – 22. In agreement with the electro- and spectroelectrochemical data discussed above, the first twelve occupied MOs (HOMO to HOMO-11) in **8** and **9** are predominantly ferrocene centered (Figure 63), while occupied π-orbitals centered on the tetraazaporphyrin core have significantly lower energies (Figure 62). LUMO to LUMO+2 in **8** and **9** are predominantly tetraazaporphyrin core-centered orbitals with the LUMO and LUMO+1 being doubly degenerate. A similar electronic structure has been

recently proposed for ferrocenyl-containing porphyrins[14l,o].

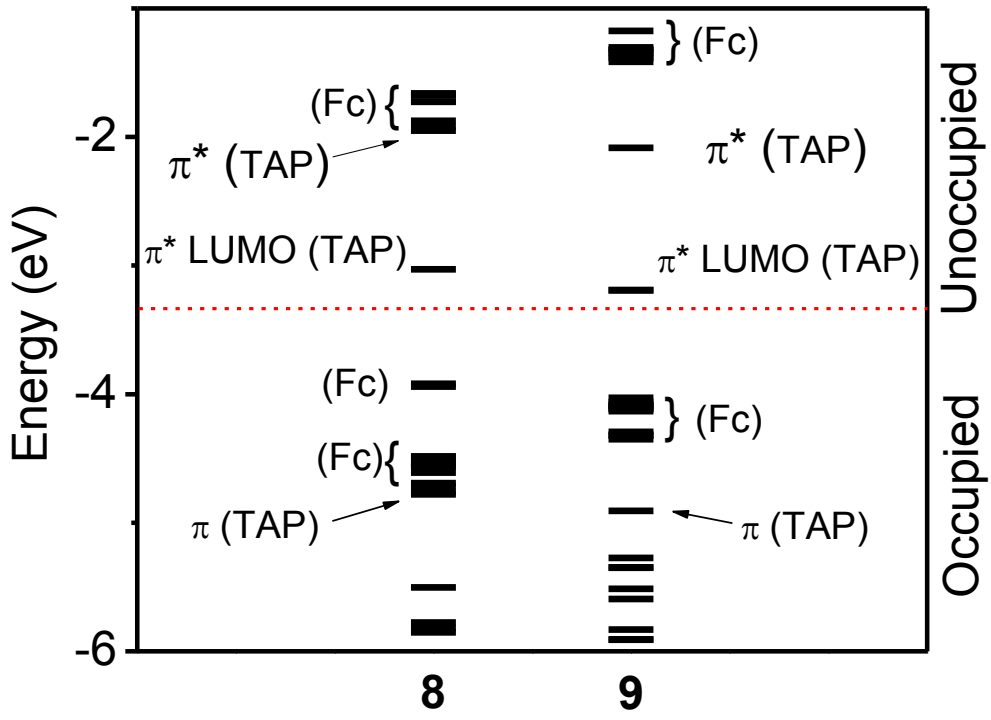


***Figure 62.*** *MO energies of* ***8*** *and* ***9*** *predicted by DFT calculations*

The presence of four electron-withdrawing groups in **9** results in the stabilization of the LUMO, HOMO, and high-energy occupied π-orbitals as well as leads to a significant decrease in the π-π* energy gap as compared to **8**. As a result, it could be expected (and confirmed by TDDFT calculations discussed below) that the energy of both MLCT and Q-bands in tetraferrocenyltetraazaporphyrins can be easily tuned by the second set of

periphery substituents. The electronic structures of **8** and **9** provide numerous possibilities for MLCT bands with lower energy than the Q-band (π-π* transition). This tentative hypothesis was further tested by a TDDFT approach, which has proven to accurately calculate the energies of π-π* and MLCT transitions in ferrocene-containing compounds, porphyrins, and phthalocyanines.[24l,35,40] Indeed, TDDFT calculations on **8** and **9** predict numerous MLCT transitions with lower energies compared to the π-π* Q-band (Figure 64).

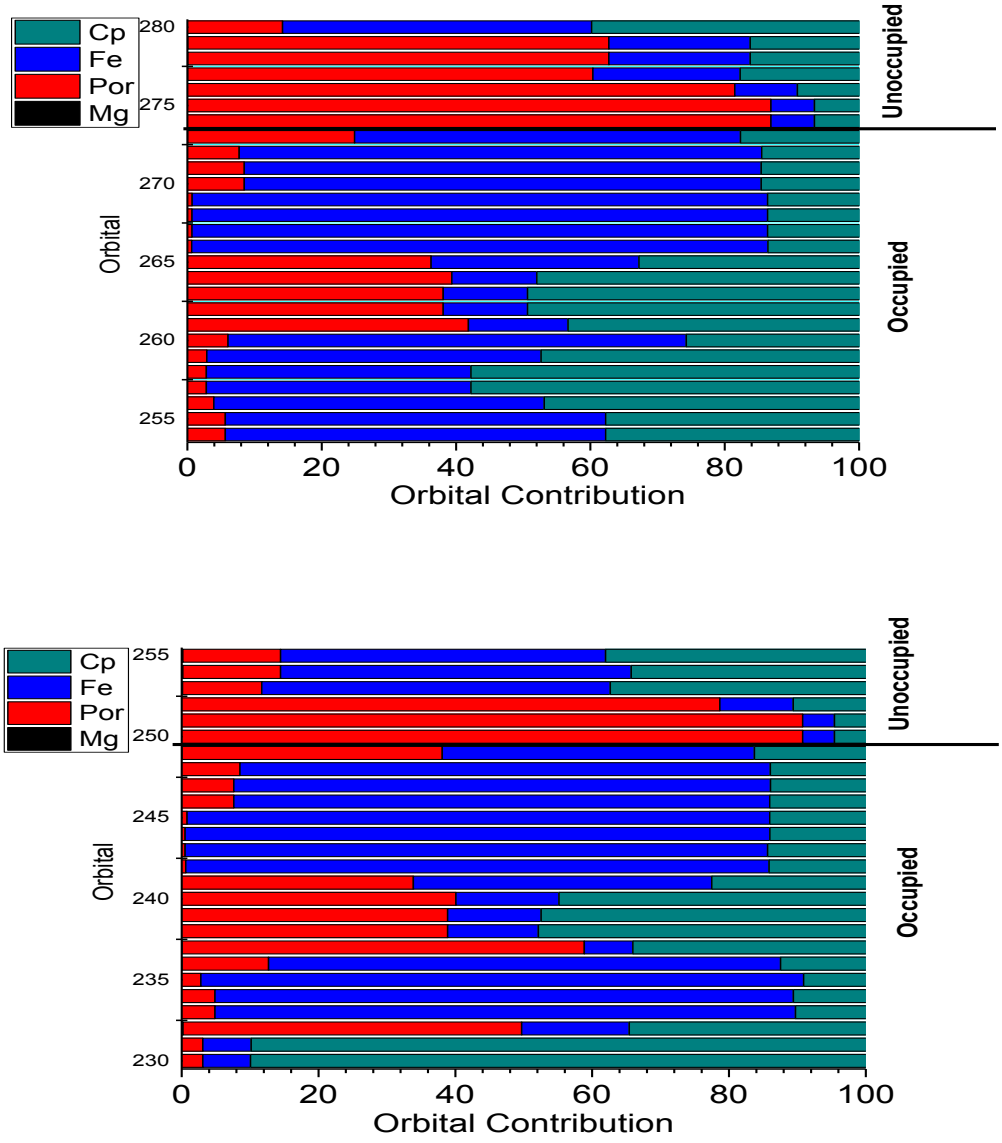


***Figure 63**: Calculated by DFT MO compositions of **9** (top) and **8** (bottom).*

In excellent agreement with the experimental data, TDDFT predicted MLCT bands in **8** are closer in energy to the Q-band, while the energy difference between the MLCT and Q-band in **9** is predicted to be larger.

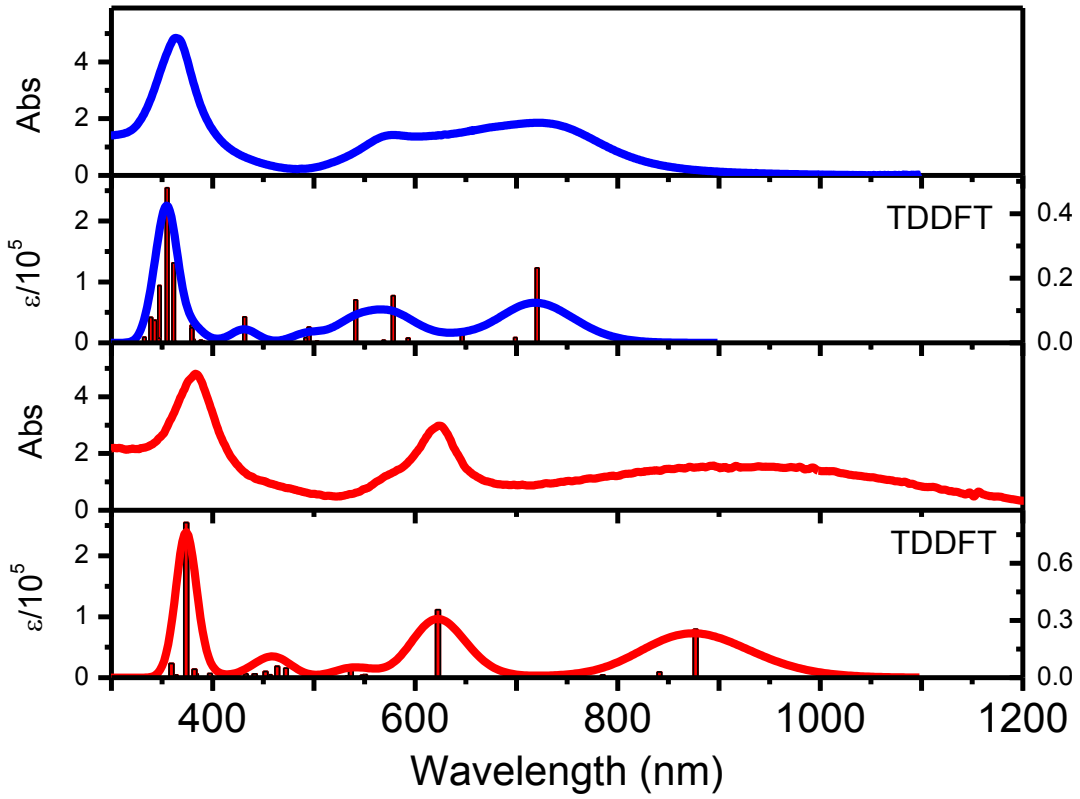


***Figure 64**: TDDFT predicted vertical excitation energies of **8** (top) and **9** (bottom) compared to the experimental UV-Vis-NIR spectra in DCM. Red bars represent predominantly π-π* and black bars represent predominantly MLCT transitions.*

In addition, the TDDFT predicted Q-band in **8** has a higher energy compared to that in **9**, in agreement with experiment. The closer energy spacing between the intense MLCT and Q-band in **8** explains the absence of the clean Faraday *A*-term centred at the Q-band. Indeed, the overlap between the positive component of the lower energy, broad NIR MLCT band and the negative component of the Q-band results in the experimentally observed spectroscopic signature of **8** (Figure 64).

## Conclusions

It was shown that the electronic structure, optical and redox properties of tetraferrocenyl-containing tetraazaporphyrins can be tuned by the second set of peripheral substituents. Further work will be directed to the incorporation of these compounds on titanium dioxide surface and constructing DSSCs by axial coordination of the electron-bridge moiety, as it is depicted in Figure 65.

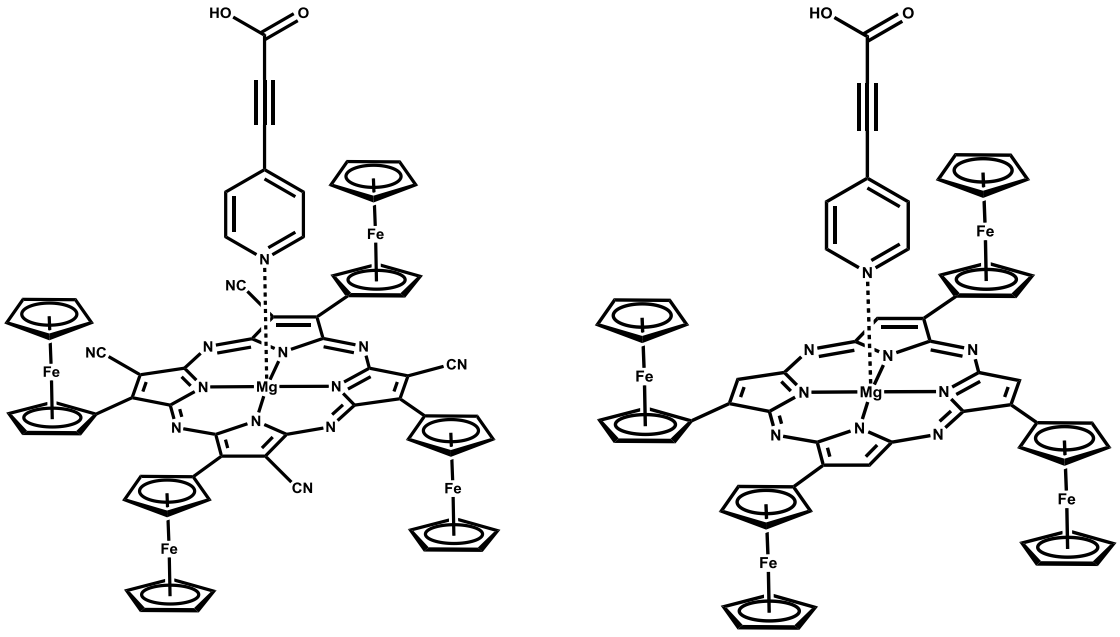


***Figure 65:*** *Modification of the structure of* ***8*** *and* ***9*** *for attaching to* $TiO_2$ *surface*

# Experimental

## Materials

All reactions were performed under dry inert (Ar, $N_2$) atmosphere with flame-dried glassware. All solvents and reagents were purchased from commercial sources and used without additional purification. Dry toluene was obtained by distillation over sodium and benzophenone indicator, dry DCM was obtained by distillation over calcium hydride prior experiments, and dry THF was obtained by distillation over Na/K alloy. Silica gel (60 Å, 63-100 μm) needed for column chromatography was purchased from Sorbent Technologies, while neutral aluminum oxide (Activity I, 58 Å, 150 mesh) was purchased from Fischer Inc. The compounds tetrabutylammonium tetrakis(pentafluorophenyl)borate (TFAB) was used in anhydrous DCM for electrochemical studies, after preparation according to literature[38].

## Synthesis of $H_2$TFcP

A mixture of 1.2 g (0.0056 mol) of ferrocenecarbaldehyde, 0.4 g (0.006 mol) pyrrole, and 0.038 ml (0.0003 mol) $BF_3 \cdot Et_2O$ in $CH_2Cl_2$ (150 ml) was reacted for 20 h at room temperature in argon atmosphere in a reactor covered with tin-foil due to photo-sensitivity. After this period, 0.98 g (0.004 mol) of p-chloranil was added and the resulting mixture was refluxed for 3.5 h. Reaction mixture was filtered through 1 cm of neutral – $Al_2O_3$ and filtrate was evaporated under reduced pressure (15 mm Hg). After

solvent evaporation, the residue was chromatographed on neutral - alumina gel using a DCM– triethylamine mixture (100 : 1 v/v) as the eluent. Finally, the product was recrystallized from toluene–hexane. Yield 0.587 g (40%).

$^1$H-NMR (500 MHz, $CDCl_3$, TMS), δ (ppm) = 9.61 (s, 8H, β-pyrr), 5.32 (m, 8H, α-Cp), 4.75 (m, 8H, β-Cp), 3.97 (s, 20H, CpH), −0.49 (s, 2H, NH).

Calc. for $C_{60}H_{46}N_4Fe_4$: C, 68.83; H, 4.40; N, 5.35%. Found: C, 68.74; H, 4.48; N, 4.81%.

## Synthesis of ZnTFcP

A mixture of $H_2$TFcP (0.200 g, 0.191 mmol) and zinc acetate (0.320 g, 1.91 mmol) in toluene (160 ml) was refluxed for 2 h (control by UV-Vis). After solvent evaporation, the residue was subjected to chromatography on alumina oxide using toluene as the eluent. Yield 0.187 g (83%).

$^1$H-NMR (500 MHz, $CDCl_3$, TMS), δ (ppm) = 9.84 (s, 8H, β-pyrr), 5.37 (m, 8H, α-Cp), 4.80 (m, 8H, β-Cp), 4.07 (s, 20H, CpH).

Calc. for $C_{60}H_{44}N_4Fe_4Zn$: C 64.93, H 4.00, N 5.05, Zn 5.89%. Found: C 64.29, H 4.31, N 5.13, Zn 5.42%.

## Synthesis of PdTFcP

A mixture of $H_2$TFcP (0.050 g, 0.0478 mmol) and $[Pd(OAc)_2]_3$ (0.075 g, 0.111 mmol) were dissolved in DMF (10 mL), and then triethylamine was added (0.2 mL). Mixture was stirred for 2 hours at 50 $^0$C (control by UV-Vis). After reaction was completed, mixture was poured into 20 mL of 5% NaCl aqueous solution. Mixture was filtered out and solid was left to dry overnight. After, dry solid was dissolved in DCM and subjected to column chromatography packed with aluminum oxide. Toluene – triethylamine mixture was used as eluent (100 : 1). Was obtained 28 mg (48%).

$^1$H-NMR (500 MHz, $CDCl_3$, TMS), δ (ppm) = 9.67 (s, 8H, β-pyrr), 5.28 (m, 8H, α-Cp), 4.75 (m, 8H, β-Cp), 3.99 (s, 20H, CpH).

## Synthesis of ClInTFcP

An amount of 800 mg (0.766 mmol) metal-free 5,10,15,20-tetraferrocenylporphyrin was measured into a 250 mL round bottom flask containing a magnetic stir-bar. $H_2$TFcP was dissolved in 160 mL dry THF. With stirring, 1.6 g (0.009 mol) $LiN[Si(CH_3)_3]_2$ was added and stirred for fifteen minutes. 4.0 g (0.018 mol) $InCl_3$ (anhydrous) was then added and refluxing began for three hours (controlled by UVVis). The mixture was then cooled down, evaporated to dryness under vacuum (15 mmHg), and the solid was set aside for column chromatography. The product was dissolved in

DCM and added to a column packed with alumina gel. Toluene – triethylamine (100 : 1) and DCM – triethylamine (100 : 1) were used as eluents. The first two bands to pass through the column were from unreacted starting materials—distinct by their light color and small amount. The main product came out in the third band (confirmed by UV-Vis spectroscopy). Solvent of the fraction with target compound was evaporated under reduced pressure. Yield: 475 mg (52%)

$^{1}$H NMR (500 MHz, $CDCl_3$, TMS), δ (ppm) = 4.25 (s, 8H, Cp), 4.86 (s, 8H, β-Cp), 5.54 (s, 20H, α-Cp), 10.02 (s, 4H, β-Pyrrole).

Calc. (found): C 60.32 (58.79), H 3.71 (3.77), N 4.69 (4.85).

## Synthesis of FcInTFcP

An amount of 196.2 mg (0.629 mol) ferrocene iodide was measured into a Schlenk flask filled with argon. A 145 mg (0.121 mmol) amount of InClTFcP was measured into another Schlenk with inert atmosphere in it as well. To the flask containing InClTFcP, 10 mL of toluene was added. The ferrocene iodide was dissolved in approximately eight milliliters of diethyl ether. While being flushed with Argon, the temperature of this solution was brought down to – 78 $^{0}$C using dry ice – acetone bath. After temperature was low enough, 0.26 mL of butyl lithium solution in hexane was added. The new orange FcLi salt was transferred to the porphyrin solution via cannula.

The reaction mixture was stirred for 45 minutes where it was then quenched with eight milliliters of distilled water. Solvent was removed under vacuum (15 mmHg) and solid was set aside for column chromatography. Column was packed with alumina gel and toluene – triethylamine (100 : 1) and DCM (100 : 1) – triethylamine were used as eluents. Yield: 94 mg (58%).

$^1$H NMR (500 MHz, THF-*d8*, TMS), δ (ppm) = 0.85 (s, 2H, α-Cp coordinated Fc), 2.49 (s, 5H, Cp Coordinated Fc), 2.99 (s, 2H, β-Cp Coordinated Fc), 4.15 (s, 20H, Cp porphyrin Fc), 4.81 (s, 8H, β-Cp porphyrin Fc), 5.54 (s, 8H, α-Cp coordinated Fc), 9.90 (s, 4H, β-Pyrrole).

Calc. (found): C 62.69 (62.625), H 4.22 (4.245), N 4.12 (3.98).

## Synthesis of $Co^{II}TFcP$

An amount of $H_2TFcP$ (100 mg, 0.1 mmol) was measured in one Schlenk flask, while $CoCl_2$ (anhydrous) was placed in another one (400 mg, 3.1 mmol). Bothe flasks were held under high vacuum (0.01 mm Hg) for an hour, and flask with $CoCl_2$ was heated to 200 $^0$C during this time. After, anhydrous THF (10 mL) was added to $H_2TFcP$ and with stirring $KN[Si(CH_3)_3]_2$ (0.200 g, 0.977 mmol) was added; solution was refluxed for 30 min. The solution was cooled down to stop refluxing and dry $CoCl_2$ was added to the reaction mixture (avoiding contact with atmosphere). The solution was refluxed for an

hour (control by UV-Vis). Resulting mixture was evaporated and subjected to column chromatography on alumina gel. Toluene – triethylamine (100 : 1) and DCM (100 : 1) – triethylamine were used as eluents. Yield: 0.025 g (44 %).

UV-vis ($\lambda_{max}$/nm, CHCl3, $\varepsilon \times 10^{-4}$): 320 (6.65), 420 (13.4), 490 sh, 660 (3.04), 590 sh, 800 sh.

Calc. for $C_{60}H_{44}N_4Fe_4Co$: C 65.32, H 4.02, N 5.08%. Found: C 68.68, H 4.52, N 5.41%

## Synthesis of $[Co^{III}TFcP]^+$

A mixture of $H_2TFcP$ (0.050 g, 0.0478 mmol) and $CoCl_2 \cdot 6H_2O$ (0.075 g, 0.111 mmol) were dissolved in Pyridine (10 mL). Mixture was refluxed for 2 hours with access of oxygen from air (control by UV-Vis). After reaction was completed, mixture was poured into 20 mL of 5% NaCl aqueous solution and it was filtered out and solid was left to dry overnight. After, dry solid was dissolved in DCM and subjected to column chromatography packed with aluminum oxide. Toluene – triethylamine mixture was used as eluent (100 : 1). Was obtained 7 mg (14%).

UV-vis ($\lambda_{max}$/nm, $CH_2Cl_2$): 338, 452, 507 sh, 718

## Synthesis of Tricyanovinylferrocene

A 2.56 g (20 mmol) sample of tetracyanoethylene was added to a preheated (100 °C) solution of 1.86 g (10 mmol) of ferrocene in 20 mL of sulfolane. Immediately after addition, the color of the solution changed first to green and later to blue and temperature of the mixture slightly dropped. The reaction mixture was heated continually with stirring for 10 min starting when temperature reached 95 $^0$C and ending with no more than 105 $^0$C, and then, it was cooled to room temperature. The resulting solution was poured into 50 mL of water, and the reaction products were immediately extracted using toluene/hexane (1:1 v/v) as a solvent. The organic layer was washed several times with water, dried over $CaCl_2$, and evaporated to dryness. The target compound was purified using column chromatography with silica gel. Toluene – hexane 4 : 1 was used as eluent. Were eluted 3 bands: 1$^{st}$ – unreacted ferrocene, 2$^{nd}$ – orange, cyanoferrocene, 3$^{rd}$ – dark – blue target compound. Yield: 740 mg (25.8%).

$^1$H NMR (500 MHz, THF-*d8*, TMS), δ (ppm) = 5.27 (t, 2H, α-$Cp_1$); 5.165 (t, 2H, β-$Cp_1$); 4.47 (s, 5H, $Cp_2$).

Calc. for $C_{11}H_9NFe$: C, 62.60, H, 4.30, N, 6.64. Found: C, 62.71, H, 4.27, N, 6.66.

## Synthesis of $MgTAP(CN)_4Fc_4$

Firstly, butyl alcohol was prepared by distillation over magnesium several times. Then 3 ml of butyl alcohol solution of tricyanovinylferrocene (70 mg, 4 mmol) and magnesium butoxide from 12 mg magnesium was refluxed for several hours under inert (Ar) atmosphere (control by UV-Vis). After the solution was cooled down to room temperature, the residue was filtered through 1cm layer of alumina gel, and then chromatographed with alumina column and using DCM – triethylamine (100 : 1) as eluent. After evaporation of dark – green fraction, it was washed for several times with ethanol – water (1 : 1) mixture. 11 mg (15%) were obtained.

Calc. for $C_{60}H_{36}N_{12}Fe_4Mg$: C, 62.22; H, 3.54; N, 13.84%. Anal. Found: C, 61.5; H, 3.1; N, 14.3%.

UV-Vis. ($\lambda_{max}$, nm (log ε), $CHCl_3$): 320sh, 382 (4.67), 430sh, 590sh, 623 (4.47), 962 (4.12).

## Instrumentation

A Varian Unity INOVA NMR instrument was used to evaluate spectra taken at 500 MHz frequency for protons. Each were referenced to TMS or peaks of the solvent as an internal standard and chemical shifts were recorded in parts per million. All UV-Vis data was obtained on a JASCO-720 spectrophotometer at room temperature. An OLIS DCM 17 CD spectropolarimeter with 1.4 T DeSa magnet was used to obtain all MCD data. Electrochemical measurements were conducted using a CHI620C electrochemical analyzer utilizing the three-electrode scheme. Platinum working, platinum auxiliary and Silver/Silver chloride reference electrodes were used in 0.05 M solution of TFAB (or 0.1 M TBAP) in DCM with redox potentials corrected using internal standard (decamethylferrocene or ferrocene) in all cases. Spectroelectrochemical data was collected using a custom-made 1 mm cell, a working electrode made of platinum mesh, and a 0.15 M solution of TFAB in DCM. Elemental analysis was performed by Atlantic Microlab, Inc. in Atlanta, Georgia.

# References


1) Creutz C. *Prog. Inor. Chem.*, **1983**, *30*, 1.

2) Robin M; Day P. *Advances in Radiochemistry*. **1967,** *10*, 248.

3) Hush N. S. *Prog. Inorg. Chem.* **1967**, *8*, 391.

4) D'Alessandro D.; Keene R. *Chem. Soc. Rev.,* **2006**, *35*, 424.

5) Shoji O, Okada S, Satake A, and Kobuke Y. *J. Am. Chem. Soc.* 2005; **127**: 2201.

6) Rochford J, Rooney AD and Pryce MT. *Inorg. Chem.* 2007; **46**: 7247.

7) Nemykin VN, Rohde GT, Barrett CD, Hadt RG, Bizzarri C, Galloni P, Floris B, Nowik I, Herber RH, Marrani AG, Zanoni R and Loim NM. *J. Am. Chem. Soc.* 2009; **131**:14969.

8) Nemykin VN, Rohde GT, Barrett CD, Hadt RG, Sabin JR, Reina G, Galloni P and Floris B. *Inorg. Chem*. 2010; **49**: 7497.

9) Solntsev PV, Sabin JR, Dammer SJ, Gerasimchuk NN and Nemykin VN. *Chem. Commun.* 2010; **46**: 6581.

10) Mishra A, Fischer Markus KR and Bäuerle P. *Angew. Chem. Int. Ed*., 2009; **48**: 2474–2499.

11) Fang Li, Qiguang Zheng Guang Yang, Nengli Dai, Peixiang Lu, *Materials Letters*, **62**: 2008, 3059-3062.

12) a) Chen J, Lee T, Su J, Wang W and Reed MA. *Encyclopedia of Nanoscience and Nanotechnology* 2004; **5**: 633. b) Weiss J. *Coord. Chem. Rev.* 2010; **254**: 2247. c) Lyshevski SE. (Ed.) *Nano and Molecular Electronics Handbook*, CRC Press: New

York, 2007; pp 912. d) Jurow M, Schuckman AE, Batteas JD and Drain CM. *Coord. Chem. Rev.* 2010; **254**: 2297. e) Lee SU, Belosludov RV, Mizuseki H and Kawazoe Y. *Small* 2008; **4**: 962.

13) a) Kaim W and Sarkar B. *Coord. Chem. Rev.* 2007; **251**: 584. b) Fabre B. *Acc. Chem. Res.* 2010; **43**: 1509. c) *Ferrocenes: Ligands, Materials and Biomolecules*, Stepnicka P. (Ed.), John Wiley & Sons, Ltd., Chichester, England, 2008; 655 pp.

14) a) Bucher C, Devillers CH, Moutet J-C, Royal G and Saint-Aman E. *Coord. Chem. Rev.* 2009; **253**: 21. b) Loim NM, Abramova NV and Sokolov VI. *Mendeleev Commun.* 1996; 46. c) Burrell AK, Campbell WM, Jameson GB, Officer DL, Boyd PDW, Zhao Z, Cocks PA and Gordon KC. *Chem. Commun.* 1999; 637. d) Narayanan SJ, Venkatraman S, Dey SR, Sridevi B, Anand VRG and Chandrashekar TK. *Synlett*. 2000; 1834. e) Rhee SW, Na YH, Do Y and Kim J. *Inorg. Chim. Acta* 2000; **309**: 49. f) Shoji O, Okada S, Satake A and Kobuke Y. *J. Am. Chem. Soc.* 2005; **127**: 2201. g) Shoji O, Tanaka H, Kawai T and Kobuke Y. *J. Am. Chem. Soc.* 2005; **127**: 8598. h) Auger A and Swarts JC. *Organometallics* 2007; **26**: 102. i) Kubo M, Mori Y, Otani M, Murakami M, Ishibashi Y, Yasuda M, Hosomizu K, Miyasaka H, Imahori H and Nakashima S. *J. Phys. Chem. A* 2007; **111**: 5136. j) Nemykin VN, Barrett CD, Hadt RG, Subbotin RI, Maximov AY, Polshin EV and Koposov AY. *Dalton Trans.* 2007; 3378. k) Rochford J, Rooney AD and Pryce MT. *Inorg. Chem.* 2007; **46**: 7247. l) Nemykin VN, Galloni P, Floris B, Barrett CD, Hadt RG, Subbotin RI, Marrani AG, Zanoni R and Loim NM. *Dalton Trans.* 2008; 4233. m) Nemykin VN, Rohde GT, Barrett CD, Hadt RG, Bizzarri C, Galloni P,

Floris B, Nowik I, Herber RH, Marrani AG, Zanoni R and Loim NM. *J. Am. Chem. Soc.* 2009; **131**: 14969. n) Galloni P, Floris B, de Cola L, Cecchetto E and Williams RM. *J. Phys. Chem. C* 2007; **111**: 1517. o) Nemykin VN, Rohde GT, Barrett CD, Hadt RG, Sabin JR, Reina G, Galloni P and Floris B. *Inorg. Chem.* 2010; **49**: 7497. p) Nemykin VN and Hadt RG. *J. Phys. Chem. A* 2010; **114**: 12062. q) Rohde GT, Sabin JR, Barrett CD and Nemykin VN. *New J. Chem.* 2011; **35**: 1440. r) Solntsev PV, Neisen BD, Sabin JR, Gerasimchuk NN and Nemykin VN. *J. Porphyrins Phthalocyanines* 2011; **15**: 612.

15) a) Burrell AK, Campbell W and Officer DL. *Tetrahedron Lett.* 1997; **38**: 1249. b) Burrell AK, Campbell WM, Officer DL, Scott SM, Gordon KC and McDonald MR. *J. Chem. Soc. Dalton Trans.* 1999; 3349. c) Jiao L, Courtney BH, Fronczek FR and Smith KM, *Tetrahedron Lett.* 2006; **47**: 501. d) Wang HJH, Jaquinod L, Olmstead MM, Vicente MGH, Kadish KM, Ou Z and Smith KM. *Inorg. Chem.* 2007; **46**: 2898. e) Gryko DT, Zhao F, Yasseri AA, Roth KM, Bocian DF, Kuhr WG and Lindsey JS. *J. Org. Chem.* 2000; **65**: 7356. f) Schmidt ES, Calderwood TS and Bruice TC. *Inorg. Chem.* 1986; **25**: 3718. g) Cheng K-L, Li H-W and Ng DKP. *J. Organomet. Chem.* 2004; **689**: 1593. h) Giasson R, Lee EJ, Zbao X and Wrighton MS. *J. Phys. Chem.* 1993; **97**: 2596. i) Muraoka T, Kinbara K and Aida T. *Nature* 2006; **440**: 512.

16) a) Maiya GB, Barbe JM and Kadish KM. *Inorg. Chem.* 1989; **28**: 2524. b) Solntsev PV, Sabin JR, Dammer SJ, Gerasimchuk NN and Nemykin VN. *Chem. Commun.* 2010; **46**: 6581.

17) a) Nemykin VN and Kobayashi N. *Chem. Commun.* 2001; 165. b) Lukyanets EA and Nemykin VN. *J. Porphyrins Phthalocyanines* 2010; **14**: 1.

18) a) Jin Z, Nolan K, McArthur CR, Lever ABP and Leznoff CC. *J. Organomet. Chem.* 1994; **468**: 205. b) Poon K-W, Yan Y, Li XY and Ng DKP. *Organometallics* 1999; **18**: 3528. c) Salan U, Altindal A, Bulut M and Bekaroglu O. *J. Porphyrins Phthalocyanines* 2006; **10**: 1263. d) Nemykin VN and Lukyanets EA. In *Handbook of Porphyrin Science*; Kadish KM, Smith KM and Guilard R. (Eds.) World Scientific: Singapore, 2010; Vol. 3, pp 1–323. e) Nemykin VN and Lukyanets EA. *ARKIVOC* 2010; **i**: 136.

19) a) Gryko DT, Piechowska J, Jaworski JS, Galezowski M, Tasior M, Cembor M and Butenschoen H. *New J. Chem.* 2007; **31**: 1613. b) Venkatraman S, Kumar R, Sankar J, Chandrashekar TK, Sendhil K, Vijayan C, Kelling A and Senge MO. *Chem. Eur. J.* 2004; **10**: 1423.

20) Dammer SJ. *M.S. thesis*, University of Minnesota Duluth, Duluth, MN, July 2011; pp 127.

21) Dawson, D.; Sangalang, J.; Arnold, J. *J. Am. Chem. Soc*. **1996**, 118, 6082.

22) a) Kadish KM and Morrison MM. *J. Am. Chem. Soc.* 1976; **98**: 3326. b) Kadish KM, Caemelbecke EV and Royal G. In *Porphyrin Handbook*; Kadish KM, Smith KM and Guilard R. (Eds.) Academic Press: New York, 2000; Vol. 8, pp 1–114. c) Ou Z, Zhu W, Fang Y, Sintic PJ, Khoury T, Crossley MJ, Kadish KM. *Inorg. Chem.* 2011; **50**: 12802. d) Zhu W, Sintic M, Ou Z, Sintic PJ, McDonald JA, Brotherhood PR, Crossley MJ and Kadish KM. *Inorg. Chem.* 2010; **49**: 1027. e) Ou

Z, EW, Zhu W, Thordarson P, Sintic PJ, Crossley MJ, Kadish KM. *Inorg. Chem.* 2007; **46**: 10840. f) Donzello MP, Agostinetto R, Ivanova SS, Fujimori M, Suzuki Y, Yoshikawa H, Shen J, Awaga K, Ercolani C, Kadish KM. *Inorg. Chem.* 2005; **44**: 8539. g) Van Caemelbecke E, Derbin A, Hambright P, Garcia R, Doukkali A, Saoiabi A, Ohkubo K, Fukuzumi S and Kadish KM. *Inorg. Chem.* 2005; **44**: 3789. h) Liu YH, Benassy M-F, Chojnacki S, D'Souza F, Barbour T, Belcher WJ, Brothers PJ and Kadish KM. *Inorg. Chem.* 1994; **33**: 4480. i) Kadish KM, D'Souza F, Van Caemelbecke E, Villard A, Lee JD, Tabard A and Guilard R. *Inorg. Chem.* 1993; **32**: 4179. j) Kadish KM, Dubois D, Barbe JM and Guilard R. *Inorg. Chem.* 1991; **30**: 4498. k) Kadish KM and Mu X. *Pure Appl. Chem.* 1990; **62**: 1051. l) Kadish KM, Liu YH, Anderson JE, Dormond A, Belkalem M and Guilard R. *Inorg. Chim. Acta* 1989; **163**: 201. m) Kadish KM, Deng YJ, Yao CL and Anderson JE. *Organometallics* 1988; **7**: 1979.

23) a) Peychal-Heiling G and Wilson GS. *Anal. Chem.* 1971; **43**: 550. b) Lanese JG and Wilson GS. *J. Electrochem. Soc.* 1972; **119**: 1039. c) Kadish KM, Cornillon JL, Cocolios P, Tabard A and Guilard R. *Inorg. Chem.* 1985; **24**: 3645.

24) a) Ding F, Wang H, Wu Q, Van Voorhis T, Chen S and Konopelski JP. *J. Phys. Chem. A* 2010; **114**: 6039. b) Santi , Durante C, Donoli A, Bisello A, Orian L, Ceccon A, Crociani L and Benetollo F. *Organometallics* 2009; **28**: 3319. c) Hadt RG and Nemykin VN. *Inorg. Chem.* 2009; **48**: 3982. d) Jones SC, Barlow S and O'Hare D. *Chem. Eur. J.* 2005; **11**: 4473. e) Solntsev PV, Dudkin SV, Sabin JR and Nemykin VN. *Organometallics* 2011; **30**: 3037. f) Semencic MC, Heinze K,

Foerster C and Rapic V. *Eur. J. Inorg. Chem.* 2010; 1089. g) Roy LE, Jakubikova E, Guthrie MG and Batista ER. *J. Phys. Chem. A* 2009; **113**: 6745. h) Romero T, Caballero A, Espinosa A, Tarraga A and Molina P. *Dalton Trans.* 2009; 2121. i) Helten H, Fankel S, Feier-Iova O, Nieger M, Espinosa Ferao A and Streubel R. *Eur. J. Inorg. Chem.* 2009; 3226. j) Pinjari RV and Gejji SP. *J. Phys. Chem. A* 2008; **112**: 12679. k) Fuentealba M, Garland MT, Carrillo D, Manzur C, Hamon J-R and Saillard J-Y. *Dalton Trans.* 2008; 77. l) Nemykin VN, Maximov AY and Koposov AY. *Organometallics* 2007; **26**: 3138. m) Nemykin VN, Makarova EA, Grosland JO, Hadt RG and Koposov AY. *Inorg. Chem.* 2007; **46**: 9591. n) Herber RH, Nowik I, Grossland JO, Hadt RG and Nemykin VN. *J. Organomet. Chem.* 2008; **693**: 1850. o) Nemykin VN and Hadt RG. *Inorg. Chem.* 2006; **45**: 8297.

25) Gratzel M, *Nature* 2001, **414**, 338.

26) Nazeeruddin MK, De Angelis F, Frantacci S, Selloni A, Viscardi A, Liska P, Ito S, Takeru B, Gratzel M, *J. Am. Chem. Soc.* 2005, **127**, 16835.

27) Gratzel M, *J. Photochem. Photobiol. A*. 2004, **164**, 3.

28) Nazeeruddin MK, Spivallo R, Liska P, Comte P, Gratzel M, *Chem. Commun.* 2003,1456.

29) Diau, E. et al. *Chem Eur. J.* 2009**, 15**, 1403-1412

30) Mishra A, Fischer, Markus KR and Bäuerle, P, *Angew. Chem. Int. Ed*. 2009. **48**, 2474–2499.

31) Gratzel M, *Inorg. Chem.* 2005, **44**, 6841.

32) Gratzel M, J. R. Durrant in *Nanostructured and Photoelectrochemical Systems for*

*Solar Photon Conversion* (Eds.: M. D. Archer, A. J. Nozik), World Scientific, Singapore, 2008, p. 503.

33) (a) Cowan DO and Kaufman F, *J. Am. Chem. Soc.* 1970, **92**, 6198; (b) Cowan DO and Kaufman F, *J. Am. Chem. Soc.* 1970, **92**, 219; (c) Jr. Morrison WH and. Hendrickson DN, *Chem. Phys. Lett.* 1973, **22**, 119; (d) Morrison WH, Krogsrud S and Hendrickson DN, *Inorg. Chem.* 1973, **12***, 1998*; (e) Morrison WH-Jr and Hendrickson DN, *Inorg. Chem.* 1975, **14**, 2331; (f) Dong TY and Hendrickson DN, *Bull. Inst. Chem., Acad. Sinica* 1987, **34**, 67; (g) Tolbert LM, Zhao X, Ding Y and Bottomley LA, *J. Am. Chem. Soc.* 1995, **117**, 12891; (h) Ribou A-C, Launay JP, Sachtleben JM, Li H and Spangler CW, *Inorg. Chem.* 1996, **35**, 3735; (i) Patoux C, Coudret C, Launay JP, Joachim C and Gourdon A, *Inorg. Chem.* 1997, **36**, 5037; (j) Hadt RG and Nemykin VN, *Inorg. Chem*. 2009, **48**, 3982.

34) Nemykin VN, Maximov AY, Koposov AY, *Organometallics*, 2007, ***26*** (13), pp 3138–3148.

35) Nemykin VN, Makarova EA, Grosland JO, Hadt RG, Koposov AY, *Inorg. Chem.* 2007, **46**, 9591 – 9601.

36) Nemykin VN, Kobayashi N, *Chem. Commun.* 2001, 165.

37) Perevalova EG, Lemenovskii DA, Alekseev VP, Grandberg KI, Nesmeyanov AN, *Izv. Acad. Nauk SSSR, Ser. Khim.* 1972, **8**, 1867.

38) (a) Waluk J and Michl J, *J. Org. Chem.* 1991, **56**, 2729; (b) Gorski A, Vogel E, Sessler JL and Waluk J, *J. Phys. Chem. A* 2002, **106**, 8139; (c) Mack J, Stillman MJ and Kobayashi N, *Coord. Chem. Rev.* 2007, **251**, 429.

39) (a) Barriere F and Geiger WE, *J. Am. Chem. Soc*. 2006, **128**, 3980; (b) Geiger WE and Connelly NG, *Advances in Organometallic Chemistry* 1985, **24***,* 87.

40) a) Mack J, Bunya M, Shimizu Y, Uoyama H, Komobuchi N, Okujima T, Uno H, Ito S, Stillman SN, Ono N, Kobayashi N, *Chem. Eur. J.* 2008, **14**, 5001; (b) Mack J, Kobayashi N and Stillman MJ, *J. Inorg. Biochem.* 2010, **104**, 310; (c) Mack J, Asano Y, Kobayashi N and Stillman MJ, *J. Am. Chem. Soc.* 2005, **127**, 17697; (d) Nemykin VN, Hadt RG, Belosludov RV, Mizuseki H and Kawazoe Y, *J. Phys. Chem. A* 2007, **111**, 12901.